UNIVERSITA' DEGLI STUDI DI NAPOLI FEDERICO II

SCUOLA POLITECNICA E DELLE SCIENZE DI BASE

DIPARTIMENTO DI INGEGNERIA CHIMICA, DEI MATERIALI E DELLA PRODUZIONE INDUSTRIALE

Dottorato di Ricerca in Ingegneria Chimica

(XXVII Ciclo)

INTENSIVE CULTURE OF AUTOTROPHIC MICROALGAE FOR ENERGY VECTOR PRODUCTION

PhD thesis

Scientific committee:

Prof. Roberto Andreozzi

Prof. Raffaele Marotta

Prof. Antonio Marzocchella

Prof. Giuseppe Olivieri

Prof. Gabriele Pinto

Prof. Antonino Pollio

Student:

Immacolata Gargano

ACADEMIC YEAR 2013-2014

ABSTRACT

The supply of renewable feedstocks for the production of convenience goods combined with the carbon capture and storage is considered a promising solution to both fossil resources depletion and global warming control. Photosynthetic microorganisms, e.g. microalgae, are good candidates for this challenging bet. Indeed, autotrophic microalgae fix CO_2 and are feedstocks for several industries involved in human nutrition, animal nutrition, cosmetics, high-added value molecules, pharmaceuticals, biofuels and wastewater treatments.

A critical issue for the intensive production of microalgae is the design of low cost and high efficiency photobioreactors. Main critical issues for the exploitation of microalgae as energy vectors are the biomass dryer and lipid extraction.

This PhD thesis was focused on the development of solutions for the critical issues listed above. The main activities were: selection of microalgal strains representative of the main phylum; the optimization of the microalgal cultures by the selection of photobioreactor design and operating conditions (effects of photobioreactor hydrodynamics, light intensity and trend, CO_2 in the gas phase, medium composition and medium pH on microalgal cultures in cylindrical and parallelepiped shape photobioreactors); the characterization of the composition of microalgae during the day/night cycle as an effect of the circadian behaviour of microalgae; the characterization of the microalgal growth rate under controlled operating conditions; the characterization of the photochemical process; the optimization of the direct transesterification on wet and dried microalgae to produce biodiesel.

Main results were:

- ✓ The CO_2 concentration typical of power plant exhaust gas (up to 15-18%) enhances lipid productivity, notwithstanding the inhibition effects on pigment synthesis. The optimal pH has been found to be 7.0, but satisfactory microalgae and lipid productivities have been obtained at low pH. The ability of microalgae to be active still a low pH suggests the real possibility to adopt acid conditions to preserve cultures from contamination. Continuous light for 24 hour did not affect the biomass and lipid productivity.

- ✓ The kinetic characterization of the photosynthetic reaction centres in microalgae by means of fluorescence methodology pointed out that: at irradiance lower than 1000 µE m^{-2} s^{-1} the photochemical process is controlled by the photons capture while at higher irradiance the photoinhibition competes with the photochemical quenching. The time-scale of repairing process is larger than the other photochemical process whatever the investigated irradiance.

✓ The optimization of the alkaline direct transesterification was carried out on *Stichococcus bacillaris* and validate on microalgal strains characterized by a different cell wall structure. Triglycerides were not converted without an alkaline catalyst and approached a maximum conversion at a catalyst concentration of 1.5% NaOH (w/w). Under alkaline conditions the pre-mixing time did not affect bio-oil yield; the bio-oil yield increased with temperature and approached a maximum at around 65°C; the bio-oil yield did not change significantly with the methanol to biomass weight ratio when the methanol is not limiting; the bio-oil yield gradually increased within the first minutes of reaction. Biomass drying was observed to play an important role in direct transesterification: the bio-oil yield reduced with an increase in biomass water content. A higher bio-oil yield was obtained increasing the methanol/wet biomass ratio. Under alkaline catalyzed conditions the direct transesterification process was more efficient than the acidic ones.

✓ The characterization of the specific growth rate and the biomass composition during the day/night cycle of *Nannochloropsis sp*. was carried out by means of a turbidosotat photobioreactor. Two irradiation strategy were been investigated :“constant irradiance day/night cycle” 16 h of light at 600 µE m^{-2} s^{-1} and 8 h of dark; “circadian cycle” 16 h of irradiation at intensity characterized by time-sinusoidal path and maximum of 1500 µE m^{-2} s^{-1} and 8 h of dark. The role of circadian clock and of the cell division of *Nannochoropsis sp.* has been highlighted during tests. The fraction of carbohydrate, protein and lipid of the biomass changes over the day: the lower value has been measured after the cell division, while the maximal values were obtained before cell division. The harvesting during the day of the biomass should be carried out when the concentration of the selected constituent is high.

✓ A model to describe the change of the specific growth rate of microalgae during the day was been proposed and validated.

The optimization on new photobioreactor systems needs to take into account the different time scale of the photochemical process and the instantaneous growth rate of microalgae. Analysis of the microalgal circadian clock is necessary to understand the right instant of the day at which to harvest the biomass with the set composition. It is also possible suggesting to develop systems to maximize the production of microalgal fractions (carbohydrates, lipids, proteins) according to the application of the process. However, the exploitation of only one microalgal fraction may not be in agreement with the maximum economic profit of the process.

ABSTRACT

La oroduzione di materie prime in grado di fornire beni di largo consumo e contemporaneamente ridurre le emissioni di anidride carbonica è considerata la sfida del 21° secolo per sopperire all'esaurimento dei combustibili fossili e all'aumento dell'effetto serra. I microrganismi fotosintetici, come ad esempio le microalghe, sono ottimi candidati in tal senso. Le microalghe, infatti, sono in grado di catturare la CO_2 e produrre, contemporaneamente, molecole ad elevato valore aggiunto sia nel campo della nutrizione umana e animale, che nel campo della cosmetica, farmaceutica e nella produzione di biocarburanti oltre che nella ficocoltura.

Tuttavia la produzione intensiva di microalghe non è ancora sostenibile per gli alti costi dei fotobioreattori. Se poi l'attenzione è rivolta alla produzione di vettori energetici, allora anche i costi dovuti alla disidratazione della biomassa e all'estrazione dei lipidi diventano rilevanti.

Durante questa tesi di dottorato l'attenzione è stata focalizzata sugli aspetti critici della produzione di vettori energetici dalle microalghe. Le attività hanno riguardato: la selezione dei ceppi microalgali rappresentativi dei vari phylum; l'ottimizzazione della crescita algale tramite l'implementazione della configurazione reattoristica e delle condizioni operative (sono stati studiati l'effetto sulla crescita dell'idrodinamica del fotobioreattore, del tipo di illumunazione e della sua intensità, la percentuale di CO_2 addizzionata all'aria, il pH e la composizione del terreno di coltura); la caratterizzazione, in condizioni controllate, della variazione della composizione delle microalghe durante le 24 ore come effetto del "circadian clock"; la caratterizzazione della variazione della velocità di crescita durante le 24 ore; la caratterizzazione del processo di fotosintesi e l'ottimizzazione della transesterificazione diretta sia sulla biomassa umida che quella secca.

I risultati hanno evidenziato:

- ✓ La produttività in biomassa e lipidi non è influenzata dalle concentrazioni di CO_2 tipiche dei gas di scarico, anche se è stato notato un effetto sulla sintesi dei pigmenti microalgali. Il pH ottimale di crescita è 7, ma buone produttività in biomassa e lipidi sono state ottenute anche a pH bassi, pertanto le contaminazioni possono essere tenute sotto controllo utilizzando temporaneamente condizioni acide di crescita. Un' irraggiamento continuo della biomassa non si traduce in un aumento della produttività in biomassa e lipidi.

- ✓ La caratterizzazione del processo fotosintetico è stata condotta attraverso analisi di fluorescenza. In particolare è stato evidenziato che: a intensità luminose inferiori a 1000 $\mu E\ m^{-2}\ s^{-1}$ il processo fotochimico è controllato dalla velocità di cattura dei fotoni, mentre a più alte intensità la

fotoinibizione entra in competizione con il quenching fotochimico. I tempi di riparo dei centri di reazione della fotosintesi sono decisamente più ampi a tutte le intensità luminose.

- ✓ L'ottimizzazione del processo di transesterificazione diretta alcalina è stata condotta su *Stichococcus bacillaris* e validata su altri ceppi algali caratterizzati da una diversa composizione della parete cellulare. I trigliceridi non vengono convertiti in assenza di catalizzatore, mentre la massima resa in esteri metilici si ottiene con una concentrazione di catalizzatore pari a 1.5% NaOH (w/w). La resa in esteri metiici non è influenzata dal tempo di pre-contatto, aumenta all'aumentare della temperatura raggiungendo un massimo a 65°C, non è infuenzata dal rapporto metanolo:biomassa secca quando il metanolo è in eccesso, aumenta nei primi minuti di reazione. L'essiccazione della biomassa gioca un ruolo fondamentale, infatti, la resa in esteri metilici si riduce drasticamente all'aumentare del contenuto di acqua nella biomassa. Il processo di transesterificazione alcalina è risultato essere più efficiente della transesterificazione diretta acida e del classico protocollo di estrazione e transesterificazione dei lipidi.

- ✓ Allo scopo di caratterizzare la velocità di crescita istantanea e la composizione della biomassa durante le 24 ore, sono stati effettuati test di crescita su *Nannochloropsis sp*. in fotobioreattori equipaggiati con un controllore di tipo turbidostato. Test con luce costante (16 ore di luce a 600 µE m^{-2} s^{-1} e 8 ore di buio) e con luce sinusoildale (16 ore di luce con un massimo di irradianza a 1500 µE m^{-2} s^{-1} e 8 ore di buio) hanno evidenziato la presenza di un "circadian clock" nel metabolismo di *Nannochoropsis sp.*. Il contenuto in carboidrati, lipidi e proteine cambia durante le 24 ore: si accumulano durante il giorno e si riducono durante la note in concomitanza con la divisione cellulare. La raccolta della biomassa dovrebbe essere condotta solo quando il costituente di interesse è alla massima concentrazione nella biomassa.

- ✓ È stato proposto e validato un modello che descrive la variazione della velocità istantanea di crescita durante le 24 ore.

L'ottimizzazione di nuovi fotobioreattori deve tener conto sia delle diverse scale temporali che caratterizzano il processo di fotosintesi, sia della variazione della velocità specifica di crescita durante le 24 ore. Analisi sul "circadian clock" permettono di conoscere l'esatto momento per raccogliere la biomassa con la composizione desiderata. Potrebbe essere interessante sviluppare sistemi che massimizzano la produttvità della frazione microalgale (carboidrati, lipidi, proteine) di interesse, ma non sempre lo sfruttamento di una sola frazione algale coincide con un ritorno economico del processo.

INDEX

LIST OF ABBREVIATIONS

λ	wavelength	[nm]
α	initial slope Photosynthesis (q^c_{CH2O})-light Intensity (I_{ph}) curve	[$(mol_{CH2O}\ mol_x^{-1})\ (E\ m^{-2})^{-1}$]
μ	specific growth rate (= specific biomass production rate)	[s^{-1}]
μ_{max}	maximal specific growth rate	[s^{-1}]
μ_{PI}	μ calculated from Photosynthesis light Intensity curve	[s^{-1}]
$\mu_{PI}(z)$	μ_{PI} at location z in photobioreactor	[s^{-1}]
$\bar{\mu}$	average specific growth rate microalgae in photobioreactor	[s^{-1}]
A_g	occupied ground area of photobioreactor	[m^2]
$A_{r,light}$	light-exposed surface area of photobioreactor	[m^2]
a_x	spectrally-averaged specific light absorption coefficient	[$m^2\ mol_x^{-1}$]
C_x	biomass concentration in photobioreactor system	[$mol_x\ m^{-3}$]
$C_{x,opt}$	optimal biomass concentration in photobioreactor (at max r_x)	[$mol_x\ m^{-3}$]
D	dilution rate of photobioreactor	[d^{-1}]
F	Liquid flow rate through photobioreactor	[$m^3\ s^{-1}$]
d	optical depth of photobioreactor	[m]
I_{ph}	PAR photon flux density (light intensity)	[$E\ m^{-2}\ s^{-1}$]
$I_{ph}(z)$	I_{ph} at location z in photobioreactor	[$E\ m^{-2}\ s^{-1}$]
$I_{ph}(0)$	I_{ph} at location z = 0 (light-exposed surface) in photobioreactor	[$E\ m^{-2}\ s^{-1}$]
$I_{ph,c}$	compensation light intensity for photoautotrophic growth	[$E\ m^{-2}\ s^{-1}$]
$I_{ph,s}$	saturation light intensity for photosynthesis (Blackman model)	[$E\ m^{-2}\ s^{-1}$]
m_{CH2O}	specific sugar consumption rate for maintenance	[$mol_{CH2O}\ mol_x^{-1}\ s^{-1}$]
PAR	Photosynthetic Active Radiation, 400 nm to 700 nm	
q_{ph}	specific photon (light) consumption rate	[$E\ mol_x^{-1}\ s^{-1}$]
q^c_{CH2O}	specific sugar (CH_2O) production rate in chloroplast	[$mol_{CH2O}\ mol_x^{-1}\ s^{-1}$]
$q^c_{CH2O,m}$	maximal specific rate of CH_2O consumption in the chloroplast	[$mol_{CH2O}\ mol_x^{-1}\ s^{-1}$]
$q^c_{CH2O}(z)$	q^c_{CH2O} at location z in microalgae culture	[$mol_{CH2O}\ mol_x^{-1}\ s^{-1}$]
q_{CH2O}	specific sugar (C_{H2O}) consumption rate in microalgae cell	[$mol_{CH2O}\ mol_x^{-1}\ s^{-1}$]
r_x	volumetric biomass production rate	[$mol_x\ m^{-3}\ s^{-1}$]
V_R	liquid volume of photobioreactor	[m^3]
$Y^c_{CH2O/ph}$	yield of sugar C_{H2O} produced in chloroplast on photons (light)	[$mol_{CH2O}\ E^{-1}$]
$Y^c_{CH2O/ph,m}$	maximal $Y^c_{CH2O/ph}$	[$mol_{CH2O}\ E^{-1}$]
$Y_{x/CH2O}$	yield of biomass on sugar	[$mol_x\ mol_{CH2O}^{-1}$]

$Y_{x/ph}$	yield of biomass on photons (light)	[$mol_x\ E^{-1}$]
$Y_{x/ph,m}$	maximal $Y_{x/ph}$	[$mol_x\ E^{-1}$]
z	shortest distance to light-exposed surface in photobioreactor	[m]
z_s	location z in photobioreactor where $I_{ph} = I_{ph,s}$	[m]
TFA	total fatty acid	
TAG	triacylglycerol	
FFA	free fatty acid	

STATE OF THE ART

1.1 Background

The 20th century has been characterized by the explosive growth of the energy consumption and rapid increase of greenhouse effects. The exploitation of renewable resources as alternative to fossil fuels is one of the most relevant priorities of industrialized Countries. The reasons are:

- the world's fossil fuel reserves are limited;
- the fossil fuel reserves are unevenly distributed in the world;
- the combustion of fossil fuel warms the earth's atmosphere as consequence of the "greenhouse effect".

Global warming has been mainly attributed to the increase of CO_2 concentration in the atmosphere (Etheridge et al., 1998). The critical threshold of 450 ppm CO_2 has been exceeded 10 years before the expectation, and the reduction of the emissions is the most appropriate strategy to face the problem (Schenk et al., 2008). Several strategies have been proposed to reduce the CO_2 concentration emissions. They include: post-combustion capture, pre-combustion capture, and *oxyfuel* capture (Russo et al., 2013). The post-combustion capture is particularly effective and requires to be associated storage processes (e.g. storage in oil/gas reservoirs). However, the captured CO_2 can be used as feedstock for photosynthetic organism cultures (Tang et al., 2011). Indeed the biofixation of CO_2 has been frequently proposed as a method to reduce the greenhouse effects through a sustainable way. The biofuel production coupled with the carbon dioxide sequestration by means of photosynthetic microorganisms has been considered as a promising process since the end of the last century (Benemann et al., 1977). Photosynthetic organisms, including plants, algae, microalgae and some photosynthetic bacteria, efficiently utilize the energy from the sunlight to convert water and carbon dioxide of the terrestrial atmosphere into biomass (Scragg et al., 2002).

$$6H_2O + 6CO_2 \rightarrow C_6H_{12}O_6 + 6O_2 \quad [1.1]$$

The crude microalgae are characterized by a biodiesel energy content ranging between 20 and 38 MJ kg_{DW}^{-1}: only 0.37 MJ $MJ^{-1}_{biodiesel}$ of energy are required in microalgal oil extraction for wet extraction and cultivation under low-nutrient conditions, while the energy required for transesterification is 0.0024 MJ $MJ^{-1}_{biodiesel}$ (Zhu, 2015). Moreover microalgae are of interest for several industries involved in human nutrition, animal nutrition, cosmetics, high-added value molecules (omega 3, pigments, vitamins, phycobilins), pharmaceuticals, biofuels (bio-oil, biodiesel, bio-hydrogen, bioethanol) and wastewater treatments (Wijffels and Barbosa 2010; Olivieri et al., 2014). As a matter of fact, it is

possible to couple CO_2 sequestration and/or biomolecules production and biofuels production. It should also be added that microalgae require less soil and water than crop cultures (Chisti, 2007; Schenk et al., 2008).

The table 1 reports a comparison of superficial productivity of some photosynthetic sources of biodiesel (Chisti, 2007).

Crop	Oil yield (L/ha)	Land area needed (M ha) [a]	Percent of existing US cropping area [a]
Corn	172	1540	846
Soybean	446	594	326
Canola	1190	223	122
Jatropha	1892	140	77
Coconut	2689	99	54
Oil palm	5950	45	24
Microalgae [b]	136900	2	1.1
Microalgae [c]	58700	4.5	2.5

[a] For meeting 50% of all transport fuel needs of the United States.

[b] 70% oil (by wt) in biomass.

[c] 30% oil (by wt) in biomass.

Table 1.1: Comparison of some sources of biodiesel (Chisti, 2007).

Chisti (2007) reported that biodiesel production rate from microalgal cultures may be 1–3 orders of magnitude larger than that from oil crops. In fact, the microalgae grow is extremely rapid and many strains are exceedingly rich in oil (50–80%wt) (Liang et al., 2010; Spolaore et al., 2006; Eichenberg et al., 1997). Moreover, the microalgal biomass fixes a large amount of carbon dioxide – 1.83 kg of CO_2 per kilogram of dry microalgae – and strongly contributes to the reduction of greenhouse gas emissions (Chisti, 2007).

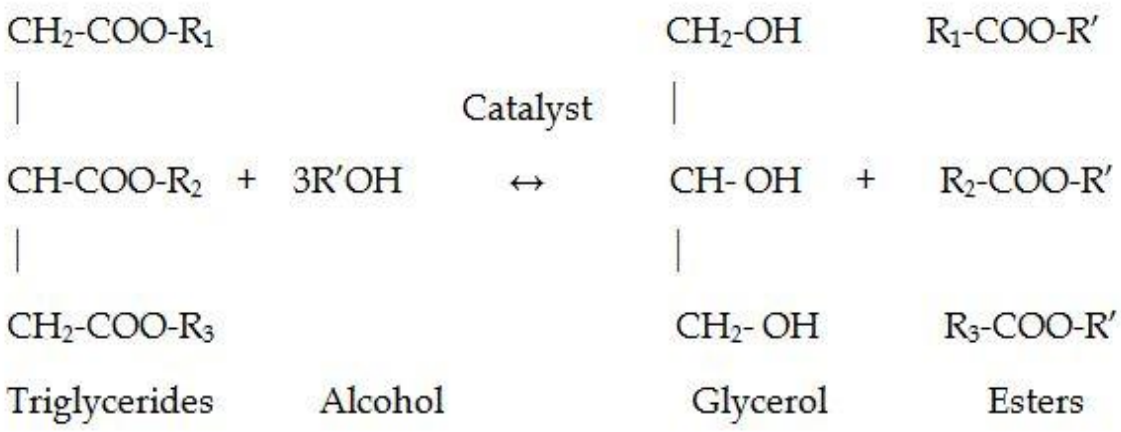

Figure 1.1: Sketch of the transesterification reaction.

Microalgae, like higher plants, produce lipids in the form of triacyglycerols (TAGs). Although TAGs can be used to produce a wide variety of chemicals, the majority of them can be employed to produce esters, which can be used as a substitute for fossil-derived diesel (Christi, 2007, Posten et al., 2009, Francisco et al., 2010). This fuel, known as biodiesel, can be synthesized from TAGs through a transesterification process in presence of alcohol under acidic or basic conditions (Sheehan et al., 1998) (figure 1.1).

1.2 Microalgae as an energy vector feedstock

The concept of using algae to make fuel was already being discussed 50 years ago (Oswald et al., 1960), but a concerted effort began with oil crisis and fuel cost increase in the 1970s (Hu et al., 2008). The US Department of Energy (DOE) from 1978 to 1996 devoted $25 million to algal fuels research at National Renewable Energy Lab (NREL).The first genetic transformation of microalgae came in 1994, and few years later scientists isolated and characterized the algal genes that express enzymes thought to enhance oil production (U.S. Department of Energy 2010 - National Algal Biofuels Technology Roadmap). From 1990 to 2000, the Japanese government funded algae research at technology for the Earth (Kyoto) (Waltz, 2009), but the real interest for this topic increased in the recent years as reported in figure 1.2.

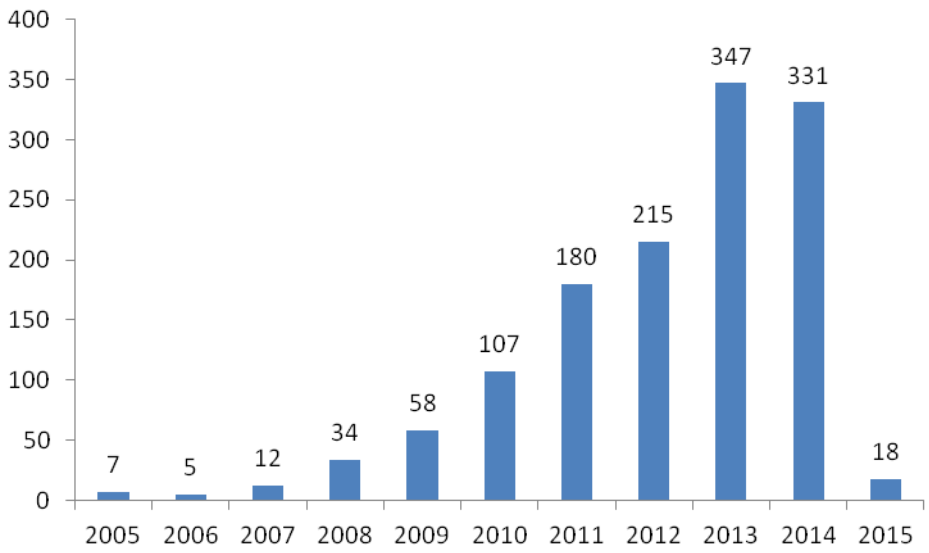

Figure 1.2: Number of paper that demonstrate the scientific interest for biodiesel production from microalgae (SCOPUS).

The advantages of microalgae as feedstock for biodiesel production, over terrestrial plant, are:

- the algal biomass growth is driven by photosynthesis;
- the algal biomass needs CO_2 to grow;

- microalgae can accumulate high lipid content;
- microalgae can grow on waste or desert land;
- microalgae don't require freshwater;
- microalgae have a high sensitivity to growth conditions and the different types of stress changes the lipid composition.

1.3 Properties and composition of biodiesel

The success of biodiesel production from microalgae depends on the content of TAG (triglyceride) which composed more than 70% of the lipid content (Spolaore et al., 2006; Eichenberger et al., 1997). In general, a TAG is a glycerol esterified with three fatty acids and it may reacts with alcohol produce FAMEs (fatty acid methyl esters) and glycerol. The FAMEs composition of algal lipids is well documented, with a high occurrence of unsaturated (and polyunsaturated) fatty acids, with half of the fatty acids having a carbon number less than C_{18}. The high concentration of unsaturated fatty acids in the extracted lipids is determinant for the fuel quality. Unsaturated FAMEs comprised over 82% of the total biodiesel content (Xu et al., 2006; Cheng et al., 2009). The FAMEs content is mainly composed of palmitic (C16:0), stearic (C18:0), oleic (C18:1), linoleic (C18:2) and linolenic (C18:3) methlyl esters (Pratoomyot et al., 2005; Riuz et al., 2009; Gao et al., 2010). The level of unsaturation affects biodiesel features (Ryan et al., 1984). Two major data characterize the quality requirements for alkyl ester-based biodiesel fuels: the ASTM D6751 in the USA and the EN 14214 in Europe. Table 1.2 compares the ASTM specifications with the features of fossil and microalgal diesel (Williams et al., 2010).

Properties	Microalgal fuel	Diesel fuel	ASTM biodiesel standard
Density [kg dm^{-3}]	0.864	0.838	0.86-0.90
Viscosity [mm^2 s^{-1}@40°C]	5.2	1.9-4.1	3.5-5.0
Flash point [°C]	115	75	Min. 100
Solidifying point [°C]	-12	-50-10	-
Filter plugging point [°C]	-11	-3.0 (max. -6-7)	Summer max. 0 Winter max. <-15
Acid value [mg_{KOH} g^{-1}]	0.374	Max. 0.5	Max. 0.5
Heating value [kJ g^{-1}]	41 [43]	40-45	-
H/C ratio	1.8 [1.9]	1.8	-

Table 1.2: Comparison of proprieties of biodiesel from microalgae, fossil diesel and ASTM standard (Williams et al., 2010).

1.4 From microalgae to biodiesel

The process from microalgae to biofuel is summarized in figure 1.3 (U.S. Department of Energy 2010 - National Algal Biofuels Technology Roadmap).

The biodiesel production process consists of two parts: the first part of the process includes the selection, growth and harvesting of biomass; the second part of the process includes the extraction and processing of microalgal lipids to produce biodiesel.

Algal biology	• Sample strains from a wide variety of environments for maximum diversity • Develop small-scale, high-throughput screening technologies • Develop open-access database and collections of existing strains with detailed characterization • Investigate genetics and biochemical pathways for production of fuel precursors • Improve on strains for desired criteria by gene manipulation technique or breeding
Algal cultivation	• Investigate multiple approaches (i.e., open, closed, hybrid, and coastal/off-shore systems; phototrophic, heterotrophic and mixotrophic growth) • Achieve robust and stable cultures at a commercial scale • Optimize system for algal productivity of fuel precursor (e.g., lipids) • Sustainably and cost-effectively manage the use of land, water, and nutrients • Identify and address environmental risks and impacts
Harvesting and Dewatering	• Investigate multiple harvesting approaches (e.g., sedimentation, flocculation, dissolved air floatation, filtration, centrifugation) • Minimize process energy intensity • Lower capital and operating costs • Assess each technology option in terms of overall system compatibility and sustainability
Extraction and Fractionation	• Investigate multiple approaches (e.g., sonication, microwave, solvent systems, supercritical fluid, subcritical water, selective extraction and secretion) • Achieve high yield of desired intermediates; preserve co-products • Minimize process energy intensity • Investigate recycling mechanisms to minimize waste • Address scaling challenges, such as operational temperature, pressure, carrying capacity, side reactions and separations
Fuel conversion	• Investigate multiple approaches to liquid transportation fuels (e.g., direct fuel production, thermochemical/catalytic conversion, biochemical conversion, and anaerobic digestion) • Improve catalyst specificity, activity, and durability • Reduce contaminants and reaction inhibitors • Minimize process energy intensity and emission over the life cycle • Achieve high conversion rates under scale-up conditions

Figure 1.3: A summary of microalgal transformation into biodiesel (U.S. Department of Energy 2010 - National Algal Biofuels Technology Roadmap).

1.5 Economics of the biodiesel production

The energy balance of the biofuel production from microalgae points out that at least 25% of the recoverable energy yield depends on the cultivation approach (Lardon et al., 2009). The cost of the conversion process can be further reduced coupling the biodiesel production with fine chemical production or applying more suitable technologies. Compared to the other biodiesel crops – e.g. palm oil and jatropha - microalgae require specific techniques for cultivation, extraction and conversion for the process to be economically feasible. Although the lipid production rate by microalgae is higher than that from other crops, the production of diesel from microalgae is still not economically sustainable and algae production on large scale is still not profitable (Bernardi et al., 2014; Sheehan et al., 1998; Alabi et al., 2009).

Table 1.3 reports biodiesel cost estimation from microalgae as recently published (Williams and Laurens, 2010). The cost details for microalgal production in photobioreactor (PBR) and raceway pond (RW) type system are reported in table 1.3.

Source	Assumed productivity g_{dw} m^{-2} d^{-1}	Assumed lipid content %dw	Biomass cost $ tonne^{-1}	
			PBR	RW
Benemann (1996)	30	50	-	241
	60	50	-	148
Molina Grima (2004)	Not given	Not given	30400	-
Chisti (2007)	72	30	470	-
	35	30	-	600
Carlsson (2007)	2.7 – 14	Not given	-	2000 – 15000
Alibi (2009)	15.3	25	5900	-
	9.4	15	-	2140
Pienkos (2009)	10	15	-	-
	25	25	-	-
	50	50	-	-
Williams (2010)	18 - 37	15-50	-	-

Table 1.3: Comparison of published data of costs for algal biomass and biodiesel production. Conversion factors: specific gravity assumed 0.88; one barrel as 159 litre; 1.28 €/$ US (Williams and Laurens, 2010).

Table 1.4 reports the major equipment costs and direct costs for microalgal biomass production and for production of crude esterified microalgal oil, assuming a continuous average biomass productivity of 1.25 kg m^{-3} d^{-1} (Molina Grima et al., 2003). According to reported analysis and successive analysis (Acien et al., 2012), the most expensive equipments are photobioreactors, the harvesting system, the freeze-dryer and the lipid extractor. Although the algae market demand is increasing, the worldwide production of microalgal biomass is about 9000 ton $year^{-1}$ and the production cost is still too high - 20

to 200 \$ kg^{-1} (Olivieri et al., 2014) – to include the microalgae among feedstock for the production of convenience goods.

Major equipment list for microalgal biomass production			
Item	Delivered cost (\$)	No. of units	Total cost
Photobioreactors (0.8 m^3)	3524	75	264300
Medium filter unit (5.99 m^3 h^{-1})	18014	1	18014
Centrifuge	123949	2	247898
Medium feed pump (0.04 m^3 h^{-1})	349	75	26175
Medium preparation tank (19.96 m^3)	34814	3	104442
Harvested broth storage tank (19.96 m^3)	34814	3	104442
Centrifuge feed pumps (2.99 m^3 h^{-1})	841	2	1682
Air compressor (240 m^3 h^{-1})	26103	3	78309
Harvest biomass conveyer belts	7100	2	14200
Seawater pump station (5.99 m^3 h^{-1})	13661	1	13661
CO_2 supply station (27.4 kg h^{-1})	3006	1	3006
Weighing station	2366	1	2366
Biomass silos (0.07 m^3)	1370	3	2740
Direct costs of biomass production			
Raw materials	Total quantity (kg)		Cost (\$)
Culture medium (at \$0.5883/kg)	65500		38534
Carbon dioxide (at \$0.4706/kg)	96940		45620
Media filters (at \$70.59/unit)	210 units		14824
Air filters (at \$94.12/unit)	105 units		9883
Other consumables (at \$117.65/kg)	13		1529
Major equipment list for production of crude esterified microalgal oil			
Item	Delivered cost (\$)	No. of units	Total cost
Ethanol tank (1.5 m^3)	2404	1	2404
Acetyl chloride tank (1 m^3)	1881	1	1881
Reactor (2 m^3)	5242	1	5242
Hexane storage tanks (60 m^3)	11613	2	23226
Holding tank (2.5 m^3)	3434	1	3434
Evaporator (50 ft^2)	14622	1	14622
Condenser (shell and tube, 5 m^2)	1678	1	1678
Direct production costs of crude esterified microalgal oil			
Raw materials	Total quantity (kg)		Cost (\$)
Ethanol, m^3 (at \$784.70 m^{-3})	33		25895
Acetyl chloride, m^3 (at \$1533 m^{-3})	7		10731
Hexane, m^3 (at \$364.7 m^{-3})	20		7294

Table 1.4: Major equipment list and costs for algal biomass production (Molina Grima et al., 2003)**.**

THE MICROALGAE AND THE EXPLOITATION PROCESS

2.1 Microalgal biology

2.1.1 Strain screening and selection

Genetics is one of the factors that affects the microalgal lipid and biomass productivity. According to this basic concept, the right selection of the species characterized by competitive potentiality in lipid production is a key issue for the success of a microalgal exploitation process. Table 2.1 reports the production rate of microalgae and of their lipid fraction.

Microalgae species	production rate (g L^{-1} d^{-1})	
	Biomass [a]	Lipid [b]
Chlorella vulgaris	0.37	0.48
Chlorella protothecoides	3.6-4.1	1.6-1.7
Botryococcus braunii	0.16	0.029-0.064
Chlorella emersonii	0.36	0.122
Nannochloropsis sp.	0.48	0.142
Schizochytrium limacinum	1.88	1.38
Scenedesmus obliquus	0.15	0.27

[a] Biomass yield based on dry weight in gram per litre per day

[b] Lipid yield based on dry weight in gram per litre per day

Table 2.1: Microalgae and lipid productivity (Suali et al., 2012).

A wide spectrum of species belonging to *Cyanophyta*, *Rhodophyta*, *Heterokontophyta*, *Dinophyta* and *Chlorophyta* has been used for intensive cultures in closed systems and open ponds (Chisti et al., 2007). *Heterokontophyta* and *Chlorophyta* are the most commercial phylum. They are characterized by high lipid productivity and CO_2 fixation rates. Therefore, these phylum could be efficiently employed for carbon dioxide capture and sequestration.

The *Nannochloropsis* – belonging to the *Heterokontophyta* phylum – is the a promising microalgal for bio-oil production. This species has been investigated with reference to the marine environment (Fawley and Fawley 2007). All *Nannochloropsis* species are small and non-motile. They are rich in chlorophyll “a” and are characterized by high concentrations of pigments like astaxanthin, but they are deficient in chlorophyll ”b” and ”c” (Lubiàn et al., 2000). *Nannochloropsis* is considered a promising alga for bio-oil production because it accumulates high levels of fatty acids (Krienitza and Wirth, 2006; Shenbaga Devi et al., 2012; Rodolfi et al., 2009) and promising features are expected because genetic manipulation is possible (Zheng et al., 2014; Zheng et al., 2013).

Two genus belonging to the *Chlorophyta* phylum are particularly interesting: *Stichococcus* and *Scenedesmus* genus. The green alga *Stichococcus* is characterized by promising performance in terms of growth rate, resistance to stress, and lipid production (Olivieri et al., 2011). *Stichococcus* is a genus of green algae (*Chlorophyta*) characterized by a simple morphology, ranging from single non-motile cells to uniseriated or unbranched filaments (Boyle et al., 2009). The species belonging to this genus are spread over continents, at latitudes extending from polar and subpolar regions to the Equatorial belt (Randawa et al., 1959, Broady et al., 1989). Some species – e.g., *S. bacillaris* - are tolerant to wide excursion of temperature, salinity and pH, and are characterized by short life cycles (Pollio et al., 1997). The lipid content (about 33%) and fatty acid distribution make *S. bacillaris* a potential candidate for commercial-scale cultivations devoted to fuel production. Indeed, recent results pointed out that the strain 158/11 of the ACUF collection (Algal Collection at University "Federico II", Naples) is characterized by high specific biomass production (about 256 mg L^{-1} d^{-1}) and high lipid productivity (about 80 mg L^{-1} d^{-1}) (Olivieri et al., 2012, 2013). *Scenedesmus* genus - one of the most common freshwater algae - are colonial and non-motile microalgae. The formation of colonies depends on a series of factors such light intensity and temperature (Lürling and Van Donk, 1999). *Scenedesmus* genus has been frequently proposed as possible candidate for phycoremediation because it has great ability to degrade phenols and their derivatives (Pollio et., 1993). Moreover *Scenedesmus* has been frequently proposed as possible candidate to produce biodiesel from microalgae (Mata et al., 2010; Rodolfi et al., 2009; Griffiths et al., 2010).

2.1.2 Microalgal physiology: photosynthesis and light utilization

Photosynthesis represents a unique process of sunlight energy conversion. The basis of algal biomass production is directly proportional to the efficiency with which the algal cells assimilate carbon dioxide from the atmosphere through photosynthesis. The simple stoichiometry of photosynthesis may be written as:

$$2H_2O + CO_2 \rightarrow [CH_2O] + O_2 + H_2 \qquad [2.1]$$

The overall reaction [2.1] may be conceptually splitted into two steps (Crill, 1977) (figure 2.1):

- ✓ a set of photochemical and redox reactions (conventionally called the "light reactions"). It is represented by the so-called photosynthetic factories (PFS), a combination of Photosystems I and II (PSI and PSII). The first step reaction is:

$$2H_2O \rightarrow 4[H] + O_2 + energy \qquad [2.2]$$

✓ a sequence of enzymatic reactions (conventionally called “dark reactions” or “light independent reactions”). The second step reaction includes enzymatic reactions:

$$4[\mathrm{H}] + \mathrm{CO_2} \rightarrow [\mathrm{CH_2O}] + \mathrm{H_2O} \qquad [2.3]$$

The light reactions operate on very short time scales (from femtosecond to millisecond), the light-independent reactions operate over timespan of seconds to hours. This profound timescale mismatch gives rise to photosynthetic inefficiencies in particular when environmental/operating conditions fluctuate, e.g. variation of irradiance and temperature over the day/year. The sensitivity of the conversion steps to the environmental/operating conditions is one of the main problem in maximizing yields of mass microalgal cultures.

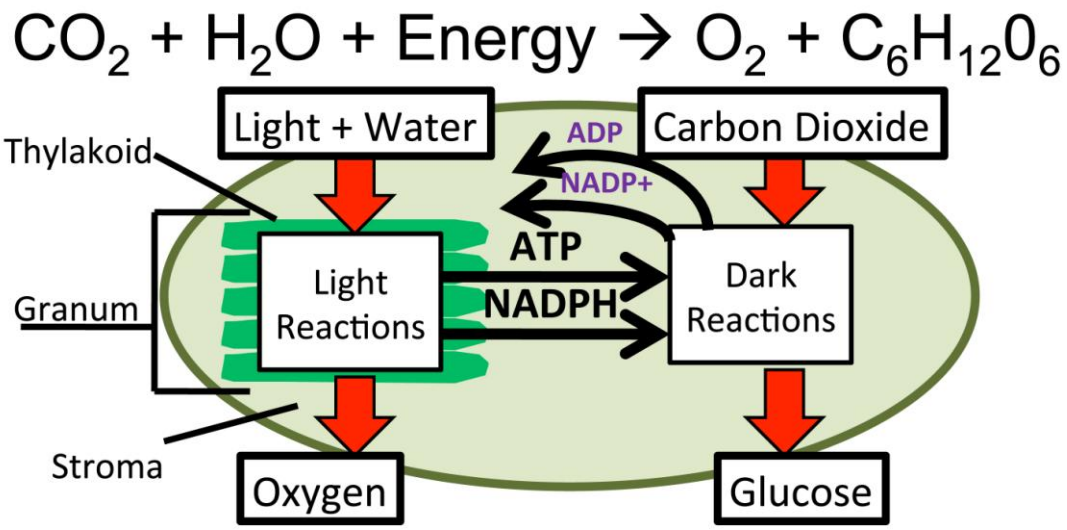

Figure 2.1: Major products of the light and dark reactions of photosynthesis: light reactions and dark reactions.

The primary pigment involved in photosynthesis is chlorophyll a that it is characterized by strong absorption bands in the regions 400-450 and 650-700 nm (figure 2.2).

These bands confine the useful range of incoming radiation to 400-700 nm: the so called photosynthetically active radiation (PAR). The sunlight energy belonging to the PAR is about 45-50% of the total incoming radiation (Mathews et al., 1990; Kirk, 1994). The low absorption of the chlorophyll in the range 450-650 nm limit the capture efficiency at the 30-40% of the photosynthetically active radiation. The microalgae may modify the accessory pigments to optimize light capture, but the adaptation process is slow compared with the time scales of the photochemical reactions.

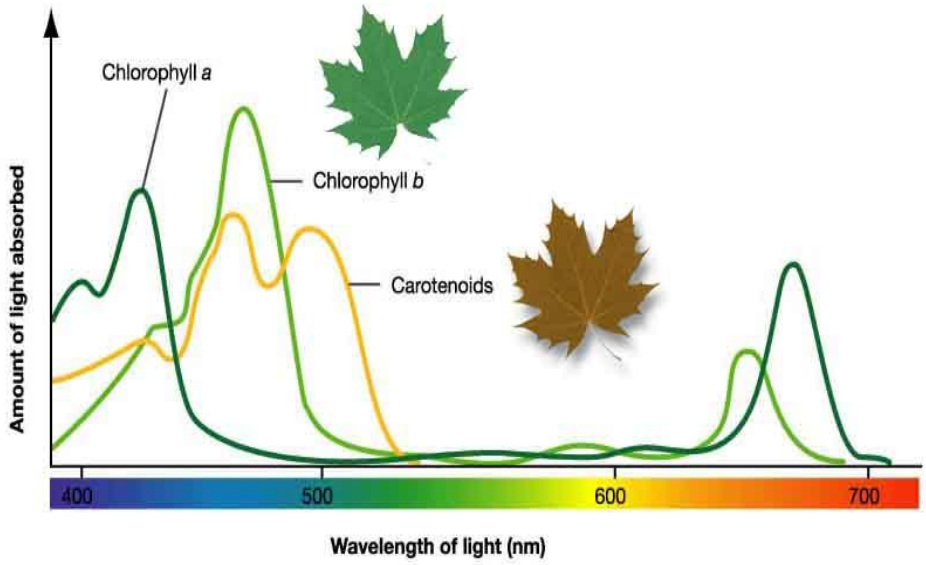

Figure 2.2: The absorption spectrum of chlorophyll a.

Figure 2.3 shows a plot of the photosynthetic activity as a function of the light intensity: the light-response (P/I) curve. It may be obtained by processing the measurements of oxygen production from microalgae exposed at irradiation.

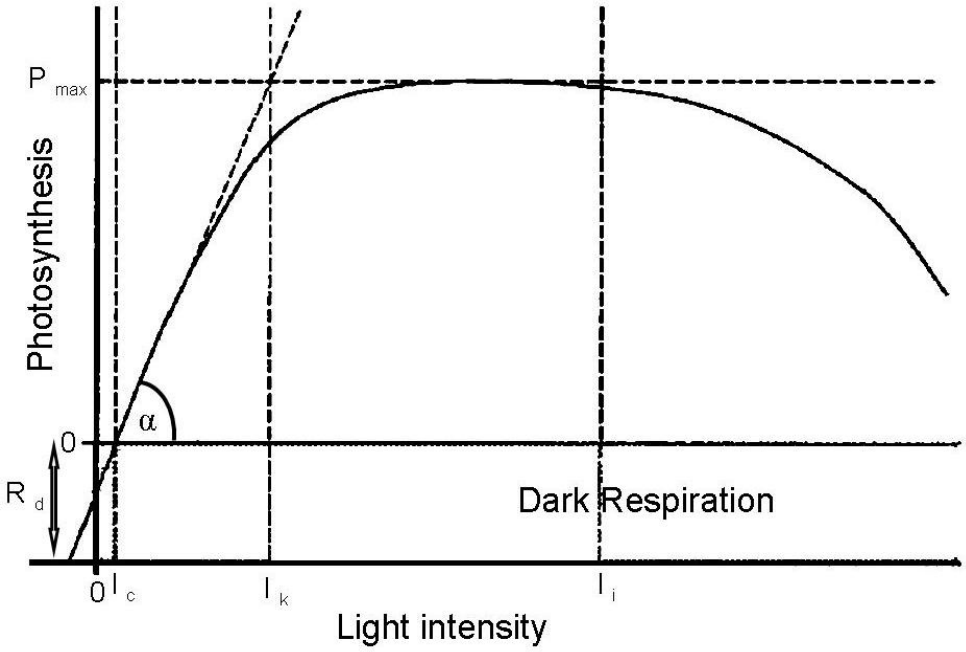

Figure 2.3: A schematic representation of photosynthetic light-response curve, i.e. the dependency of photosynthesis vs. irradiance.

The initial slope α is the P_{max}/I_k ratio, where I_k is the saturation irradiance and P_{max} the maximum rate of photosynthesis. Under dark conditions, there is a net consumption of oxygen as a consequence of

respiration (the negative part of the curve in figure 2.3). Therefore, gross photosynthesis is considered as the sum of net photosynthesis (O_2 evolution) and respiration (O_2 uptake). At low irradiance, the rate depends linearly on light intensity. Increasing the light intensity, photosynthesis becomes less and less efficient. Photosynthesis reaches a plateau at high irradiance when enzymatic reactions utilizing fixed energy become rate limiting. Under prolonged supra-optimal irradiance, photosynthetic rate usually declines from the light-saturated value. This phenomenon is commonly referred to as photoinhibition of photosynthesis.

Routine measurements of photosynthetic oxygen production in algal cultures are usually carried out with an oxygen electrode. Optical oxygen sensors have recently been developed. They are based on the fluorescence and phosphorescence quenching of some luminosphere in the presence of oxygen. Chlorophyll fluorescence characterization has become one of the most common and useful technique in photosynthesis research. It is non invasiveness and very sensitive to photosynthesis efficiency.

Chlorophyll fluorescence directly reflects the performance of photochemical process in PSII; the contribution of PS I emission in the total signal at ambient temperature is rather small and for practical purposes it is often neglected. Under light conditions, photosynthetic reaction centres are excited to a excited state. The energy of excited state is transferred to the reaction centres to be used for photochemical charge separation. Alternatively, the excitation energy can be dissipated as heat, or re-emitted as fluorescence (figure 2.4). The sum of energy of these three competing process is equal to the absorbed light energy.

Figure 2.4 shows the three-states model proposed by Eilers and Peeters (1988), the transition through the states and the kinetics proposed for the transition among the states. The three states of the reactor centres proposed by Eilers and Peeters (1988) are: 1 – *open-state*, 2 – *closed-state*, 3 – *inhibited-state*. x_1, x_2 and x_3 reported in figure 2.4 are the fraction of the reaction centres under state 1, 2 and 3 states, respectively. Four routes are identified for the reaction centres:

i) the *open-state* jumps to the *closed-state* conditions when hit by photons. The rate of the photon capture is:

$$r_{PC} = \alpha I x_1 \qquad [2.4]$$

Where I is the light intensity.

ii) the *closed-state* typically restores the *open-state* with photochemical quenching and fluorescence. The rate of the photochemical quenching - and of the associated fluorescence - is:

$$r_{PQ} = \gamma x_2 \quad [2.5]$$

iii) the *closed-state*, if hits by further photons, jumps to *inhibited-state* and releases heat. The rate of the photoinhibition is:

$$r_{PI} = \beta I x_2 \quad [2.6]$$

Where I is the light intensity.

iv) the *inhibited-state* restores the *open-state* by repairing processes. The rate of the repair process is:

$$r_{REP} = \delta x_3 \quad [2.7]$$

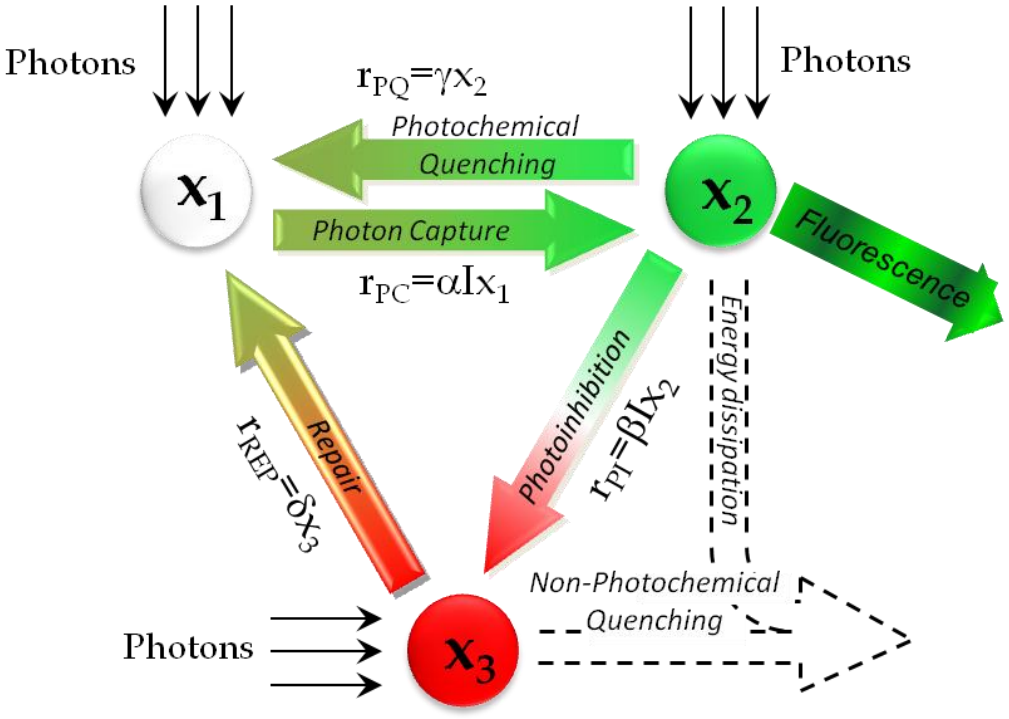

Figure 2.4: Schematic representation of the kinetic model proposed (after Eilers and Peters, 1988).

Figure 2.5 shows a sketch of the time resolution measurement of microalgal fluorescence under a wide set of operating conditions. ML marks the beginning of the modulated measuring light after the microalgae have been kept under prolonged dark adaptation. LP marks a light pulse under ML conditions. AL marks the beginning of microalgal illumination with actinic light. SP marks a saturated light pulse under AL conditions. The pulse is characterized (inset of figure 2.5) by: pulse light intensity (I_P) and pulse width (W_P).

The microalgal fluorescence behavior depends on the irradiance strategy: combination of intensity of basal irradiance (ML vs. AL) and intensity of the light pulse (LP vs. SP). In particular, the irradiance conditions reported hereinafter are used.

- Modulated measuring light (ML). The basal value (F_0) of fluorescence is recorded. Under this condition, all reaction centres of microalgae are at the *open-state* and the fluorescence is at the minimum value (Masojidek et al., 2004).

- Irradiation by a light pulse (LP) under ML conditions. A maximum of the fluorescence (F_M) is recorded. The reaction centres are progressively *closed* (x_2 increases) during the pulse action. The presence of a fraction of closed reaction centres leads to an overall reduction in the efficiency of photochemical process and to an increase in the fluorescence. In particular, the fluorescence increases proportionally to the closure of the reaction centres because the *open-state* acts as a fluorescence quencher. The F_M increases with the energy (intensity and/or period) of the LP until saturation conditions are reached. Under saturation conditions the LP is called saturation pulse (SP) and the maximum F_M is known as $F_{M,max}$.

- Irradiation by actinic light (AL). The fluorescence increases at the constant value F'. The fluorescence increases because the activation of photochemical processes.

- Irradiation by a saturating pulse (SP) under AL conditions. The fluorescence increases from F' to F'_M. The photochemical processes are suppressed.

- No irradiation after AL period. The fluorescence decreases at F'_0 lower than F_0 as soon as the AL is switched off and increases gradually to F_0.

Fluorescence data are processed to assess the following parameters:

F_V - the difference between the maximum fluorescence value achieved during the LP (F_M) and minimum fluorescence (F_0).

F_V/F_M - assessed as $(F_M-F_0)/F_M$ - is the photochemical efficiency of PSII for the AL used under ML condition. This efficiency is maximum when a SP is used. The maximum value of F_V/F_M measured in several healthy microalgae is around 0.650 (Kolber and Falkowskj, 1993).

NPQ - assessed as $(F_M-F'_M)/F'_M$ - is the "non-photochemical quenching". NPQ is proportional to the fraction of reactor centres that do not produce fluorescence and dissipate the excitation energy as heat. The NPQ is inversely proportional to photochemistry and it is a "safety valve" of the cells to protect reaction centres from photoinhibition at high irradiance level (Masojidek et al., 2004).

Φ_{PSII} - assessed as $(F'_M-F')/F'_M$ - is the effective PSII photochemical efficiency (quantum yield of PSII linear electron transport). The ϕ_{PSII} is a feature of the beginning of photosynthesis and it is a measure of the reaction center fraction under *open* and *closed-states*. This parameter can be assigned as $\Phi_{PSII} = x_1 + x_2$.

The kinetic model and the assessment procedure of the photochemical process are reported hereinafter. The equation set [2.85] through [2.11] derives from the model proposed by Eilers and Peeters (1988). It describes the behavior of reaction centres involved in the photochemical processes (figure 2.4):

$$\frac{dx_1}{dt} = -\alpha I x_1 + \gamma x_2 + \delta x_3 \qquad [2.8]$$

$$\frac{dx_2}{dt} = \alpha I x_1 - \gamma x_2 - \beta I x_2 \qquad [2.9]$$

$$\frac{dx_3}{dt} = \beta I x_2 - \delta x_3 \qquad [2.10]$$

$$x_1 + x_2 + x_3 = 1 \qquad [2.11]$$

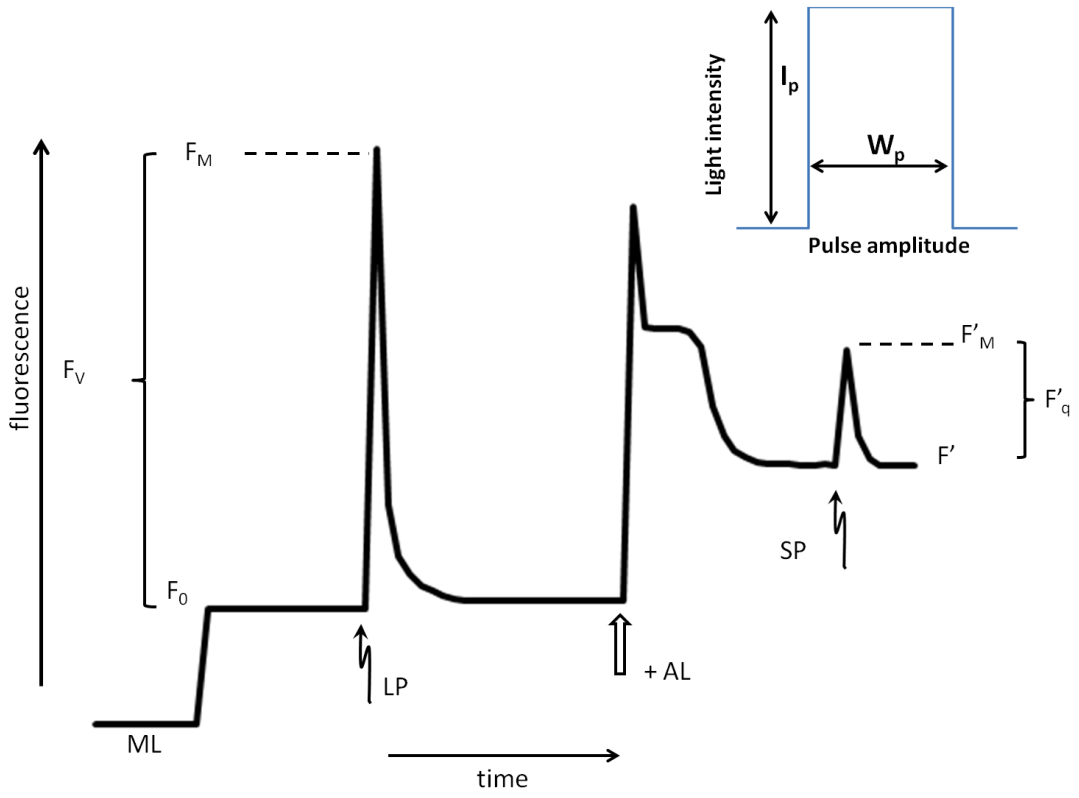

Figure 2.5: Typical signal of chlorophyll fluorescence emission. The inset represents the pulse characteristics: pulse light intensity (I_P) and pulse width (W_P).

2.1.3 The parameters affecting the microalgal growth

✓ **Dissolved oxygen**

High level of dissolved oxygen (DO) inhibits photosynthesis. The inhibition concentration depends on the microalgal species.

✓ **Carbon dioxide**

The low CO_2 concentration of atmospheric air is sufficient for cell growth. The response to the CO_2 concentration depends on the microalgal strain: additional CO_2 may enhance biomass growth and/or lipid content. Widjaja et al. (2009) showed that the CO_2 concentration plays an important role in increasing the lipid content, lipid composition and biomass yield. Indeed, Chiu et al. (2009) showed that microalgal culture aerated with 2-15% CO_2 was characterized by the increase of the microalgal specific growth rate up to 0.66 g day^{-1}. Olivieri et al. (2012, 2013) showed that CO_2 concentration higher than the air level (0.035%) improved the process performances in terms of productivity and concentration of lipids in *Stichococcus bacillaris* strain. No strong differences were observed for the selected CO_2 concentrations (5 and 15%) under the operating conditions investigated. Pegallapati et al. (2012) reported that the expression of specific growth rate includes the carbon dioxide substrate and light as growth limiting factors along with temperature effects. They interpreted the substrate effects according to Haldane type kinetic expression. The growth rate as a function of the carbon dioxide concentration (C_{CO_2}) is:

$$\mu = \mu_{max} \frac{C_{CO_2}}{k_n + C_{CO_2} + \frac{(C_{CO_2})^2}{k_i}} \qquad [2.12]$$

where K_n is half saturation constant of carbon dioxide, and k_i the inhibition constant of carbon dioxide.

✓ **Nitrogen source**

After carbon, the nitrogen is most important element of an algal culture medium. Indeed, the nitrogen content in the biomass ranges from 1 to 10 % of the total dry weight. The supply of nitrogen may be reduced to fulfil specific request: e.g. the production of lipids. Additionally, numerous studies pointed out that under nitrogen starvation the lipids biosynthesis and accumulation is favoured (Solovchenko, 2008). The effects of nitrogen source/supply may be furtherly tuned by the culture methods (batch, fed-batch, semi-continuous). Recently, Pignatelli et al. (2013) studied the interaction between glucose and nitrate in mixotrophic growth of *Chlorella vulgaris* and *Nannochloropsis*

oculata. They proposed a Monod-like model to describe the dependence of the growth rate on the nitrate concentration (C_N).

$$\mu = \mu_{max} \frac{C_N}{k_n + C_N} \quad [2.13]$$

The values for the maximum specific growth rate μ_{max}, the half saturation constant k_N and the yield factor $Y_{X/N}$ were computed by processing the data measured during microalgal growth in flasks. The assessment was based on the mass balance equations referred to the nitrogen, the carbon and the glucose. Table 2.5 reports the parameters assessed by Pignatelli et al. (2013) for autotrophic growth of *Chlorella* and *Nannochloropsis*.

Chlorella			**Nannochloropsis**		
μ_{max} (day^{-1})	k_N ($g\ L^{-1}$)	$Y_{X/N}$ (10^9 cell g^{-1})	μ_{max} (day^{-1})	k_N ($g\ L^{-1}$)	$Y_{X/N}$ (10^9 cell g^{-1})
0.39 ± 0.01	0.03 ± 0.02	12 ± 1	0.36 ± 0.01	0.02 ± 0.01	5.4 ±0.33

Table 2.5: Kinetics parameters assessed by Pignatelli et al. (2013).

✓ **Temperature**

The optimal growth temperature of microalgae strongly depends on the species. It depends on the environment where the species has been isolated: see, rivers, tropical rainforest, dry, wet, snow or highland climate. The cultivation temperature of microalgae characterized by good potential as biofuel feedstock has been discussed by Suali et al. (2012). Pegallapati et al. (2012) proposed equation [2.14] to describe the temperature effects on *Chlorella*, *Scenedesmus* and *Nannochloropsis*:

$$I_{(T)} = 1.066^{(T-20)} \quad [2.14]$$

where $I_{(T)}$ is the enhancement factor that depends on the deviation of the temperature (expressed in Celsius degree) from the optimal growth temperature (20°C).

✓ **pH**

Olivieri et al. (2011) investigated the pH effects on *Stichococcus* strains cultures. They pointed out that the specific growth rate depends on the pH and that the optimal pH was about 7 for all investigated strains.

2.1.4 Circadian cycle

The biochemical composition of the algal biomass is a key issue to address their exploitation as feedstock for the production of biofuels, chemicals, materials, foods, feeds and high-value bioactives.

Indeed, high lipid concentration is the requisite for the microalgal exploitation as feedstock for biofuel production. Moreover, it has been pointed out that biomass composition changes over the day whatever the irradiation scenario (e.g. day/night cycle, constant irradiation): carbon storage reserves - like carbohydrates and lipids – are accumulated during the day-time and are consumed during the night-time (Post et al., 1985; Sukenik and Carmeli, 1990; Fàbregas et al., 2002; de Winter et al., 2014). The chlorophyll concentration of microalgae reaches the maximum value during the day-time and decreases before the night-time (Falkowski and Raven, 2007). The observed fluctuation of the microalgal composition is due to the day-periodic modulation of the metabolism: carbon reserves and energy accumulated during the day-time are used for the synthesis of proteins during the night-time (Cuhel et al., 1984). For example, microalgal starch fraction fluctuates between 45% of biomass dry weight (DW) before cell division to 4–13% of DW after cell division (Brànyikovà et al., 2011). This cyclic behaviour is known as circadian clock of the microorganisms and it is responsible of the process schedule in the microalgae within a suitable temporal window. For synchronized cultures, all cells are at the same stage of the cell cycle at a given instant and the cell division occurs at the same instant.

It is worth to note that there is no relationship between the circadian clock and the day-night sun light cycle (de Winter et al., 2013). The circadian cycle is characterized by a frequency of about 24 h and regulates metabolic, physiological and/or events (Mittag et al., 2005). In particular, events are triggered to occur at the optimal time of the daily cycle (figure 2.6). The circadian cycle is observed even under 24/24 h constant irradiation conditions (de Winter et al., 2013).

Winter de et al. (2013) have reported that cell division of *N. oleoabundans* under controlled irradiation was controlled by the circadian clock and that multiple fission is observed during the night. Fluctuations in starch, protein and pigment content were measured during the synchronized cell division cycle. The maximum concentration of protein, starch and lipid was measured just before the beginning of the cell division process. Outdoor cultures - natural day/night cycle – are affected by the uncontrolled operating conditions (e.g. temperature irradiance). The interference between the circadian clock and the environmental conditions is expected to affect the average composition of microalgal cultures. However, composition fluctuation is still expected but the oscillation amplitude should be reduced.

The behaviour and physiological circadian cycle observed in *Chlamydomonas reinardtii* is reported in figure 2.6: diagrammatic. The arrows are the active time of reported cellular process (Matsuo and Ishiura, 2010).

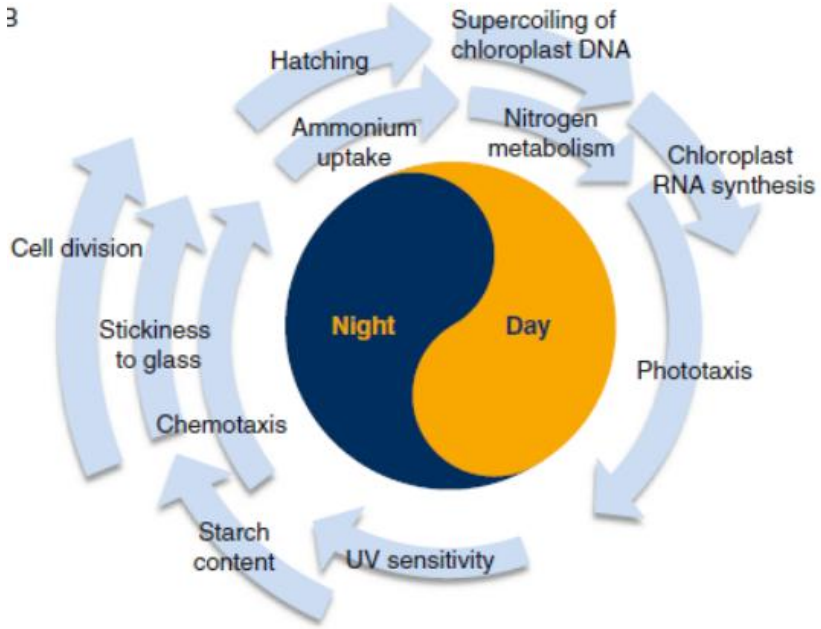

Figure 2.6: Behaviour and physiological circadian cycle observed in *Chlamydomonas*: diagrammatic representation of the circadian cycle of *Chlamydomonas*. The arrows are the active time of reported cellular process (Matsuo and Ishiura, 2010).

2.1.5 Season cycle

The culture performances remarkably reduce when microalgal cultures move from laboratory to industrial scale (Rawat et al., 2013). The technology for large-scale production of microalgae is mainly limited to open pond systems. Singh and Gu (2010) reported that no industrial plant finalized to produce low-value products – e.g. lipids for biodiesel - from microalgae is operated throughout the world. The basic requisite for the development of large-scale production of oil from microalgae is to make the process environmentally and economically sustainable/feasible (Rawat et al., 2013). To become economically feasible, the cultivation of microalgae requires high biomass and lipid productivity per unit area and minimum plant investment and operating costs.

A key issue for the process based on outdoor photobioreactors (PBR) is the efficient utilization of the photosynthetically active radiation (PAR) (Suali and Sarbatly, 2012). The efficient conversion of the sunlight – variable during the day and the year – requires the optimization of operating conditions and PBR design. In particular, attention must be paid at aspects as reactor orientation, light variation during the day, reflection of light, light gradient in the reactor (Slegers et al., 2011). Continuous PBRs operated at steady state conditions have been proved to be more reliable and reproducible (Ghasemi et al., 2012). Indeed, continuous PBRs are characterized by higher controllability than batch ones, making continuous operations more advantageous at industrial scale. Recent investigations are mainly focused on the characterization of the continuous operation mode (Gonzàles et al., 2012;

Zijffers et al., 2010; Olivieri et al., 2011; de Winter et al., 2014), the effect of light on growth and the modelling of light distribution in PBRs (Gutierrez et al., 2012; Janssen et al., 2010; Hindersin et al., 2013).

Bertucco et al. (2014) have simulated the algal growth in continuous PBRs under sunlight regimes of the four seasons at mid-latitudes. The aim has been to evaluate the effects of seasonal irradiation on microalgae growth, biomass productivity and energy conversion to biomass. The interest has been to address the industrialization and large-scale application of continuous PBRs. They have developed a mathematical model to evaluate the effect of seasonal irradiation on *S. obliquus* growth in a flat-plate PBR operated continuously. Four months representative of each season of the year were simulated with respect to light irradiation energy. Biomass concentration in the produced stream, biomass productivity and energy conversion efficiency have been calculated. The maximum energy conversion has been found for growth during the winter time. It is expected that the low average light irradiance reduced photosaturation, photoinhibition and energy dissipation. Nevertheless, a remarkable productivity has been assessed for all seasons even though the energy conversion was lower at high irradiation (summer time).

2.2 Microalgal cultivation systems

Solar photosynthetic active radiation (PAR) is the main limiting growth factor in photoautotrophic microalgal cultures provided that temperature and nutrient concentration are not growth limiting. Several solutions have been proposed to optimize the light regime for cells in the culture and to achieve high biomass productivity under outdoor conditions. The attentions has been paid to several parameter/phenomena involved in intensive cultivations. Parameter/phenomena to be tuned include: cell density, rate and method of culture mixing, photobioreactor depth, day/night cycle frequency, growth inhibition, photosynthetic rates, efficient energy conversion under high irradiance, monoalgal cultures. Moreover, the reactor should be designed to increase the efficiency of the light capture.

2.2.1 Open pond and photobioreactors

Reactor systems for autotrophic cultures must provide the environmental conditions for the efficient supply of carbon dioxide to the medium and of the light to the cells. They can be classified as open and closed systems (Flickinger, 1999).

- ✓ **Open systems** known as raceway ponds and open ponds. These systems are the simplest method of algal cultivation and offer advantages in terms of cost - fixed and operation - and of operation. Open culture systems require large surface area and a shallow depth of about

12–15 cm to improve light utilization. Furthermore, the culture is mixed to prevent the cells from sedimentation at the bottom as well as to distribute efficiently cell growth at the sunlight. The agitation was provided by a recirculation pump (Benemann et al., 1977). The main problems of the open raceways are: the low CO_2 transfer rate into the medium; culture contamination by different algal species and other organisms; water evaporation (it produces salinity increase in the culture medium).

- ✓ **Closed systems** known as photobioreactors. They are characterized by several advantages: low contamination risk; no water loss; high biomass productivity at high cell density; harvesting costs reduced with respect to the open system; possibility to grow a wide spectrum of species by tuning the operating conditions. However, the design of efficient and reliable large-scale culture systems requires to take into account several issues: light-utilization efficiency, homogeneous mixing (turbulence), low-shear conditions, temperature control, and efficient gas transfer (Weissman et al., 1988). The yield of light to algal biomass depends on the surface-to-volume ratio that play a key role in the efficient light utilization. The closed systems are usually classified according to geometry in: tubular and flat; horizontal, inclined, vertical and spiral; manifolds and serpentine.

Variable	**Photobioreactor facility**	**Raceway pond**
Annual biomass production (kg)	100000	100000
Volumetric productivity (kg m^{-3} d^{-1})	1.535	0.117
Areal productivity (kg m^{-2} d^{-1})	0.048[a]	0.035[b]
	0.072[c]	
Biomass concentration in broth (kg m^{-3})	4.00	0.14
Dilution rate (d^{-1})	0.384	0.250
Area needed (m^2)	5681	7828
Oil yield (m^3 ha^{-1})	136.9[d]	99.4[d]
	58.7[e]	42.6[e]
Annual CO_2 consumption (kg)	183333	183333
System geometry	132 parallel tubes/unit;	978 m^2/pond;
	80 m long tubes;	12 m wide;
	0.06 m tube diameter	82 m long;
		0.30 m deep
Number of units	6	8

[a] Based on facility area

[b] Based on actual pond area

[c] Based on projected area of photobioreactor tubes

[d] Based on 70% by wt oil in biomass

[e] Based on 30% by wt oil in biomass

Table 2.6: Comparison of photobioreactor and raceway production method (Chisti et al., 2007).

Table 2.6 reports a comparison of photobioreactor and raceway systems. The analysis of the reported data points out the high potential of PBRs with respect to raceway ponds.

The main disadvantage of closed systems are the photo-oxidative damage of the cells and the pH increase. The oxygen produced during the photosynthesis may accumulate at concentration that inhibits the cell growth and the chlorophyll expression. The CO_2 uptake during the microalgal growth is associated to the pH increase that may inhibit/stop the cell growth (Camacho Rubio et al., 1999). Potential solutions to reduce these effects are: degasser systems to limit the increase the oxygen accumulation (Molina Grima et al., 2001); CO_2 injection along the PBR to prevent CO_2 starvation. The length of the reactor tube depends on: biomass concentration, light intensity, CO_2 flow rate and O_2 inlet concentration.

2.2.2 Photobioreactor mixing

The type of system used to mix and circulate the culture play a key role in the optimization of photobioreactors. Mixing is necessary to prevent the biomass sedimentation, to prevent thermal stratification, to distribute nutrients and to smooth diffusion gradients at the cell surface, to remove the oxygen generated from photosynthesis and to guarantee all cells receive the adequate length of light and darkness. The hydrodynamics of the culture medium and the type of mixing influence the average irradiance and the light regime at which the cells are exposed. The mixing rate in the tube photobioreactors controls turbulence and mass transfer rate. The latter phenomenon significantly affects the oxygen concentration in the culture and carbon dioxide supply (Molina Grima, 1999).

The selection of the mixing system and of the mixing rate depends on the features of the cultivated microorganism. It should be taken into account that the air bubbling may cause stress to the cells when bubbles form/break-up. It is reported that bubble columns and airlift systems are characterized by low shear stress and therefore they are recommended for fragile microalgae (Sanchez Miron et al., 1999). Torzillo (1997) reviewed the mixing systems and the power requirement for microorganism mixing. Camacho Rubio et al. (1999) studied the gas–liquid mass transfer and mixing in serpentine airlift bioreactors. The Authors developed a model to describe the mass transport to assess the composition of the outlet gas (dissolved oxygen concentration included), the carbon dioxide flow rate required and the culture pH as functions of solar hour. The predictive capacity of the model has been validated by outdoor cultures of *P. tricornutum* (Camacho Rubio et al., 1999).

2.3 Microalgal downstream processes

A large number of potential pathways have been proposed for the conversion of algal biomass to energy vectors. These pathways can be classified into the following two general categories:

- ✓ processes of algal extracts (e.g. lipids) to produce biofuel (as conventional extraction and transesterification);
- ✓ processes focused on the direct production of biodiesel from microalgae without any extraction (direct transesterification and enzymatic transesterification).

The processes proposed to produce biofuel from microalgae extends the processes developed for the conversion of terrestrial plant-based oils to biofuels. A synoptic summary of the proposed processes is reported in figure 2.8.

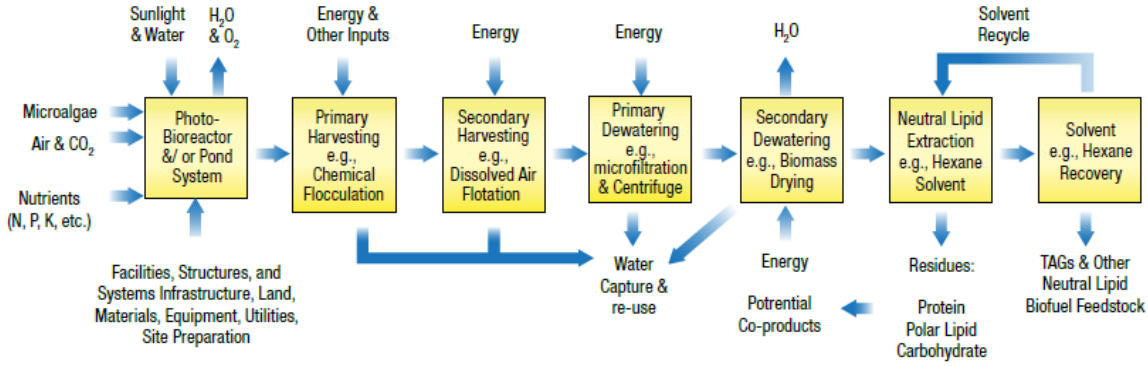

Figure 2.8: A schematic summary of the biomass to fuel conversion technology.

2.3.1 Lipid extraction and transesterification

The conversion of algal triglycerides to biodiesel proposes two step processes: the first step is focused on lipid extraction by using organic solvent (e.g. hexanes, chloroform and methanol) (Folch et al., 1957) and includes solvent recovery; the second step is focused on the conversion of lipids by the mixing with a catalyst (acid, base, enzyme) and alcohol to produce fatty acid methyl esters (FAMEs).

Direct use of triacylglycerols (TAGs) as combustible fuel is not suitable due to their high kinematic viscosity and low volatility. Furthermore, its long term use posed serious problems such as deposition, ring sticking and injector chocking in engine. Therefore, TAGs must be subjected to chemical reaction such as transesterification to reduce the viscosity. In that reaction, in the presence of short chain alcohol, such as methanol or ethanol, and a catalyst, such as basic or acid, triglycerides are converted into esters and glycerol (Vasudevan et al., 2008).

Table 2.7 reports the most relevant catalysis method for the triacylglycerol (TAG) transesterification (homogeneous acid and base, heterogeneous acid and base and enzymatic) and the potential of heterogeneous acid catalysts towards a more sustainable biodiesel industry production (Kee Lam et al., 2010).

Type of catalyst	Advantages	Disadvantages
Homogeneous base catalyst	• Very fast reaction time • Reaction can occur at mild reaction condition and less energy intensive • Catalyst such as NaOH and KOH are relatively cheap and widely available	• Sensitive to FFA content • Soap will formed if the FFA content is more than 2wt% • Too much soap formation will decrease the biodiesel yield and cause problem during purification
Heterogeneous base catalyst	• Relatively faster reaction rate than acid-catalyzed transesterification • Reaction can occur at mild reaction condition and less energy intensive • Easy separation of catalyst from product • High possibility to reuse and regenerate the catalyst	• Poisoning of the catalyst when exposed to ambient air • Sensitive to FFA content • Soap will formed if the FFA content is more than 2wt% • Too much soap formation will decrease the biodiesel yield and cause problem during purification • Leaching of catalyst active sites may result to product contamination
Homogeneous acid catalyst	• Insensitive to FFA and water content in the oil • Esterification and transesterification occur simultaneously	• Very slow reaction rate • Corrosive catalyst • Separation of catalyst from product is problematic
Heterogeneous acid catalyst	• Insensitive to FFA and water content in the oil • Esterification and transesterification occur simultaneously • Easy separation of catalyst from product	• Complicated catalyst synthesis procedures lead to higher cost • High temperature of reaction, high alcohol:oil molar ratio and long reaction time • Energy intensive
Enzyme	• High possibility to reuse and regenerate the catalyst • Insensitive to FFA and water content in the oil • Only simple purification step is required • Transesterification can be carried out at low reaction temperature, even lower than homogeneous base catalyst	• Very slow reaction rate • High cost • Sensitive to alcohol

Table 2.7: Advantages and disadvantages of different types of catalysts used in transesterification (Kee Lam et al., 2010).

Fatty acids vary in terms of carbon chain length and number of unsaturated bonds (double bonds). Biodiesel is a mixture of fatty acid alkyl esters. A mixture of fatty acid methyl esters is produced when methanol is used as reactant; while fatty acid ethyl esters are produced when ethanol is used. Methanol is commonly and widely used in biodiesel production due to its low cost and high availability. Table 2.8 shows the common composition of FAMEs in biodiesel (Ma et al., 1999).

Methyl ester	Formula	Common acronym	Molecular weight
Methyl palmitic	$C_{17}H_{34}O_2$	C16:0	270.46
Methyl stearate	$C_{19}H_{38}O_2$	C18:0	298.51
Methyl oleate	$C_{19}H_{36}O_2$	C18:1	296.50
Methyl linoleate	$C_{19}H_{34}O_2$	C18:2	294.48
Methyl linolenate	$C_{19}H_{24}O_2$	C18:3	292.46

Table 2.7: Chemical structures of common FAMEs.

2.3.2 Direct transesterification

The transesterification of TAGs in a one-pot process is aimed at suppressing the pre-extraction step and bypassing the use of large quantities of organic solvent. This process has been proposed as a significant simplification of the bio-diesel production. This process - known as in situ or direct transesterification – has been adopted in the past as an analytical technique in the preparation of FAMEs in connection with the determination of the fatty acid composition in lipids. Different authors (Johnson et al., 2009; Wahlen et al., 2011; Ehimen et al., 2010; Xu et al., 2011 and Velasquez-Orta et al., 2012) have recently evaluated acid-catalysed in situ transesterification. Johnson et al. (2009) have produced biodiesel from *Schizochyrtium limacinum* using different solvents (methanol, chloroform and hexane). They have obtained a maximum 68% yield of FAMEs under the following operating conditions: chloroform or hexane added to methanol, 1.5 mol of sulfuric acid, 132:1 molar ratio of methanol to solvent, 90°C, reaction time 40 min. Ehimen et al. (2010) have processed *Chlorella* algae at different temperature, alcohol molar ratio, reaction time, and moisture contents. They have pointed out a maximum lipid to FAME conversion of about 88% for a reaction time of 2 h, 0.04 mol of sulphuric acid, 500:1 molar ratio methanol to solvent, temperature of 90°C. Xu et al. (2011) have carried out an alkaline in situ transesterification of *Spirulina* in order to test different co-solvent. Velasquez-Orta et al. (2012) have assessed to the FAME production by alkali-catalyzed in situ transesterification of *Chlorella vulgaris* at different reaction time, methanol-to-solvent ratio, and catalyst concentrations. Lepage et al. (1984, 1986) and Vincente et al. (2009) have compared conventional and direct transesterification and have pointed out the direct method is characterized by a higher FAME yield.

AIM OF THE THESIS

The critical issues of the production of energy vectors from microalgae have been identified in the photobioreactors, biomass dryer and lipid extraction. The aim of the PhD thesis is to develop solutions for these critical issues that contribute to reduce the biodiesel cost. The partial goals of the study have also been identified taking into account the time scale of the phenomena involved in the growth of microalgae as well as the in the production rate of the component of interest. Figure 3.1 reports the time scale of the main phenomena investigated. The wide spectrum of the time scale has required the design of *ad hoc* tests. In particular, the devices as well as the experimental techniques have been purposely designed/selected for the phenomenon under investigation.

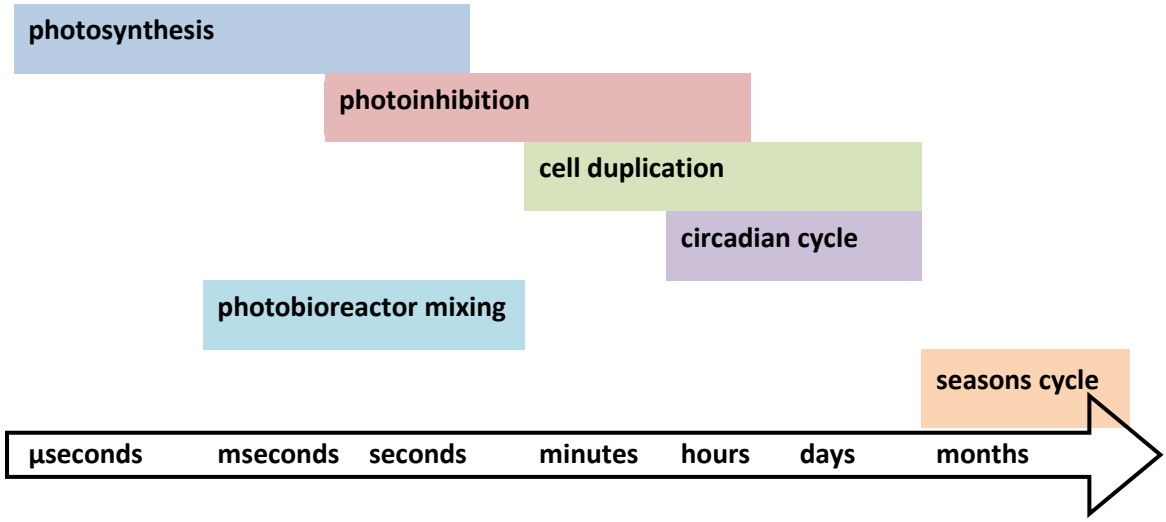

Figure 3.1: Synoptic scheme of the time scale of the investigated phenomena.

Partial goals of the study are reported hereinafter.

- ✓ Selection of microalgal strains representative of the main phylum. The investigated strains were selected in order to study the effects of: lipid fraction, cell wall composition, fresh vs. saline water. The investigated strains were: *Nannochloropsis sp.*, *Scenedesmus vacuolatus*, *Stichococcus bacillaris*, *Stichococcus fragilis*, *Stichococcus cylindricus*, *Stichococcus deasonii*, *Stichococcus jenerensis*, *Stichococcus chodatii, Chlorella vulgaris*, *Chlamydomonas reinhardtii*, *and Maesotaenium caldariorum.*

- ✓ Optimization of the microalgal cultures by the selection of photobioreactor design and operating conditions.

- ✓ Characterization of the composition of microalgae during the day/night cycle as an effect of the circadian behaviour of microalgae. The characterization has been aimed at addressing

the production maximization of a selected component of the cells (e.g. lipids for the biofuel production). *Nannochloropsis sp*. has been investigated in a photobioreactor turbidostat operated under conditions close to the outdoor operations in North Europe (16 hours of light and 8 of dark). Tests have been carried out under optimal temperature, and no limitation of nutrients and light. Nitrogen starvation has been also investigated. Some tests have also been carried out in an outdoor facility.

- ✓ Characterization of the microalgal growth rate under controlled operating conditions. The characterization has been carried out in a photobioreactor turbidostat operated under controlled conditions of irradiance and nutrients.

- ✓ Characterization of the photochemical process. The attention has been focused on the development of a procedure to assess the kinetics of the photosynthesis. The procedure is based on the processing of the fluorescence dynamics of pulse-amplitude modulation fluorimetric measurements. The kinetic parameters of the photochemical model proposed by Eilers and Peeters (1998) have been assessed for a selected collection of strains growth under a wide interval of operating conditions.

- ✓ Direct transesterification of microalgae to produce fatty acid methyl esters (FAMEs). The efficiency of the process – expressed in term of FAME yield - has been assessed for several strains characterized by different composition of the cell wall. The role of both alkaline and acid catalyst has been investigated. The attention has also been focused on the effects of operating conditions - pre-contact time, catalyst concentration, methanol/dried-biomass weight ratio, temperature, reaction time, water content of microalgal biomass – on the FAME yield. The direct transesterification efficiency has been compared with results of the conventional extraction-transesterification process.

MATERIALS AND METHODS

4.1 Organism and medium

Nannochloropsis sp. 211/78 was achieved from culture collection of Algae and Protozoa, Oban, Argyll, Scotland, United Kingdom. Natural seawater, from de Oosterschelde, the Netherlands, was used for the medium preparation (Table 4.1) (Benvenuti et al., 2014). To remove any contaminations, seawater containing 5mM Na_2EDTA was sterilized for 60 minutes at 121°C. After autoclaving all other medium components were added and the pH was set to 7.5. The final medium was filter sterilized with a 0.2µ filter.

Component	Molar concentration in final medium
HEPES	$1.00 * 10^{-01}$ M
$NaNO_3$	$7.00 * 10^{-02}$ M
$CaCl_2 * 2H_2O$	$2.50 * 10^{-03}$ M
$MgSO_4 * 7H_2O$	$5.00 * 10^{-03}$ M
K_2HPO_4	$2.30 * 10^{-03}$ M
KH_2PO_4	$8.80 * 10^{-04}$ M
NaCl	$4.20 * 10^{-02}$ M
EDTA-Fe(III)-Na-salt	$1.10 * 10^{-04}$ M
$NaHCO_3$	$1.00 * 10^{-02}$ M
Biotin	$1.00 * 10^{-07}$ M
Vitamin B1	$3.70 * 10^{-06}$ M
Vitamin B12	$1.00 * 10^{-07}$ M
$Na_2EDTA * 2H_2O$	$1.80 * 10^{-04}$ M
Na_2SO_4	$3.50 * 10^{-03}$ M
$CoCl_2 * 6H_2O$	$1.20 * 10^{-06}$ M
$MnCl_2 * 2H_2O$	$1.55 * 10^{-05}$ M
$CuSO_4 * 5H_2O$	$1.30 * 10^{-06}$ M
$ZnSO_4 * 7H_2O$	4.00 * 10-06 M

Table 4.1: Composition of the medium for *Nannochloropsis sp*.

Scenedesmus vacuolatus, *Stichococcus bacillaris*, *Stichococcus fragilis*, *Stichococcus cylindricus*, *Stichococcus deasonii*, *Stichococcus jenerensis*, *Stichococcus chodatii, Chlorella vulgaris*, *Chlamydomonas reinhardtii*, *and Maesotaenium caldariorum* were achieved from the ACUF collection of the Department of Biological Science at the University of Studies of Napoli — Federico II (http://www.biologiavegetale.unina.it/acuf.html). These algae have only minimal requirements to the medium for the growth. There is the need of inorganic ions and a minimal quantity of organic compounds, such as vitamins. Carbon, nitrogen and phosphor are the most important nutrients for

the autotrophic algal growth (Becker et al., 1986). Bold Basal medium (Bold 1949, Bischoff et al., 1963) is an artificial freshwater medium, which is practical for growing green algae. Bold Basal Medium (BBM) supplemented with $NaNO_3$ (40 mg L^{-1}) as nitrogen source was adopted. After preparing the medium (table 4.2) it was autoclaved for 20 minutes. The final pH should be 6.8.

Component	Molar concentration in final medium
$NaNO_3$	$2.94 * 10^{-03}$ M
$CaCl_2 * 2H_2O$	$1.70 * 10^{-04}$ M
$MgSO_4 * 7H_2O$	$3.04 * 10^{-04}$ M
K_2HPO_4	$4.31 * 10^{-04}$ M
KH_2PO_4	$1.29 * 10^{-03}$ M
NaCl	$4.28 * 10^{-04}$ M
EDTA anhydrous	$1.71 * 10^{-04}$ M
KOH	$5.52 * 10^{-04}$ M
H_3BO_3	$1.85 * 10^{-04}$ M
$FeSO_4 * 7H_2O$	$1.79 * 10^{-05}$ M
H_2SO_4	$1.79 * 10^{-05}$ M
$ZnO_4 * 7H_2O$	$3.07 * 10^{-05}$ M
$MnCl_2 * 4H_2O$	$3.07 * 10^{-05}$ M
MnO_3	$4.93 * 10^{-06}$ M
$CuSO_4 * 5H_2O$	$6.29 * 10^{-06}$ M
$Co(NO_3)_2 * 6H_20$	$1.68 * 10^{-06}$ M

Table 4.2: Composition of the Bold Basal Medium.

4.2 Photobioreactor set-up

Tests were carried out in bubble column photobioreactors characterized by circular cross section (CBC) and rectangular cross section (RBC).

- ✓ *Cylindrical bubble column photobioreactor (CBC)*: the 1 L bench scale photobioreactor had a cylindrical shape (figure 4.1). It was made of glass (0.04 m ID, 0.8 m high) and closed at the top by a removable silicon cap. The photobioreactors were housed inside a climate chamber (M2M engineering; type: Solar neon) with a temperature set at 23±1 °C. 10 lamps (Philips Master, TL-D 90 de luxe; 36 W/940) continuously illuminated the front side of the photobioreactor. Air supplemented with CO_2 was provided at the bottom of the photobioreactor by means of a porous ceramic diffuser to provide the aeration and mixing of the bubble column. A flowmeter (ASA, Sesto S. Giovanni; model: E5-2600/H) was used to measure the gas flow rate. A T-shaped valve connected and mixed the CO_2 and the air flow rates before entering the photobioreactor. Three tubes were fixed in the silicon cap on the top of the reactor. Two of them were destined for the gas flow inlet

and the gas flow outlet. The third line was provided for the sampling operation and was closed by a clamp.

The chamber was equipped with two type of lamps: white light lamps and red/blue light lamps. The CBC were operated under vertical configuration for all investigated conditions.

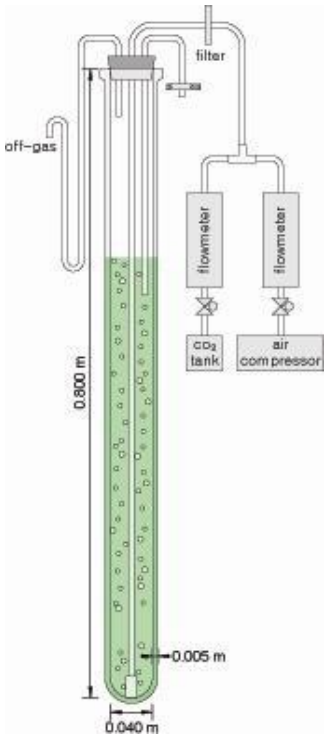

Figure 4.1: Sketch of CBC photobioreactor.

✓ *Parallelepiped-shape bubble column photobioreactor (RBC)*: the 1 or 2 L bench scale photobioreactor had a square shape (figure 4.2). They are made of glass with a working volume of 0.6L and 1.7 L, respectively. The photobioreactors differ in their thickness: 2 L photobioreactor is 8 cm of depth, while 1 L photobioreactor 5 cm of depth. A removable silicon cap equipped three tubes closed the reactor at the top. The RBC were operated under inclined conditions: the longitudinal axis was inclined with respect to the vertical of 2 and 45°.

Indoor tests were carried out in a climate chamber (Heraeus Vötsch GmbH; type: HPS 500) with a temperature set at 23±1 °C. Lamps (M2M engineering) fixed inside the climate chamber illuminated, depending on the experimental designs, continuously or in day/night cycle the photobioreactor from above or side. For the aeration and mixing air was sparged at the bottom of the photobioreactor by means of a plastic tube with many holes in a distance of about 1 cm. One T-shaped valve mixed the air from a compressor and the CO_2 from a tank. A flow meter (ASA, Sesto S. Giovanni; model: E5-2600/H) was used to measure the in-gas flow rate. The gas-off line was

connected to a gas fermenter analyser (Solaris biotechnology) to determine the concentration of CO_2 and air outgoing of the reactor.

The RBC during the outdoor tests were housed in a water bath kept at constant temperature by means of a crio-thremostatic bath. The temperature of the bath was set at 23°C. The day/night temperature fluctuations introduced a test temperature fluctuation of ± 2 °C.

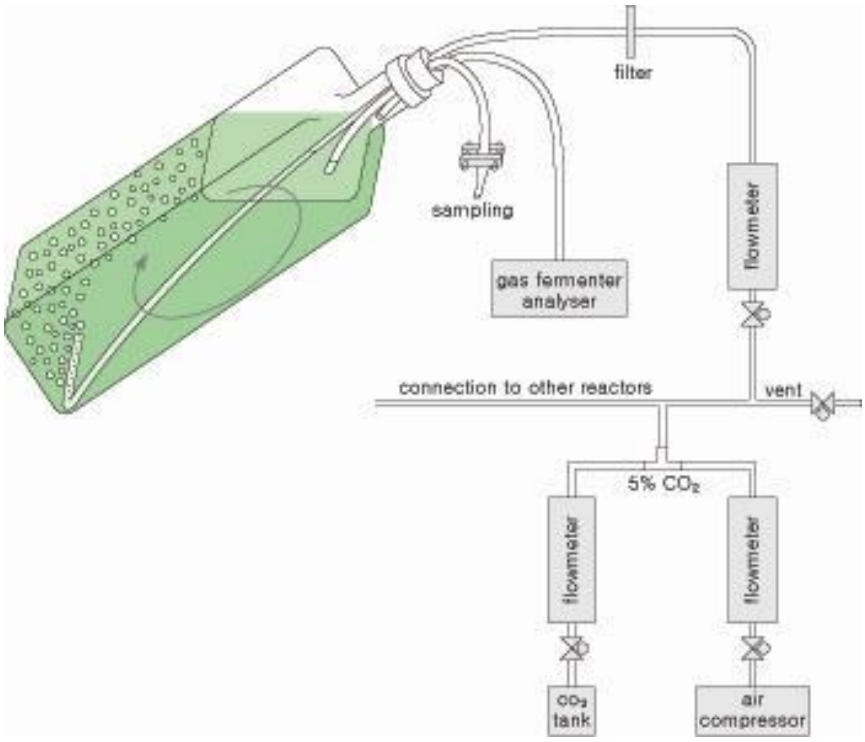

Figure 4.2: Sketch of the RBC photobioreactor (not on scale). The arrow denotes the direction of mixing.

✓ *Flat photobioreactor*: the photobioreactor consists of three glass plates, which are held in place by three aluminium cover frames, all mounted on the stainless steel inner frame of the culture chamber (figure 4.3). The three glass plate formed two chambers, one for the biomass culture and the second for the water jacket. The culture chamber has a working volume of 1.7 L, a light path of 20 mm and an illuminated area of 0.085 m^2 (22.5 x 40 cm^2, minus the rounded corners). The illumination was provided by LED panels of 20x20 cm (LED Light Source SL 3500, average optimum 630-635 nm and a spectral half width of 20 nm, PSI, Czech Republic). The photon flux density at the surface of the algal culture was measured by a LI-COR 190-SA 2π sensor (PAR range 400-700 nm). A similar measurement at the back of the reactor gave the amount of light falling through the system during cultivation. To obtain the proper value for light leaving the culture the measured value was corrected for the light absorbed by the water jacket and the back glass panels. This was done by measuring the light leaving the system when only medium and no cells

were present. The light sensor (LI-COR 190-SA 2π sensor, PAR range 400-700 nm) attached to the front and back glass panels of the reactor are connected to an ADAM-5000/485-AE data acquisition and control module (Advantech) and controlled via a LabView virtual instrument running on a PC (LabView 7.1, National Instruments Corporation, Austin) (Klok et al., 2013).

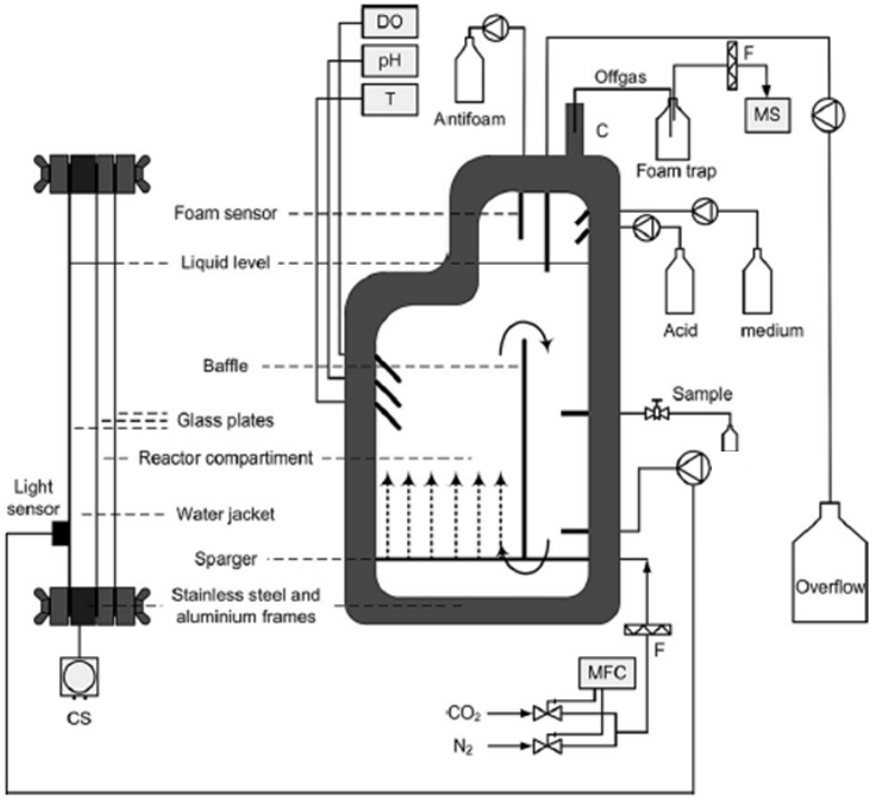

Figure 4.3: Sketch of the flat photobioreactor. C = condenser connected to separate cryostat (not shown), DO = dissolved oxygen sensor, F = air filter, MFC = mass flow controllers for both nitrogen and carbon dioxide, MS = mass spectrometer for off-gas analysis, pH = pH sensor connected via controller to acid pump, T = temperature sensor connected cryostat, CS = cryostat.

✓ *Thin flat photobioreactor*: the 0.25 L thin flat photobioreactor had a square shape (figure 4.4). It was made of glass with a working volume of 0,25 L. The dimensions are shown in figure 6.4. A non-removable silicon cap equipped three tubes closed the reactor at the top. The photobioreactors were housed in a vertical position inside a climate chamber with a temperature set at 23±1 °C. Blue and red led (M2M engineering) fixed on the front side of the photobioreactor continuously illuminated the reactor from above. For the aeration and mixing air was sparged at the bottom of the photobioreactor by means of a plastic tube with many holes in a distance of about 1 cm. One T-shaped valve mixed the air from a compressor and the CO_2 from a tank. A flow meter (asa, Sesto S. Giovanni; model: E5-2600/H) was used to measure the in-gas flow rate.

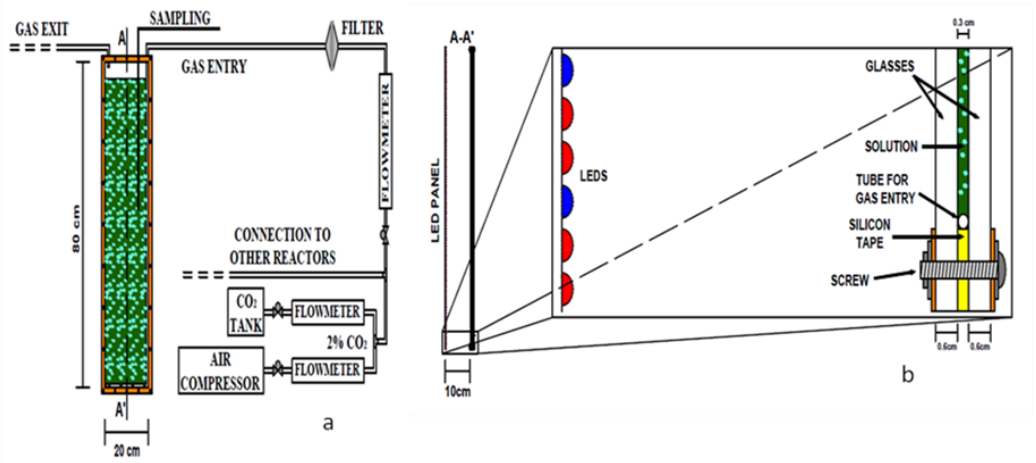

Figure 4.4: Sketch of the thin flat photobioreactor (on scale): a) front; b) section.

4.3 Contamination assessment

The determination of bacterial and fungal contamination in the reactors was performed by a microscope with a magnification factor of 40 x and 100 x respectively (Leitz Wetzler; 567146; Germany). A Nikon Eclipse 800 fluorescence microscope was used to visualize the chlorophyll content in the algal cells.

4.4 Chlorophyll a

A fluorometer (AquaFluorTM; Handheld Fluorometer/Turbidimeter; Turner Designs) was used to measure the content of in vivo chlorophyll a in the untreated samples. Therefore the excitation light of the fluorometer passes through the medium and causes the chlorophyll a inside the cells to fluoresce. This signal allows estimating the concentration of Chlorophyll a in the sample.

4.5 Photosynthesis and respiration rates

Photosynthesis is an indication of the health of algal cells and can be measured by means of an Hansatech Oxygraph. It consists of two connected sections: the upper section of the Oxygraph that contains a transparent, thermostated sample chamber, and the lower electrode part. A thin Teflon membrane is used to separate the sample from the electrode compartment. A magnetic stirrer mixes the sample continuously. The adjustable stopper is used to prevent room air dissolving during the experiments. To start the measurement a small polarising voltage is applied between the anode and the cathode. Now the oxygen diffuses through the Teflon membrane and is converted into an electrical signal which can be detected. The oxygen control unit is connected to a PC, so it is possible to observe the oxygen gradient during the oxygen uptake (respiration) and the oxygen production (photosynthesis).

If the photosynthesis was active (light phase), a positive slope (R_{Light}) in the oxygen vs time plot can be measured. If only the respiration was active (dark phase) a negative slope (R_{Dark}) in the oxygen vs time plot can be measured. The real photosynthetic rate (R_{Ph}) and respiration rate (R_{Resp}) were calculated as following:

$$R_{Ph} = R_{Light} + R_{Dark} \quad [4.1]$$

$$R_{Resp} = R_{Dark} \quad [4.2]$$

4.6 Microalgal fluorescence

A Chlorophyll Fluorimeter (or fluorometer) is designed specifically to detect the chlorophyll fluorescence emission from a sample. The "Fluorescence Monitoring System" of Hansatech Instruments was used in the present investigation. The System was based on 2 different measurement techniques, Pulse Modulated Chlorophyll Fluorometers and Continuous Excitation or Prompt Chlorophyll Fluorimeters.

4.7 Biomass characterization

The concentration of algal biomass was estimated by measuring the optical density at 600 nm with a spectrophotometer (Specord 50 – Analytic Jena). The dry weight of the inoculum was used to establish the basis for converting the optical density in g L^{-1} of algal biomass. Therefore a Whatman filter GF/A was dried at 60°C overnight and then weighed. A part of the inoculum was filtered using the dried Whatman filter. The wet biomass retained. The filter with the biomass on it dried overnight at 60°C and was then weighed out. The microalgal dry weight can be calculated from the difference in weight between the dry filter with and without biomass.

The composition of the biomass was assessed on samples harvested from the cultures. The samples from a bioreactor - in triplicate - were centrifuged for 10 min at 2500 rpm and the pellets were washed with water or 0.5 mM ammonium formate. The pellets were stored at -20ºC, then freeze dried.

- ✓ *Proteins*. Protein content was analyzed with the DC protein assay (BioRad). Freeze dried pellets containing 7.5 mg of DW were dissolved in 1 mL of lysis buffer, containing 60 mM Tris pH 9 and 2% SDS. Subsequently, the cells were disrupted using a beat beater (Precellys 24, Bertin Technologies, France) at 6000 rpm for 3 cycles of 60 s with 120 s breaks. The samples were incubated for 30 min at 100 °C in a heating block. After incubation samples were centrifuged for 10 min at 3500 RPM. Supernatant was transferred in new tubes and diluted 2X with lysis buffer

solution. 10 µL of samples were mixed with reagents Bio-Rad Dc protein assay kit and incubated in dark condition for 15 minutes at room temperature. Protein content was analyzed by measuring absorbance at 750 nm using the Tecan M200 Plate Reader.

✓ *Carbohydrate.* Total carbohydrate content was determined using the protocol in according to Dubois et al., 1956. 5 mL of 2.5M HCl were added to freeze dried pellets containing 10 mg of DW. The biomass was incubated in a boiling waterbath for 3 hours and vortexed every hour. To neutralize 2.5M of NaOH solution were added to the biomass. 50µL of supernatant were transferred in a fresh glass tube and 450 µL of MilliQ water were added to the supernatant. Then 500 µL of 5% phenol solution and 2.5 mL of concentrated sulphuric acid were directly added on the liquid surface. The samples were incubated for 10 minutes at room temperature and then for 30 minutes in water bath at 35 ºC. The carbohydrate concentration was analyzed by measuring the absorbance at 483 on a spectrophotometer (DU 640, Beckman, U.S.A.).

✓ *Lipid.* The lipids identification requires several steps: biomass harvesting; biomass freeze-drying; lipid extraction and weight; lipid transesterification and methyl esters analysis. The direct transesterification process was done in both conditions using basic or acid catalysts.

4.8 Lipid analysis and transesterification

4.8.1 Alkaline-catalyzed condition

✓ *Conventional protocol*: the fraction of lipids was extracted from the algal cells according to a method proposed by others (Guckert et al., 1988). A pre-weighed spherical flask was loaded with: i) a cellulose extraction thimble with about 0.4 g of freeze-dried algal biomass put into the main chamber of the Soxhlet extractor; ii) the extraction solvents made of chloroform/methanol in a ratio 2:1. The flask was heated until a solvent reflux was observed from the condenser. At the end of the extraction operation, the solvents were evaporated at 60 °C under vacuum conditions. After the solvent evaporation, the spherical flask, containing lipids, was weighed and the total lipid content was calculated. The samples extracted were stored at 4°C. A literature procedure (Rashid and Anwar, 2008) was adopted for the conventional alkaline transesterification reaction. The extracted lipids were mixed with 10mL of alkaline solution of methanol in a flask equipped with a condenser and thermostat at 60 °C in a water bath for 3 minutes under magnetic stirring. After a fixed time, the mixture was filtered and the liquid phase stored at 4 °C, before the GC analysis.

✓ *Direct transesterification in alkaline-catalyzed conditions*: a sample of algal biomass (0.1 g dry matter) was suspended in closed glass test tubes containing methanol alkaline solution.

Tests were carried out under a wide interval of operating conditions obtained by changing the biomass water content, methanol/biomass weight ratio, concentrations of sodium hydroxide in methanol, pre-contact time, temperature, reaction time. The reaction system was quenched by cooling at room temperature, filtered and the liquid phase stored at 4 °C, before the further GC analysis. For the experiments on biomass with different water content, samples of wet algal biomass recovered from bioreactor were submitted to lyophilisation process for different times.

4.8.2 Acid-catalyzed condition

✓ *Conventional protocol:* a sample of algal biomass (10 mg DW) was suspended in methanol:chloroform 1.25:1 solution. The cells were disrupted using a beat beater (Precellys 24, Bertin Technologies, France) at 2500 rpm for 5 cycles of 60 s with 120 s breaks. The solution was transferred in glass tubes and the bead beater tubes were rinsed 3 times with methanol:chloroform solution and transferred in the glass tubes. The samples were vortexed for 5 second and sonicated for 10 minutes. 2.5 mL of 50 mM + 1 M NaCl pH 7.5 were added to the samples. The samples were vortex and sonicated again. The samples were centrifuged for 5 minutes at 2500 rpm at 15 ºC and the CHCl3 phase was transferred to new tubes. A 1 mL of chloroform was added to old tubes, vortex, sonicated and centrifuged: the $CHCl_3$ phase was collected and pooled with the first chloroform fraction. The chloroform was evaporated under nitrogen gas stream and 3 mL of methanol containing 5% H_2SO_4 were added. The samples were vortex and incubated for 3 hours at 70 ºC in a block heater. 3 mL of water and 3 mL oh hexane were, then, added and the samples were mixed for 15 minutes with an incanter. The samples were centrifuged and the hexane phase was collected and washed with 2 mL of water. The hexane phase containing the fatty acid were analyzed by GC (Hewlett Packard 6890 Series) (Solvent A: n-hexane, column: Supelco Nucoltm col. 355 33-03A, gas carrier: helium, flow rate: 20mL/min) (Breuer at al., 2013).

The triacylglycerols and polar acyl lipids were separated and quantified by using SPE columns (Sep-Pak Vac Silica cartridge 6cc/1000mg). The samples, after the chloroform evaporation, were dissolved in 1.5 mL hexane:diethylether 7:1 v/v solution and transferred to the pre-equilibrate columns. The apolar lipids (TAG) were eluted by 5 columns volume of hexane:diethylether 7:1 v/v solution. The polar acyl lipids were, then, eluted in new glass tubes by 5 columns volume of methanol:acetone:hexane 2:2:1 v/v/v solution. The solvents was evaporated under nitrogen gas stream and the samples were then transesterified in acidic condition (Breuer et al., 2012).

✓ *Direct transesterification in acidic-catalyzed conditions: a*cidic-catalyzed direct transesterification was carried out according to two protocols previously reported (Johnson and Wen, 2009). Samples of freeze-dried algal biomass (0.1 g) were placed in different closed glass test

tubes and mixed with a mixture of methanol (3.4 mL) and sulphuric acid (0.6 mL). Depending on the experimental design, 4 mL of chloroform (or methanol) was added to the test tube. The transesterification process was carried out at 90 °C for 40 minutes under magnetic stirring and controlled reflux. After the reaction, the samples were cooled, filtered and the liquid phase stored at 4 °C, before the further GC analysis.

4.9 Analytic methods

- ✓ **Nitrate concentration.**

The analysis of nitrate concentration in the medium was made using a nitrate electrode Metter-Toledo.

- ✓ **pH**

The pH of the medium was measured with a pH-meter of the type - Crison; Basic 20. The pH reflects the content of dissolved carbon dioxide and carbonic acid salts ($HCO_3^- \leftrightarrow CO_2 \leftrightarrow CO_3^{2-}$).

- ✓ ***FAME***

The FAMEs produced by lipid transesterification were extracted by hexane (Wang and Wang, 2012). The organic layer with the FAMEs was transferred to a tube and dried under nitrogen stream of nitrogen. The residue was re-suspended in methanol. The qualitative and quantitative analysis of FAMEs was carried out using an Agilent 7820A GC equipped with a Flame-ionization detector (FID) and Agilent DB-WAXTER column (30m x 0.320mm x 0.50 film thickness). The temperature was increased from 100 °C to 230 °C at 10 °C min^{-1}). Helium (1mL min^{-1} in constant flow) as used as the carrier gas and the detector temperature was 300 °C. The calibration was done with chemical standards from Fluka Sigma-Aldrich. Peak areas were used to quantify each FAME relative to the internal standards. The total fatty acid content was calculated by adding all the individual FAME peak areas.

RESULTS: MICROALGAL CULTIVATIONS

The analysis of the critical issues for intensive microalgal cultures reported in the introduction section has pointed out the necessity to focus the attention on the photobioreactor design, the medium composition and the illumination strategy. Results of the investigation reported in this section refer to the characterization of the effects of the recalled issues on the microalgal productivity. The lipid productivity was also investigated as a potential exploitation of microalgae as biofuel feedstock.

5.1 Operating conditions and procedures

Tests were carried out in bubble column photobioreactors characterized by circular cross section (CBC) and rectangular cross section (RBC). The operating volume of CBC and of RBC characterized by 5 cm depth was 0.6 L; the operating volume of RBC characterized by 8 cm depth was 1.7 L. The temperature in the climate chambers was set at 23 ± 1 °C and the pH was kept constant at about 7 by the CO_2 feeding. The medium was Bold Basal Medium (BBM) per *Stichococcus bacillaris* and *Scenedesmus vacuolatus*. The irradiance strategy was: a) continuous irradiance at 140 and 250 µE m^{-2} s^{-1}; circadian irradiance characterized by 16/8 h light/dark cycle with a sinusoidal light period having 140 and 250 µE m^{-2} s^{-1} irradiance as maximum.

Tests in photobioreactors started under batch conditions until the concentration of the nitrogen source was higher than 10 mg L^{-1}. As soon as the nitrogen source was lower than the reported threshold, fed-batch cultivation method started by supplementing the photobioreactor – when necessary - with concentrated medium to restore the nutrient concentration at initial value. Semi-continuous cultivation started when the biomass concentration under fed-batch conditions reached about 5-6 g_{DW} L^{-1}. The semi-continuous condition was characterized by the weekly replacement of 30% of the suspension with fresh medium: dilution rate (D) – the ratio between the average feeding volumetric rate and the photobioreactor working volume - 0.043 d^{-1}. The broth removed each week was used for the characterization of both the liquid phase and biomass phases. The continuous cultures was kept under steady state conditions for some weeks, then nitrogen-starvation culture was adopted (no nitrogen source feeding). After 1 week under nitrogen starvation, the reactors were stopped and the biomass was harvested for the analysis.

The tests were characterized in terms of time-resolved measurements of biomass concentration and chlorophyll a content. Steady state cultures were characterized in terms of: biomass concentration (X, g L^{-1}); biomass productivity (W_X, mg $L^{-1}d^{-1}$); chlorophyll a content, (Chl a, mg g_{DW}^{-1}); concentration of lipid content of the dry weight biomass ($\%_{Lipid}$, g g_{DW}^{-1}); fraction of identified FAME with respect to

the dry weight of the biomass, (% g g_{DW}^{-1}). The characterization of the photosynthesis rate, respiration rate and biomass fluorescence were also carried out.

5.2 Effect of the medium

✓ Effect of CO_2 concentration

Tests were aimed to assess the effect of CO_2 concentration in the gas stream fed to the culture on the photobioreactor performance. The tests were carried out in CBC photobioreactors irradiated continuously at 140 µE m^{-2} s^{-1} with white light. *Scenedesmus vacuolatus* and *Stichococcus bacillaris* were investigated. The CO_2 concentration in the gas stream fed to the photobioreactors ranged between 0.5 vvm (air) up to 15%v/v. The highest CO_2 concentration was investigated for *S. bacillaris* cultures to assess the behaviour under typical exhaust gas. Figure 5.1 and 5.2 report data measured during *S. vacuolatus* and *S. bacillaris* cultures, respectively. Data refer to growth carried out feeding air (a) and 2% CO_2 stream (b). Photobioreactors were operated under batch, fed-batch, and semi-continuous conditions.

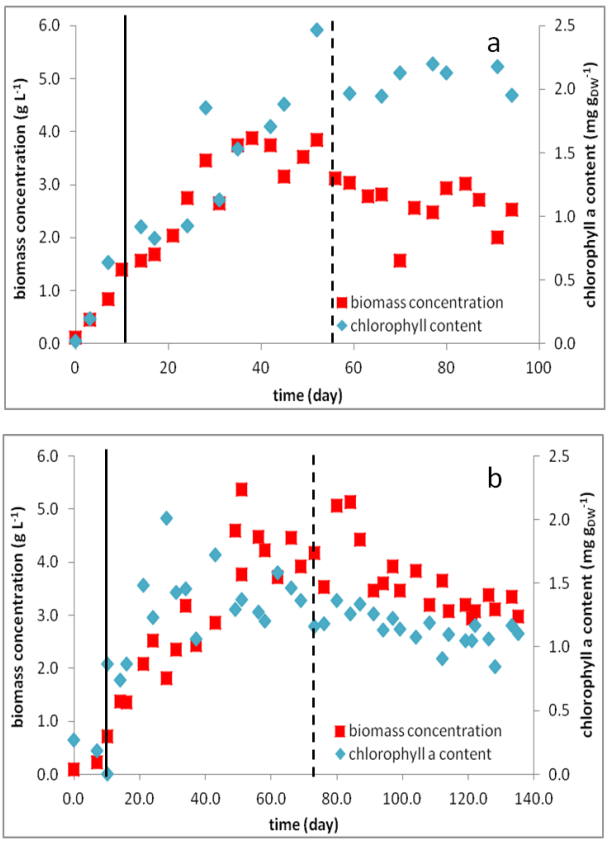

Figure 5.1: Characteristics of a *Scenedesmus vacuolatus* culture running through batch, fed-batch and semi-continuous conditions, a) with only air sparged and b) with 2% of CO_2 added to air; ■ biomass concentration (g L^{-1}), ♦ chlorophyll a (mg g_{DW}^{-1}). Continuous line marks the beginning fed-batch mode; dashed lines the semi-continuous mode.

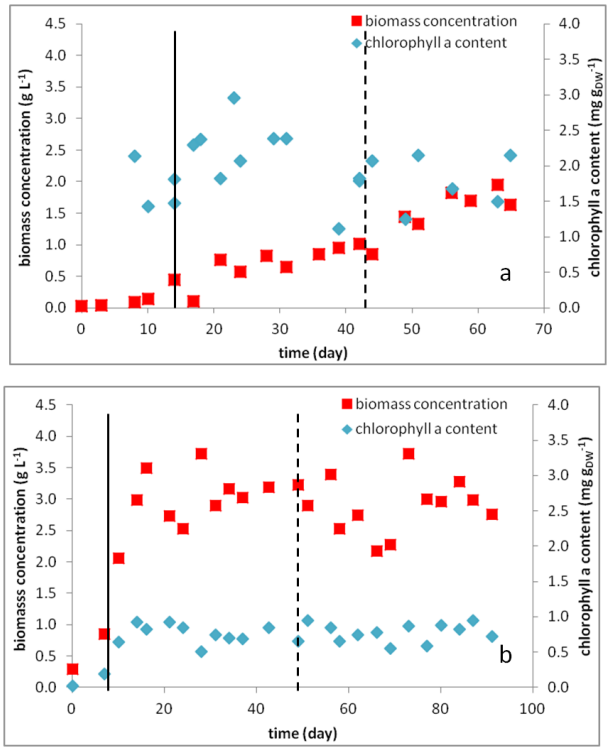

Figure 5.2: Characteristics of a *Stichococcus bacillaris* culture running through batch, fed-batch and semi-continuous conditions, a) with only air sparged and b) with 2% of CO_2 added to air; ■ biomass concentration (g L^{-1}), ♦ chlorophyll a (mg g_{DW}^{-1}). Continuous line marks the beginning fed-batch mode; dashed lines the semi-continuous mode.

Photobioreactor	**CBC**													
Organism	*S. bacillaris*										*S. vacuolatus*			
CO_2 (%)	**0.035**		**2**		**5**		**10**		**15**		**0.035**		**2**	
pH	~7													
I (µE $m^{-2}s^{-1}$)	140													
X (g L^{-1})	1.30±0.18		2.64±0.5		2.48±0.3		2.62±0.5		2.78±0.3		2.99±0.26		3.46±0.1	
					5									
W_x (mg$L^{-1}d^{-1}$)	/		110		100		110		120		130		140	
Chl a (mg g_{DW}^{-1})	2.56		0.80		0.30		0.32		0.27		1.85		1.11	
N conditions	+	-	+	-	+	-	+	-	+	-	+	-	+	-
% Lipid (% g g_{DW}^{-1})	29	28	33	37	34	27	36	25	27	27	18	15	30	25
% FAME (% g g_{DW}^{-1})	5.8	6.1	7.5	7.7	5.2	8	8	8.4	5.6	7.8	2.9	5	7.3	7.8

Table 5.1: Steady state data of semi-continuous tests in VBC photobioreactors under N sufficient (+) and N starvation (-) conditions.

Table 5.1 reports data measured under steady state conditions of *S. vacuolatus* and *S. bacillaris* cultures carried out at different CO_2 concentration. The analysis of data reported in the figures 5.1 and 5.2 and table 5.1 points out the following issues:

- *S. bacillaris* and *S. vacuolatus* were able to grow under all the investigated CO_2 concentrations.
- Both strains grown very slow when sparged with air. *Stichococcus* never reached steady-state biomass concentration.
- The biomass concentration was higher in a photobioreactor sparged with CO_2 supplemented air.
- The maximum specific biomass productivity (W_X) was 110 mg L^{-1} d^{-1} per *Stichococcus bacillaris* and about 140 mg L^{-1} d^{-1} per *Scenedesmus vacuolatus*.
- The chlorophyll a content decreases in the culture with additional CO_2 was lower than in the culture with only air sparged. This result is in agreement with Huertas et al. (2000), Ge et al. (2011) and Sergeenko et al. (2000) that reported a decrease in chlorophyll pigments in several algal strains cultivated under high CO_2 concentration.
- The total lipid fraction of biomass was maximum for cultures carried out spreading gas streams at CO_2 concentration in the range 2-10% for both investigated strains.
- The fraction of FAME per grams of biomass dry weight increased when CO_2 supplemented air stream was fed to the photobioreactors. The fraction was practically no dependent on the CO_2 concentration in the range 5-10%.

The composition of esterified lipids (data not show) did not change with the strain and with the CO_2 concentration in the sparged gas stream. The linolenate and linoleate fractions were the highest in the cultures grown with CO_2 supplemented air. The oleate fraction was dominant for cultures carried out under nitrogen starvation condition and sparging CO_2 supplemented air. Elaidate was found in FAME from *S. bacillaris* cultures carried out under nitrogen sufficient condition and sparging 15% CO_2 air stream.

✓ **Effect of pH**

Tests were aimed to assess the effect of different pH values in the medium to the microalgal culture of *Stichococcus bacillaris* (figure 5.3). These tests were carried out in RBC photobioreactor irradiated continuously at 250 µE m^{-2} s^{-1} with white light and sparged with gas mixture consisted of air with 5% additional CO_2. The cultures ran under batch, fed-batch and semi-continuous mode. At the end of the experiment, the photobioreactor was cultivated in nitrogen starvation for one week. Table 5.2 reports data of semi-continuous tests with different pH values in the culture medium. The following effects could be noticed by considering all cultures in the experiment.

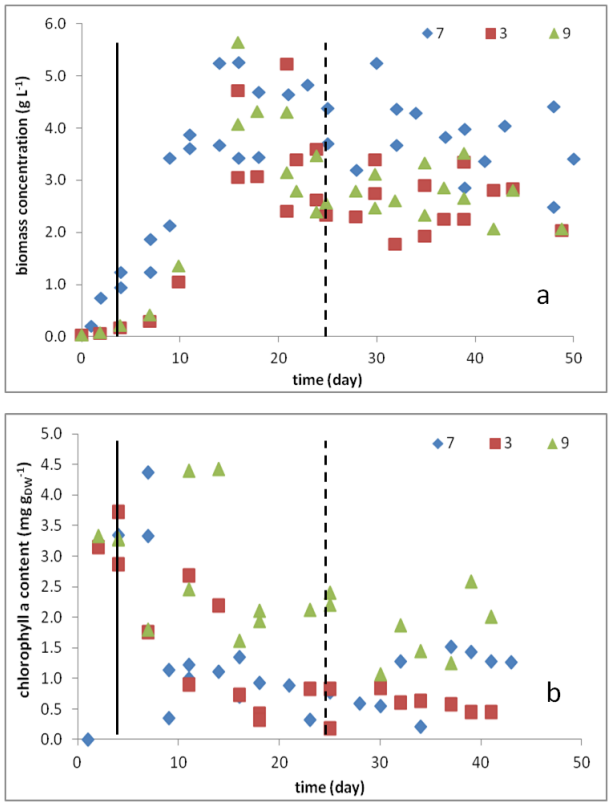

Figure 5.3: Characteristics of a *Stichococcus bacillaris* culture running in square vertical bubble column with 8 cm of depth irradiated at 250 $\mu Em^{-2}s^{-1}$ through batch, fed-batch and semi-continuous conditions, a) biomass concentration (g L^{-1}); b) chlorophyll a content (mg g_{DW}^{-1}); ■ culture growth at pH 3; ♦ culture growth at pH 7; Δ culture growth at pH 9. Continuous line marks the beginning fed-batch mode; dashed lines the semi-continuous mode.

Photobioreactor	**RBC**					
Organism	*Stichococcus bacillaris*					
CO_2 - %	5					
initial pH	**3**		**7**		**9**	
I ($\mu E\ m^{-2}s^{-1}$)	250					
X (g L^{-1})	3.42±0.06		4.27±0.55		3.4±0.48	
W_x (mg $L^{-1}\ d^{-1}$)	205		256		204	
Chl a (mg g_{DW}^{-1})	0.79		0.57		2.16	
N conditions	+	-	+	-	+	-
% Lipid (% g g_{DW}^{-1})	28	24	32	40	14	/
% FAME (% g g_{DW}^{-1})	5.5	6.4	14	12	6.2	/

Table 5.2: Steady state data of semi-continuous tests in square bubble column photobioreactors under N sufficient (+) and N starvation (-) conditions.

Table 5.2 reports data measured under steady state conditions of *S. bacillaris* cultures carried out at different pH. The analysis of data reported in the figure 5.3 and table 5.2 points out the following issues:

- *Stichococcus bacillaris* was able to grow in all the investigated pH conditions.
- The cultures grown at pH 3 and at pH 9 achieved a lower biomass concentration than the culture a pH 7.
- The cultures grown at pH 7 achieved the higher biomass concentration during the steady-state at about 4 g L^{-1}.
- The specific biomass productivity (W_X) in the culture grown at pH 3 and 9 was about 200 mg L^{-1} d^{-1}. The cultures grown at pH 7 achieved a biomass productivity about 250 mg L^{-1} d^{-1}.
- The chlorophyll a content was at 2.0 mg g_{DW}^{-1} at the beginning of the experiments. It started to decrease during the semi-continuous mode to a concentration of about 1.5 g L^{-1}. The chlorophyll a content decreased continuously in the cultures grown at pH 3 until it settled down at about 0.7 mg g_{DW}^{-1} during the semi-continuous mode.
- The total lipid fraction achieved its maximum at pH 7 with 40 % under nitrogen starvation.

Table 5.2 regards also data obtained under different pH conditions. Probably not only the total amount of lipid fraction was effected by different pH conditions but also the amount of esterified lipids. The highest amount of total esterified lipids was achieved in cultures grown at pH 7 (about 14 %). The culture grown at pH 3 showed a very low value (about 5.5 %) of esterified lipids.

Test showed that *Stichococcus bacillaris* cells were able to live in a low and high pH environment (about pH 3 and 9). It seems like the effect of pH on total lipid content is acceptable considering that the culture obtained a lipid content of almost 30 %. But consider that the total amount of esterified lipids was very low compared to the value achieved at pH 7. Furthermore, the growth rate was negatively influenced by the low pH.

Microscopic observations of the suspension sampled (Figure 5.4) from cultures at pH 3, 7, 9 pointed out that:

- ✓ at pH=7.0 cells appeared uniform and characterized by high motility;
- ✓ at pH=9.0 the agglomerated cells were: not motile, not uniform in size and shape, typically curved, in some cases very plump;
- ✓ at pH=3.0 the cells were agglomerated, very small, roundish and not motile.

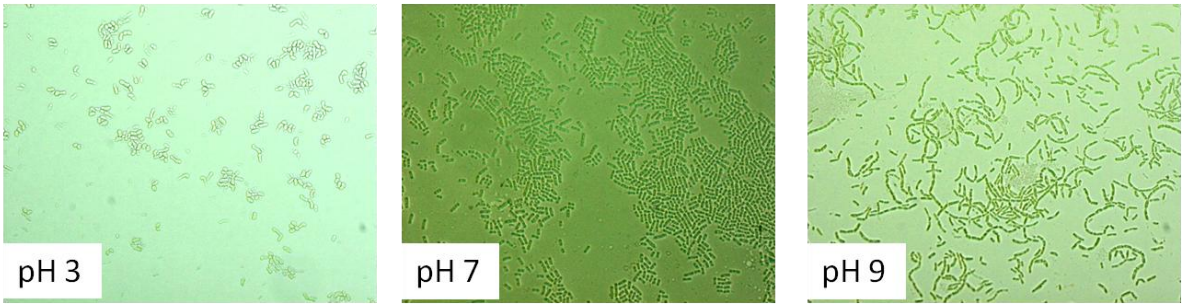

Figure 5.4: Microscopic observation of the cultures carried out at pH=7.0, 3.0 and 9.0.

5.3 Effect of the illumination

✓ Effect of light source

These tests were aimed to assess the effect of light on the *S. vacuolatus* (figure 5.5) and *S. bacillaris* culture (figure 5.6) grown in CBC photobioreactors irradiated continuously at 140 µE m^{-2} s^{-1} with white light or selected red and blue light. The red and blue light were selected because the primary pigment involved in photosynthesis, the chlorophyll a, has strong absorption bands in the regions 400-450 (blue light) and 650-700 nm (red light). The measurements on biomass concentration are reported in grams per litre of culture (g L^{-1}) while the chlorophyll a content in milligrams per grams of biomass dry weight (mg g_{DW}^{-1}).

Figures 5.5 and 5.6 reported data regarding the cultures carried out in CBC photobioreactors. In table 5.3 the results in terms of maximum achieved biomass concentration (X), biomass productivity calculated in steady state condition (W_X), chlorophyll a content (Chl a) and total lipid content (% Lipid) and percentage of esterified lipids (% FAME) were reported.

Photobioreactor	**CBC**							
Organism	*Stichococcus bacillaris*				*Scenedesmus vacuolatus*			
Light	**white**		**red and blue**		**white**		**red and blue**	
CO_2 (%)	2							
pH	7							
I (µE $m^{-2}s^{-1}$)	140							
X (g L^{-1})	2.64±0.5		2.80±0.15		3.46±0.11		2.99±0.10	
W_X (mg$L^{-1}d^{-1}$)	111		111		140		128	
Chl a (mg g_{DW}^{-1})	0.80		1.92		1.11		2.11	
N conditions	+	+	+	+	+	-	+	-
Lipid concentration(% g g_{DW}^{-1})	33	37	38	36	30	25	27	25
FAME concentration(% g g_{DW}^{-1})	7.5	7.7	4.3	8.2	7.3	7.8	5.4	5.3

Table 5.3: Steady state data of semi-continuous tests in square bubble column photobioreactors under N sufficient (+) and N starvation (-) conditions.

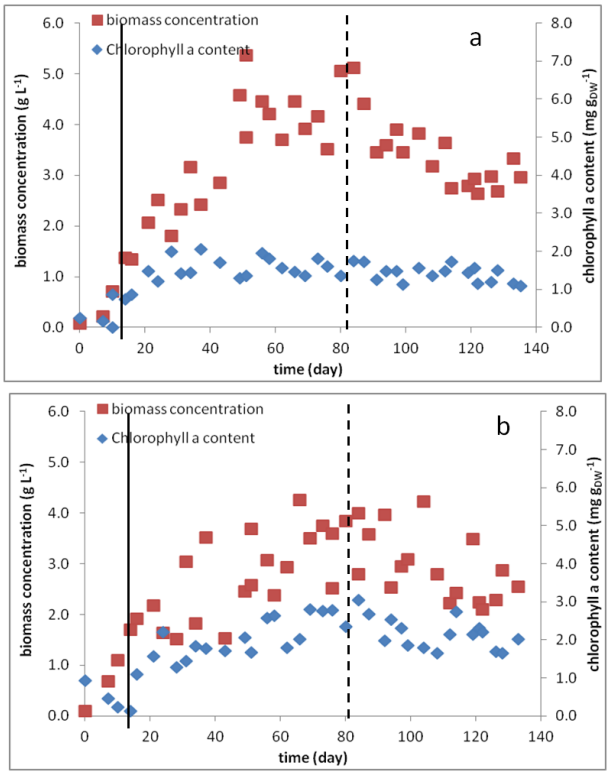

Figure 5.5: Characteristics of a *S. vacuolatus* cultures, illuminated a) with all spectrum and b) with red and blue light; ■ biomass concentration (g L^{-1}), ♦ chlorophyll a (mg g_{DW}^{-1}). Continuous line marks the beginning fed-batch mode; dashed lines the semi-continuous mode.

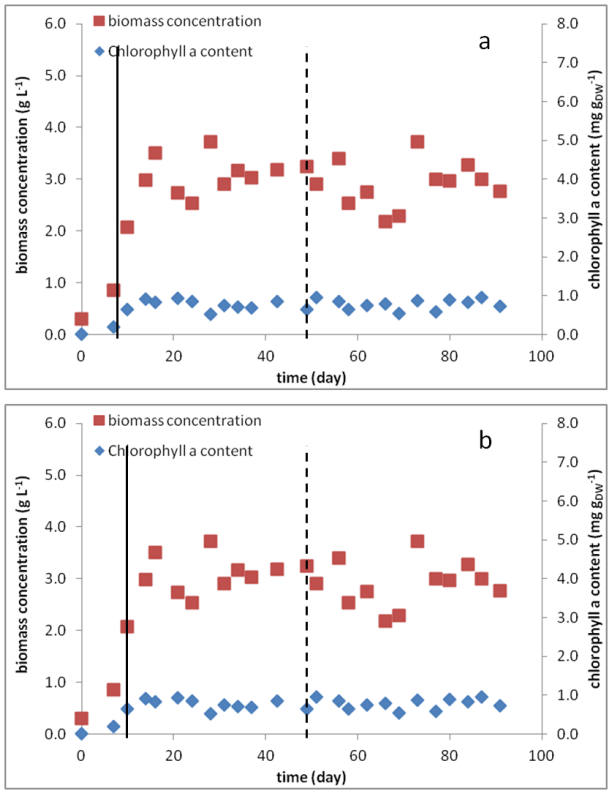

Figure 5.6: Characteristics of a *S. bacillaris* cultures, illuminated a) with all spectrum and b) with red and blue light; ■ biomass concentration (g L^{-1}), ♦ chlorophyll a (mg g_{DW}^{-1}). Continuous line marks the beginning fed-batch mode; dashed lines the semi-continuous mode.

- The biomass productivity resulted equal for both operating conditions and microalgal genus.
- Big difference was observed analyzing the chlorophyll a content, in particular it resulted double in the biomass irradiated with only red and blue light. This is due to the fact that the biomass, acclimatized to the operating condition, increased the chlorophyll a content in order to collect more light. This increase in chlorophyll a content didn't result in higher biomass productivity, probably because the photosynthetic apparatus was already working at maximum rate. Kim et al. (2014) reported the effects of cultivation under monochromatic illumination on the growth and lipid contents of *Nannochloropsis gaditana*. They also reported that no significant difference in growth rates was observed in cultures growth under blue and red light condition. Moreover they observed an increase of photosynthetic oxygen evolution, carbon fixation and nutrient uptake.
- Some significant physiological changes were observed under red than under blue light.

✓ **Effect of light cycle and light intensity**

Illumination is one of the main factor that influence the microalgae growth rate. Therefore, in order to achieve a satisfactory biomass productivity, an efficient use of light must be optimized. In fact, light provides all the energy required to support metabolism, but, if present in excess, it can damage cells, leading to oxidative stress and photoinhibition and thus lower photosynthetic efficiency (Sforza et al., 2014). These tests were aimed to analyze the influence of continuous and sinusoidal light at low and high light intensity on biomass growth rate and biochemical composition of *Scenedesmus vacuolatus* and *Stichococcus bacillaris* species. These tests were conducted growing the biomass in RBC photobioreactors with 5 cm of depth. Figure 5.7 and 5.8 report data obtained per *Scenedesmus vacuolatus* and *Stichococcus bacillaris*, respectively, grown under (a) continuous light and (b) circadian illumination. While, figure 5.9 and 5.10 report data obtained per *Scenedesmus vacuolatus* and *Stichococcus bacillaris*, respectively, grown under (a) 140 µE m^{-2} s^{-1} of continuous light and (b) 250 µE m^{-2} s^{-1} of continuous light.

The influence of continuous illumination and alternation of light and dark cycles and subsequently different light intensities (140 and 250 µE m^{-2} s^{-1}) were investigated using both microalgal species. In order to understand the real effect of the light, all experiments were carried out under a non-limiting CO_2 supply, with CO_2-enriched air bubbled through the culture. In this apparatus, it was measured growth rate, chlorophyll a content and % FAME extracted and transesterified by direct transesterification protocol of *Scenedesmus vacuolatus* and *Stichococcus bacillaris*.

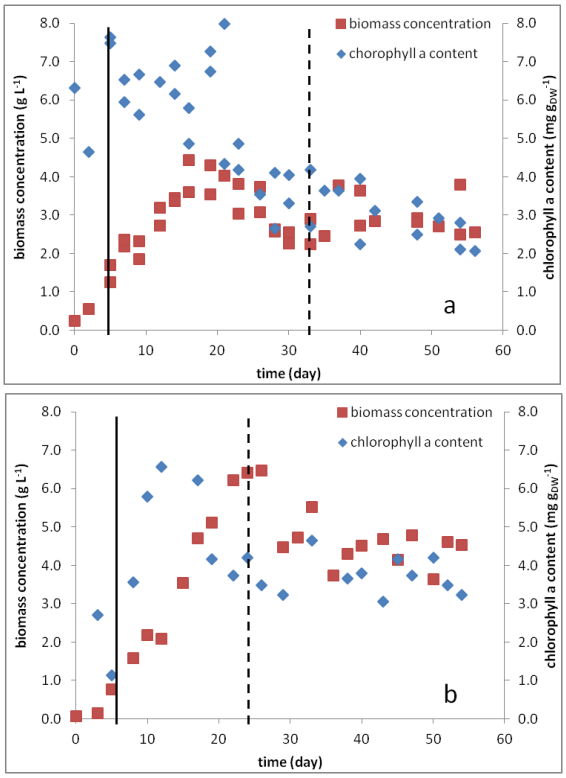

Figure 5.7: Characteristics of a *S. vacuolatus* cultures grown in RBC irradiated under a) 24 h of light and b) 16h light/8 dark; ■ biomass concentration (g L^{-1}), ♦ chlorophyll a (mg g_{DW}^{-1}). Continuous line marks the beginning fed-batch mode; dashed lines the semi-continuous mode.

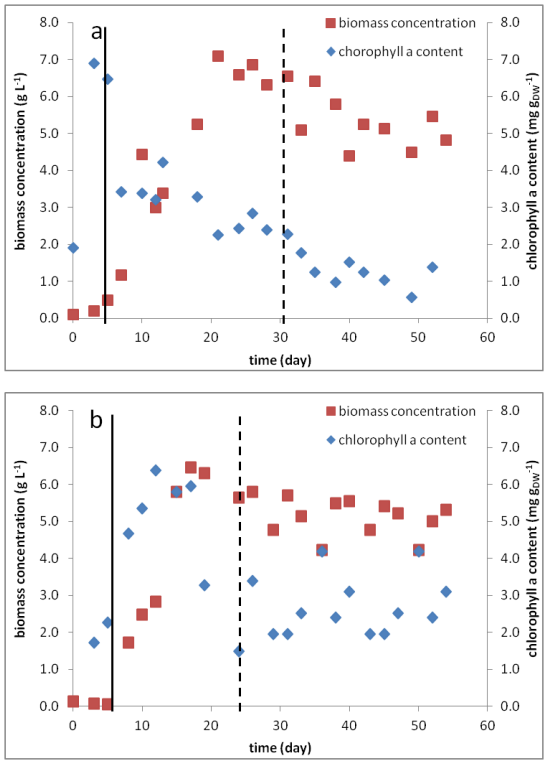

Figure 5.8: Characteristics of a *S. bacillaris* cultures grown in RBC irradiated under a) 24 h of light and b) 16h light/8 dark; ■ biomass concentration (g L^{-1}), ♦ chlorophyll a (mg g_{DW}^{-1}). Continuous line marks the beginning fed-batch mode; dashed lines the semi-continuous mode.

Photobioreactor	**RBC**							
Organism	*Stichococcus bacillaris*				*Scenedesmus vacuolatus*			
Light	**continuous**		**circadian**		**continuous**		**circadian**	
CO2 (%)	2							
pH	7							
I (µE $m^{-2}s^{-1}$)	140							
X (g L^{-1})	5.47±0.24		5.29±0.14		3.13±0.35		4.94±0.28	
[X] (mg$L^{-1}d^{-1}$)	235		227		140		212	
Chl a (mg g_{DW}^{-1})	1.34		2.73		2.45		3.7	
N conditions	+	-	+	-	+	-	+	-
% FAME (% g g_{DW}^{-1})	13	12	14	17	6.4	5.9	6.2	6.3

Table 5.4: Steady state data of semi-continuous tests in square bubble column photobioreactors under N sufficient (+) and N starvation (-) conditions.

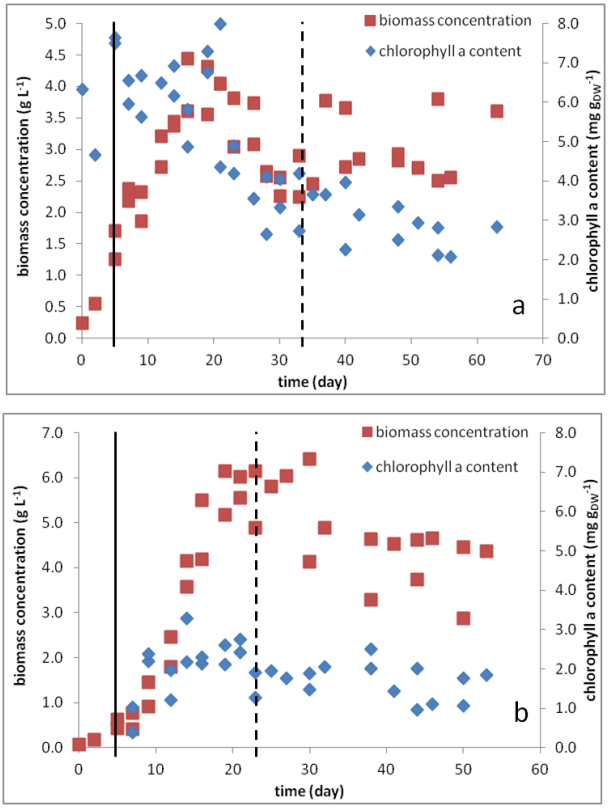

Figure 5.9: Characteristics of a *Scenedesmus vacuolatus* culture running through batch, fed-batch and semi-continuous conditions, grown in RBC irradiated in continuous light a) at 140 µE m^{-2} s^{-1} and b) at 250 µE m^{-2} s^{-1}; ■ biomass concentration (g L^{-1}), ♦ chlorophyll a (mg g_{DW}^{-1}). Continuous line marks the beginning fed-batch mode; dashed lines the semi-continuous mode.

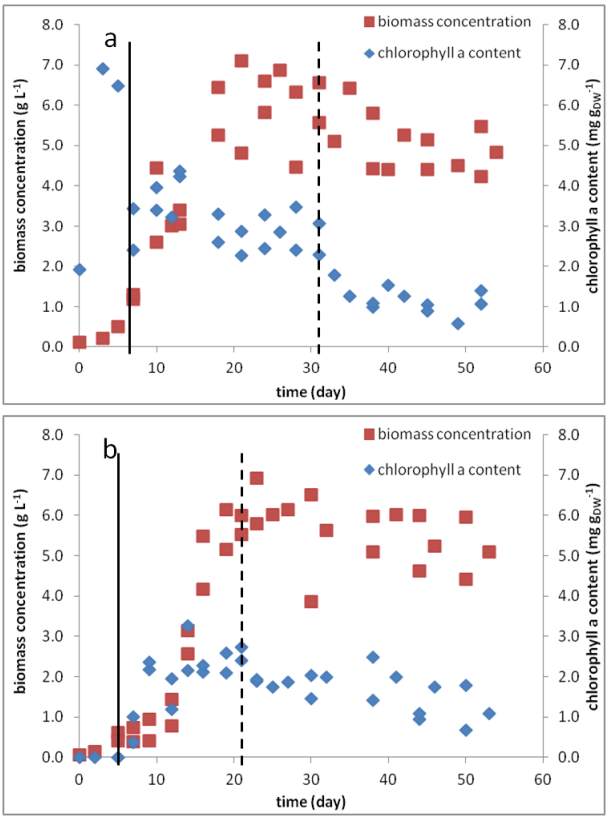

Figure 5.10: Characteristics of a *Stichococcus bacillaris* culture running through batch, fed-batch and semi-continuous conditions, grown in RBC irradiated in continuous light a) at 140 µE m^{-2} s^{-1} and b) at 250 µE m^{-2} s^{-1}; ■ biomass concentration (g L^{-1}), ♦ chlorophyll a (mg g_{DW}^{-1}). Continuous line marks the beginning fed-batch mode; dashed lines the semi-continuous mode.

Photobioreactor	**RBC**							
Organism	*Stichococcus bacillaris*				*Scenedesmus vacuolatus*			
Light	continuous							
CO2 (%)	2							
pH	7							
I (µE $m^{-2}s^{-1}$)	**140**		**250**		**140**		**250**	
(g L^{-1})	5.47±0.24		4.87±0.7		3.13±0.35		3.57±0.8	
W_X (mg$L^{-1}d^{-1}$)	235		209		140		153	
Chl a (mg g_{DW}^{-1})	1.34		1.24		2.45		1.64	
N conditions	+	+	+	+	+	-	+	-
% FAME (% g g_{DW}^{-1})	13	12	14	13	6.4	5.9	4.8	7.2

Table 5.5: Steady state data of semi-continuous tests in RBC photobioreactors under N sufficient (+) and N starvation (-) conditions.

- The species didn't show a higher growth rate at 250 µE m^{-2} s^{-1}. Probably, at this value the growth was inhibited, while the algae was found still able to exploit light, even if at lower efficiency.

- Both strains showed a decreased pigment content during the tests.
- The resistance of the species to prolonged time of irradiances was confirmed in the experiment with continuous light, where microalgae were able to adapt to continuous illumination.
- In addition, the lipid content was not affected by the variation light intensity and light cycle, making this species suitable to industrial application.

5.3 Effect of photobioreactor design

✓ **Geometry**

The results and observations of the performed tests (tables 5.1 and 5.2) were used to compare algal growth and also biomass composition in different reactor shapes, but under same cultivating conditions. CBC photobioreactors, and RBC photobioreactors, respectively, were operated with 5 % additional CO_2 to the air and a pH of about 7. The reactors followed a stepwise operation method (batch, fed-batch, and semi-continuous mode). Table 5.6 reports data in steady state for the culture of *Stichococcus bacillaris.*

Organism	*Stichococcus bacillaris*			
Photobioreactor	**RBC**		**RBC**	
CO_2 (%)	5			
pH	7			
I (µE $m^{-2}s^{-1}$)	140			
X (g L^{-1})	2.48±0.35		4.27±0.5	
W_X (mg$L^{-1}d^{-1}$)	104		256	
Chl a (mg g_{DW}^{-1})	0.30		0.57	
N conditions	+	+	+	-
% Lipid (% g g_{DW}^{-1})	34	27	32	40
% FAME (% g g_{DW}^{-1})	5.2	7.9	14	12

Table 5.6: Steady state data of semi-continuous tests in RBC photobioreactors under N sufficient (+) and N starvation (-) conditions.

The culture grown in the RBC photobioreactor achieved the highest biomass concentration with a value about 4.27 g L^{-1}. In contrast the culture in the CBC photobioreactor obtained the highest chlorophyll a content at about 0.57 mg g_{DW}^{-1}. Table 5.6 reports data concerning biomass and cell composition at semi-continuous mode in both reactor shapes.

Reactor shape may have an influence on the growth rate and the composition of microalgal cells. Possible reason could be the effect of shear stress and the impact of light limitation due to the reactor design. Microalgal cultures obtained their maximal biomass concentration at a defined value

although enough nutrients were accessible in the medium. The biomass productivity could be an indicator for a light limitation due to the fact that it was approximately the same value in all CBC photobioreactors. For example, at an optical density of 4 only 0.018 % of incident light passes through the first centimetre of algal culture. A much higher optical density than 4 was achieved during the tests. So, almost all the light was absorbed by the cells at the surface area without entering the centre of the reactors. A possibility to offer light also to inner layers would be an increase of light intensity. Optimizing the reactor shape would be another method. The biomass productivity at pH 7 and with 5% CO_2 was higher in the square bubble column photobioreactors than in the vertical bubble column photobioreactors for both microalgal species. Probably the differential reactor shape and a better mixing mode were reasons for a higher biomass concentration (figure 5.11). Microalgal cells passed the light irradiation about every 2-3 seconds in the inclined square bubble column photobioreactors. The algal cells, which were grown in the vertical bubble column photobioreactors, probably spent more time (minutes) in the dark layer in the centre of the photobioreactors, where no light enters (Olivieri et al., 2013; 2014).

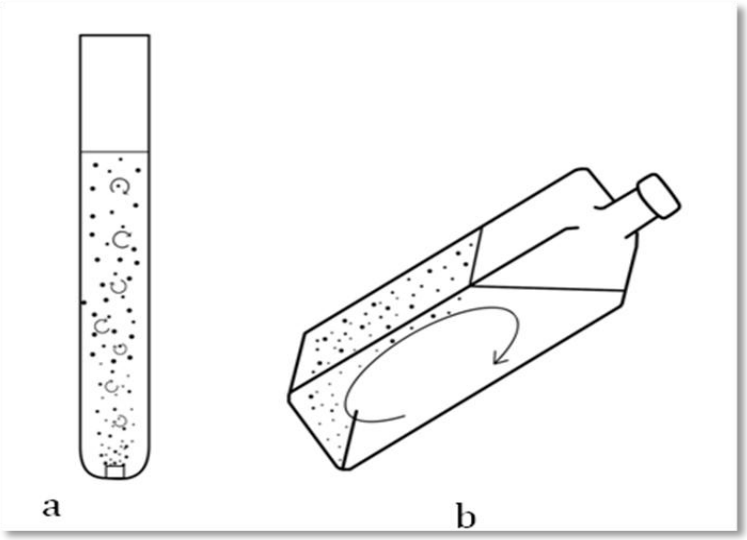

Figure 5.11: Schematic overview of the different reactor shapes and their bubbling mechanisms. The CBC photobioreactor: a) produces much turbulence, also in the middle of the reactor where the light is completely missing. An overall mixing takes place but needs more time compared to the RBC photobioreactors, b) which generate a gentle mixing. Shear stress due to the bubbling could be another influence for the microalgal growth rate.

Figure 5.11 illustrates the mixing mode. The RBC photobioreactors provided a carefully mixing without a lot of turbulences. The biomass constantly circled in one direction. Bubble size and strength of mixing seemed to be almost insignificant due to the soft stirring. In contrast the CBC photobioreactors generated much turbulence with different size bubbles. The airstream went

through the reactor distributing bubbles all over the liquid volume. Strong turbulences occurred everywhere inside the culture.

✓ **Effect of photobioreactor depth**

The next step regards the effects of reactor design on biodiesel production and *Stichococcus bacillaris* (figure 5.12). The attention was focused on the effects of the depth of subhorizontal flat photobioreactors on the performances of continuous cultures. Two square shape columns were investigated of depth 5 and 8 cm. Tests were carried out at 23°C and pH 7. The continuous irradiance level was set at 250 µE m^{-2} s^{-1}, gas flow rate at 0.5 vvm, CO_2 concentration in the gas stream set at 2%v. Figures 5.11 reports data regarding two tests carried out in RBC photobioreactors (a) of 5 cm of depth and (b) with 8 cm of depth, respectively.

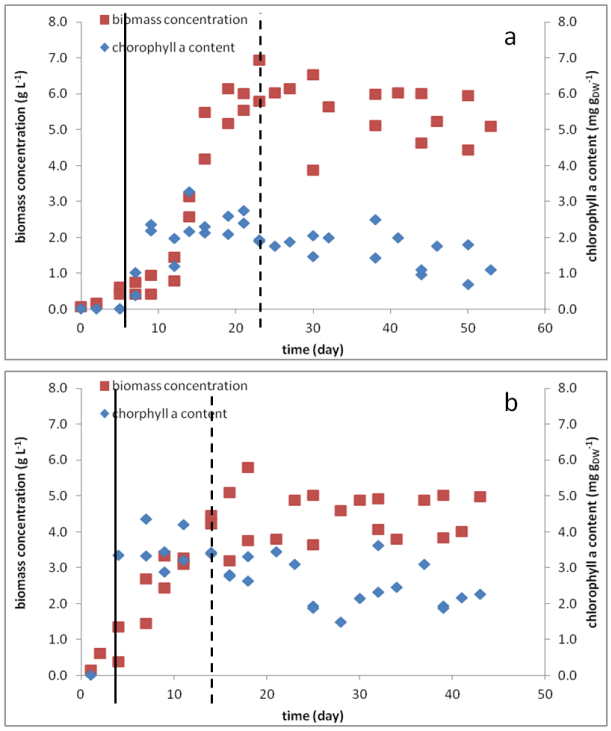

Figure 5.12: Characteristics of a *Stichococcus bacillaris* culture running through batch, fed-batch and semi-continuous conditions, grown at 250 µE$m^{-2}s^{-1}$ a) in RBC with 5 cm of depth and b) in RBC with 8 cm of depth; ■ biomass concentration (g L^{-1}), ♦ chlorophyll a (mg g_{DW}^{-1}). Continuous line marks the beginning fed-batch mode; dashed lines the semi-continuous mode.

Table 5.7 reports the results of tests in terms of concentration of biomass (g L^{-1}), chlorophyll a content (g g_{DW}^{-1}), volumetric biomass productivity (mg L^{-1} d^{-1}) and areal biomass productivity (mg m^{-2} d^{-1}) assessed for test under steady state. The % of identified FAME per gram of dry matter is also reported.

Photobioreactor	5 cm of depth				8 cm of depth			
organism	*Stichococcus bacillaris*							
pH	2							
I (µE $m^{-2}s^{-1}$)	250							
CO_2 (%)	2							
X (g L^{-1})	5.00		4.99		5.83		5.12	
W_X (mg $L^{-1}d^{-1}$)	215				230			
A_X (mg m^{-2} d^{-1})	0.0125				0.023			
Chl a (mg g_{DW}^{-1})	0.46		0.49		0.23		0.24	
N conditions	+	-	+	-	+	-	+	-
FAME biomass^{-1} (% g g_{DW}^{-1})	6.01	6.06	4.99	7.07	5.54	9.79	5.57	12.02

Table 5.7: Steady state data of semi-continuous tests in RBC photobioreactors under N sufficient (+) and N starvation (-) conditions.

It is interesting to note that under steady state conditions, the biomass concentration (X) and the biomass productivity W_X were about constant with the photobioreactor depth of 5 and 8 cm: about 5.0 g L^{-1} and 0.24 g L^{-1} d^{-1}, respectively. On the contrary, chlorophyll a content and biomass superficial productivity changed with the biomass depth. The chlorophyll a content decreased with the photobioreactor depth from 0.48 mg g^{-1} (5 cm depth) to 0.23 mg g^{-1} (8 cm depth). Accordingly, the biomass superficial productivity (A_X) increased with the photobioreactor depth from 0.0125 g m^{-2} d^{-1} (5 cm depth) to 0.023 g m^{-2} d^{-1} (8 cm depth). No real difference was observed in terms of percentage of transesterified lipids under nitrogen sufficient conditions. The effects of the photobioreactor depth deserve some considerations. The microalgal productivity was about constant with the depth and the chlorophyll content decreased with the depth. The first issue suggests that the reaction volume of the inclined column photobioreactor was exploited with the same efficiency for both depths. However, the microalgal concentration was sufficiently high to affirm that the light decay rapidly within the photobioreactor and just a few mm layer close to the exposed surface should be under sufficient irradiated source. It may infer that the frequency of microalgae turnover at the irradiated surface was sufficient to expose microalgae at the light source at sufficient frequency and period. It is known that chlorophyll a content of numerous algae is inversely proportional to the light intensity during growth (Algal physiology and biochemistry, ed. W.D.P. Stewart, 1974, University of California Press). The strong reduction of chlorophyll a content observed in 8cm-depth photobioreactors could be due to the more frequent exposition of algal cells to the light source.

✓ **Effect of outdoor circadian cycle**

To reduce the biodiesel production costs is essential to use outdoor cultivation in open systems, but the main problem associated with this type of cultivation is the contamination of the culture by other

algal species Moreover, during outdoor culture with solar energy as the light source, the biomass productivity is strongly affected by environmental factors such as irradiation and temperature. These tests reports the results of outdoor cultures of *Scenedesmus vacuolatus* strain in thermostated RBC. The reactors were inclinated at 45°, so they were characterized by 250 cm^2 irradiated surface. Cultures were carried out outdoor: i) a test campaign during the May-July 2012 period under shadow conditions and direct sun light, irradiance maximum of 450 µE m^{-2} s^{-1}; ii) a test campaign during the May-July 2013 period under direct sun light, irradiance maximum and 2100 µE m^{-2} s^{-1}; iii) a test campaign during the September-November 2013 period under direct sun light, irradiance maximum of 2000 µE m^{-2} s^{-1}; iv) a test campaign during the June-July 2014 period under direct sun light, irradiance maximum of 2000 µE m^{-2} s^{-1}. Cultures were operated under fed-batch or semi-continuous mode. Harvested microalgae were processed in order to characterize the methyl-ester distribution of transesterified lipid. Figure 5.13 reports the light intensity and temperature profile of summer 2014.

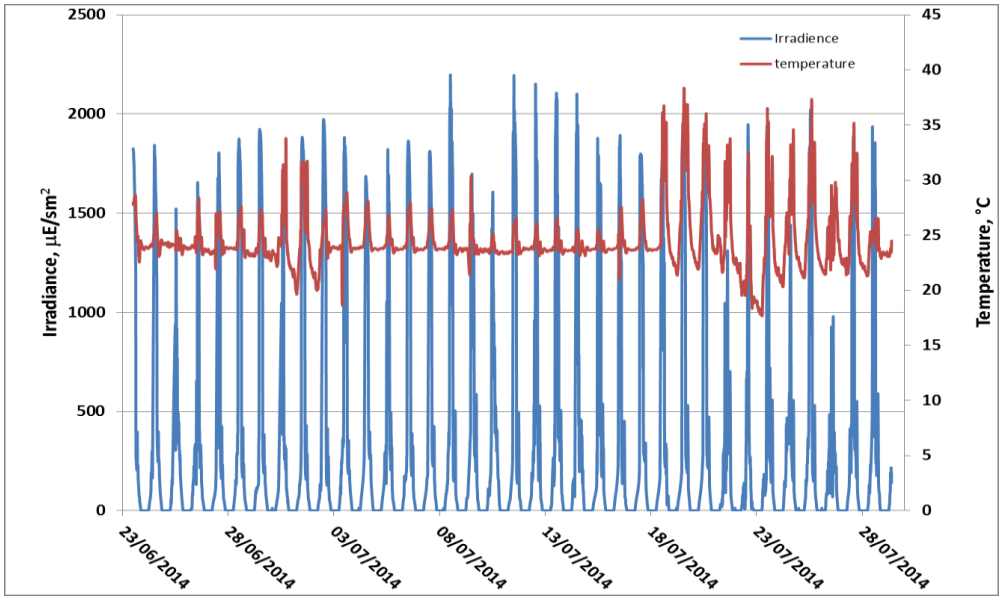

Figure 5.13: Profile of the light intensity and temperature during summer 2014.

The analysis of the results shows that *S. vacuolatus* was able to grow under all investigated conditions. The pH measured during tests was steady at 7 as a result of the equilibrium between acid action of the dissolved CO_2 and the buffer action of the carbonate/bicarbonate system. Except for summer 2014, a very slight increase in biomass productivity from 0.12 to 0.13 g L^{-1} d^{-1} and chlorophyll a content from 4.9 to 5.1 mg g_{DW}^{-1} may be observed under direct sunlight conditions. The invariance of the biomass productivity rate may be interpreted considering that the basis of algal biomass production is directly proportional to the efficiency of photosynthesis. When the light intensity is very high, photosynthesis become less efficient (Camacho Rubio et al., 2003). Probably, the considered irradiance are very high and the photosynthesis is jet inhibited under these conditions

(Chisti 2007). The fraction of FAMEs – a relevant feature for biodiesel application – was characterized. No very differences in terms of percentage of identified FAMEs were observed in all outdoor considered conditions. As regard the lipid composition methyl-oleate, linoleate, linolenate and elaidate were the identified chemicals present at the highest concentrations in FAME mixture. Results of the microalgal characterization under steady state in outdoor conditions are reported in table 5.8.

Photobioreactor	RBC			
organism	*Scenedesmus vacuolatus*			
pH	7			
year	**summer 2013**		**winter 2013**	**summer 2014**
irradiance condition	**Shadow condition**	**Direct sunlight**	**Direct sunlight**	**Direct sunlight**
max I (µE $m^{-2}s^{-1}$)	**450**	**2100**	**2000**	**2100**
CO_2 (%)	2			
X (g L^{-1})	2.9	3.1	3.2	2.4
W_X (mg L^{-1} d^{-1})	124	133	137	103
Chl a (mg g_{DW}^{-1})	4.94	5.11	5.12	2.1
N conditions	+	+	+	+
% FAME (% g g_{DW}^{-1})	4.80	4.20	6.42	/

Table 5.8: Results of tests in terms of average biomass concentration (X), chlorophyll a content (Chl A), biomass productivity (W_X) assessed for each steady state.

RESULTS: BIOMASS GROWTH CHARACTERIZATION

6.1 Microalgal growth in flat photobioreactor under turbidostat control

The investigation on *Nannochloropsis sp*. growth was carried out in the flat photobioreactor equipped with turbidostat described in the section 4.2. Tests were carried out sparging 1% CO_2 supplemented air at 27 °C. The volumetric flow rate of the medium fed to the reactor (table 4.1) was controlled to kept the biomass concentration of the suspension in the photobioreactor at 1.5 g_{DW} L^{-1}. Two irradiation strategies were investigated to simulate a typical summer day in the Netherlands: "constant irradiance day/night cycle" 16 h at 600 µE m^{-2} s^{-1} and 8 h of dark (figure 6.1a); "circadian cycle") 16 h of irradiation at intensity characterized by time-sinusoidal path and maximum of 1500 µE m^{-2} s^{-1} and 8 h of dark (figure 6.1b). The integral of the irradiance over the day was constant in both investigate strategies: 35 E m^{-2}. The light was switched on at 6:00 and turned off at 22:00.

The specific growth rate of microalgae under turbidostat operating condition was calculated according to the relationship:

$$\mu = D = \frac{\Delta V}{t}\frac{1}{V_{PBR}}[=]\, d^{-1} \qquad [6.1]$$

Figure 6.1 shows the time resolved measurements of the irradiance and of the dilution rate under steady state conditions for the two irradiation strategies. Data of the dilution rate are averaged over a couple of weeks. With reference to the test carried out under:

- ✓ "constant irradiance day/night cycle" (figure 6.1a), the specific growth rate: i) was equal to zero when the light irradiance was equal to zero; ii) started to increase after about one hour from the light switch on and approached a constant value within three hours; iii) was almost constant for about five hours; iv) then decreased even though the irradiance was constant and larger than zero; v) approached zero in about one hour after light switch off.
- ✓ "circadian cycle" (figure 6.1b), the specific growth rate: i) was equal to zero when the light irradiance was equal to zero; ii) increased very fast after about one hour from the light switch on, and – except for a underdamped behaviour - approached a constant value within three hours; iii) was almost constant for about five hours, iv) then decreased even though the irradiance was constant and larger than zero; v) approached zero just after light switch off.

The day-averaged specific growth rate of the biomass was 0.52 and 0.46 day^{-1} for the "constant irradiance day/night cycle" and "circadian cycle", respectively.

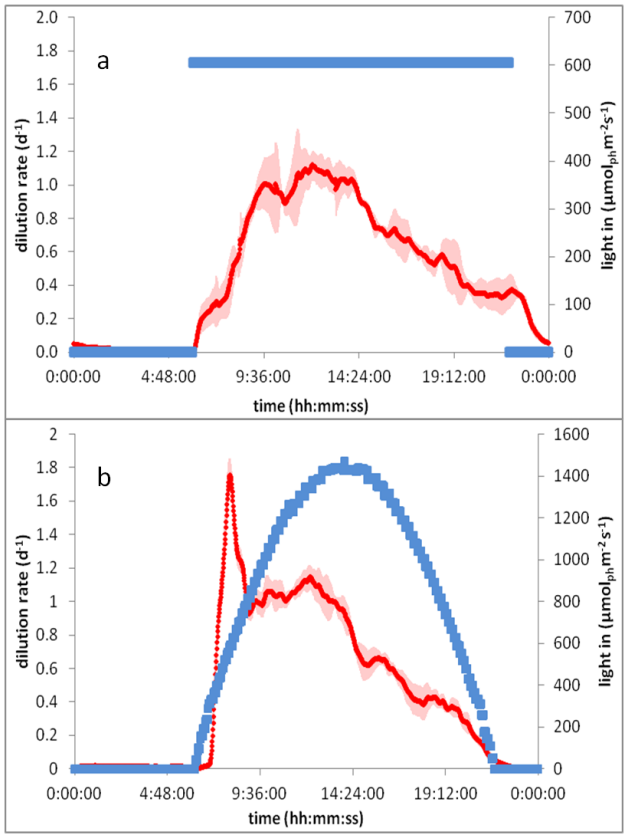

Figure 6.1: Light intensity and growth rate of *Nannochloropsis sp*. grown in flat photobioreactor under turbidostat condition: a) "constant irradiance day/night cycle"; b) "circadian cycle".

The health of the cells was characterized in terms of the maximum quantum yield (measured by Aquapen AP 100, photon systems instruments) of the biomass (figure 6.2). The high level of irradiance and the low biomass concentration (1.5 g L^{-1}) in the photobioreactor are responsible of the very low value of the maximum quantum yield assessed for both tests. The maximum quantum yield was almost constant under "constant irradiance day/night cycle" conditions for all the day. The maximum quantum yield was function of the day time under "circadian cycle" conditions and it was characterized by a minimum at about after two hours of irradiance peak.

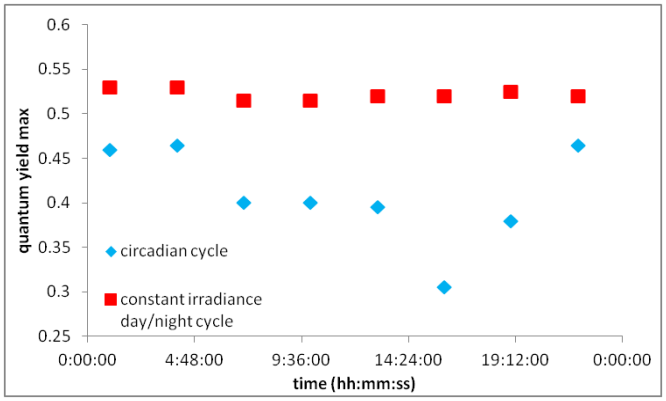

Figure 6.2: Maximum quantum yield of *Nannochloropsis sp*. grown in flat photobioreactor under turbidostat condition: ♦) "circadian cycle"; ■) "constant irradiance day/night cycle".

Measurements were carried out to determine cell size and number during 24 hour cycle. Results are reported in figure 6.3 for “constant irradiance day/night cycle” and figure 6.4 for “circadian cycle”.

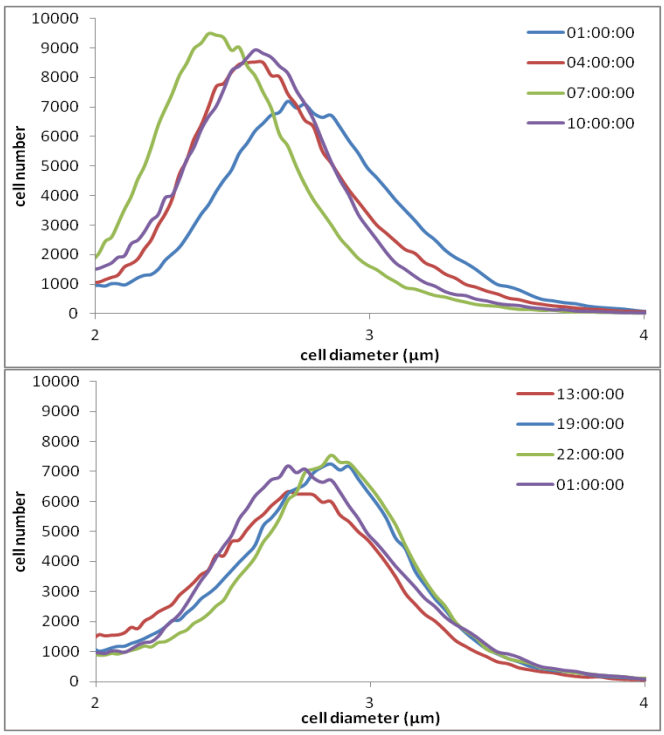

Figure 6.3: Cell number as a function of cell size of samples taken at 1:00, 4:00, 10:00, 13:00, 16:00, 19:00, 22:00 hour of *Nannochloropsis sp*. culture in the flat photobioreactor under turbidostat conditions under “constant irradiance day/night cycle”.

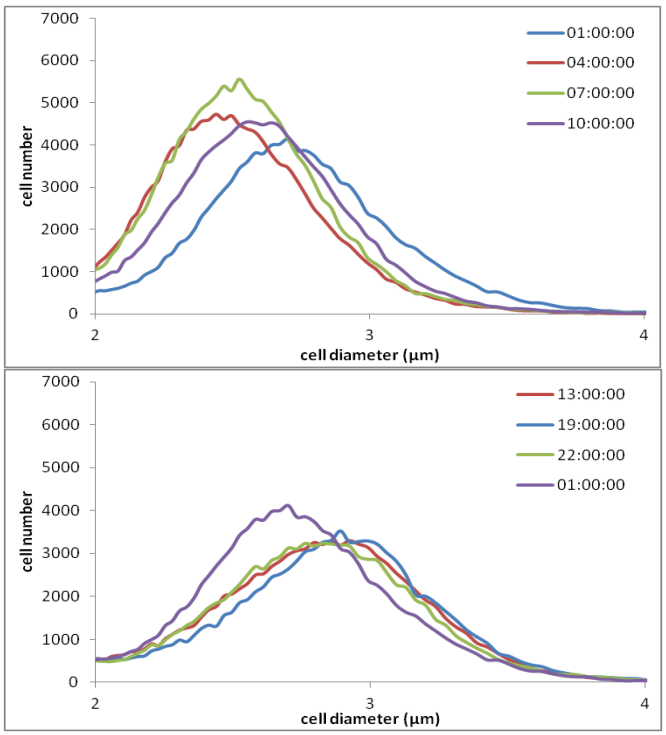

Figure 6.4: Cell number as a function of cell size of samples taken at 1:00, 4:00, 10:00, 13:00, 16:00, 19:00, 22:00 hour of *Nannochloropsis sp*. culture in the flat photobioreactor under turbidostat conditions under “circadian cycle”.

According to the assessed cell population, the cell number decreases during the light period while the cell diameter increases. It may be affirmed that cells are synchronized and all cells divided in one day. In other words, under both operating conditions cell division was synchronized. This finding is in agreement with the observation that the specific growth rate in the day changed even though the irradiance was constant.

The biomass harvested during a 24-hour cycle was characterized in terms of protein, carbohydrate and total fatty acid (TFA) composition (figure 6.5), triacylglycerol (TAG) and polar acyl lipids (figure 6.6), fatty acid profile (figure 6.7), biomass dry weight and supernatant dry weight (figure 6.8). Protein, carbohydrate and TFA content decreased during the night and increased during the day. Results were similar to data obtained for *N. oleoabundas* culture by de Winter at al. (2014). The variation of the protein and carbohydrate concentration was more pronounced than that of TFA concentration. Whatever the component analysed, the concentration value was restored after 24 hours. This observation is in agreement with the results reported by de Winter et al. (2013): they pointed out that the variation of the biomass composition was observed over the 24 hour cycle and that the composition was constant when the sampling was carried out each 24 hours. The TFA content is due to the sum of triacylglycerols (TAG) and acyl lipids content. Analysis of the time-resolved measurements of the TAG and acyl lipids content pointed out a day-cyclic behaviour as shown by TFA. The fatty acid (FA) composition was determined over the 24 hour cycle. In general, C14:0, C16:0, C16:1, C18:1, C18:2 and C20:3 populations are the most relevant. The FA distribution is still characterized by a day-cyclic behaviour. The biomass dry weight increased during the day and decreased during the night. The liquid phase after biomass harvesting by centrifugation was characterized in terms of dry weight. The results points out that some fine materials are present in the liquid phase but it is negligible with respect to the dry biomass concentration and the oscillations over the day are not significant. The main observations are:

- the growth of *Nannochloropsis sp*. in the flat photobioreactor under turbidostat conditions was not constant during the day even though the culture conditions were constant. This finding is in agreement with previous observations reported by de Winter et al. (2013, 2014) for continuous cultures of *N. oleoabundans*;
- the concentration of the main biomass constituents of *Nannochloropsis sp.* increases during the day and the number of cells increases during the night. The observed phenomena are in agreement with those observed for many green microalgae (Lacour et al., 2012; Matsuo et al., 2010; Sukenik and Carmeli, 1990).
- although a day-averaged specific growth was assessed, the instantaneous specific growth rate changes the day.

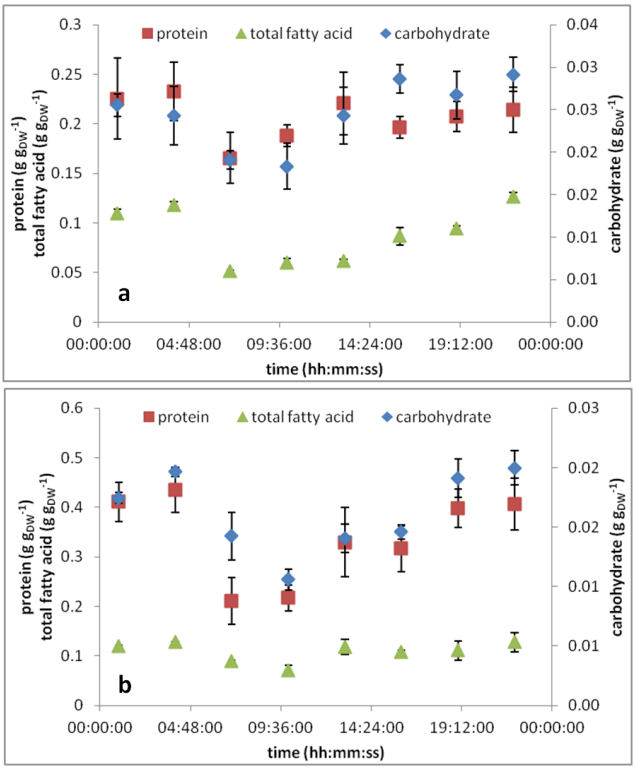

Figure 6.5: Carbohydrate (♦), protein (■) and total fatty acid (▲) content per biomass dry weight in (g g_{DW}^{-1}) of *Nannochloropsis sp*. biomass grown in flat photobioreactor under turbidostat condition: a) "constant irradiance day/night cycle"; b) "circadian cycle".

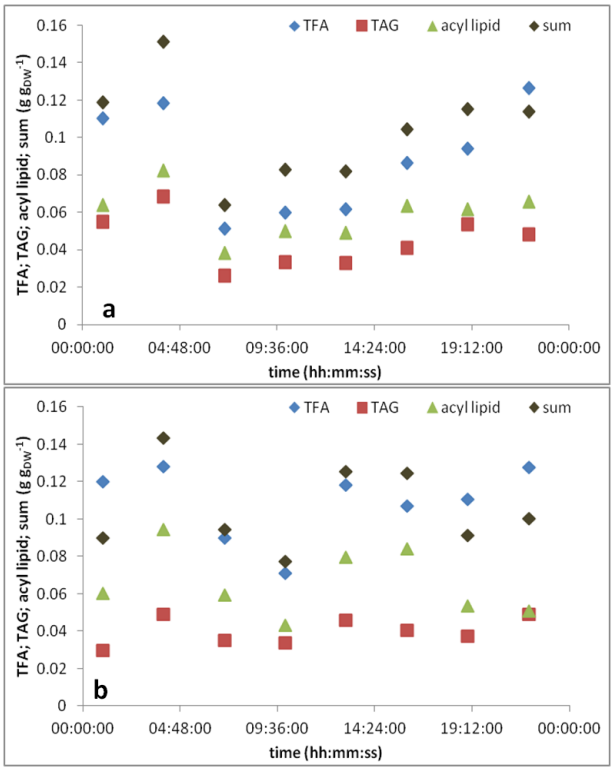

Figure 6.6: Total fatty acid (TFA) (♦), triacylglycerol (TAG) (■), acyl lipid (▲) and sum of TAG plus acyl lipid (♦)content per biomass dry weight in (g g_{DW}^{-1}) of *Nannochloropsis sp*. biomass grown in flat photobioreactor under turbidostat condition: a) "constant irradiance day/night cycle"; b) "circadian cycle".

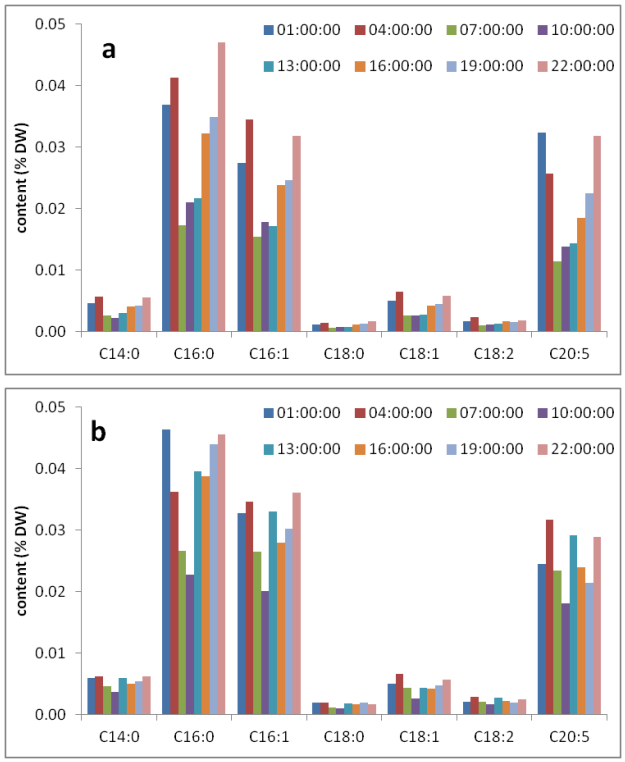

Figure 6.7: Fatty acid (FA) composition of *Nannochloropsis sp*. biomass grown in flat photobioreactor under turbidostat condition: a) "constant irradiance day/night cycle"; b) "circadian cycle".

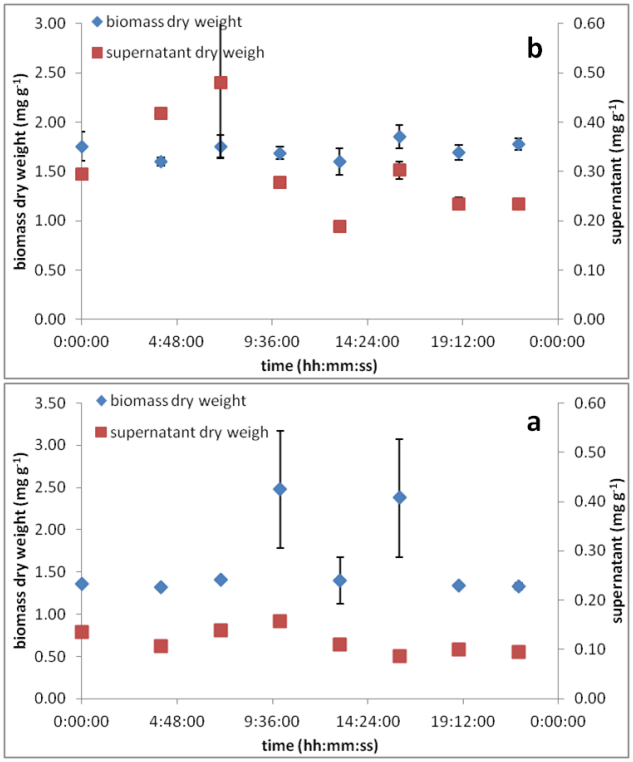

Figure 6.8: Biomass (♦) and supernatant dry weight (■)of *Nannochloropsis sp*. biomass grown in flat photobioreactor under turbidostat condition. Error bars represent standard deviation between triplicate measurements: a) "constant irradiance day/night cycle"; b) "circadian cycle".

The analysis of the reported results suggests that the continuous culture of *Nannochloropsis sp.* in the turbidostat is controlled by the circadian clock of the cells. Assumed that at 4 AM the cell division ended, the dynamics of constituent accumulation depends on the constituents: the protein accumulation starts soon after the end of the cell division, and after about four hours the carbohydrates and TGA accumulate. The observed dynamics is in agreement with finding reported by de Winter at al. (2013) for *N. oleoabundans* cultures and Cuhel et al. (1984) for *Dunaliella tertiolecta* cultures. In particular the reported results confirm the observation of Cuhel et al. (1984) that proteins accumulate until the cell division. Proteins started to be synthesized soon after the cell division to prepare the light harvesting system (e.g. chlorophyll protein complexes). Only when the cell is able to harvest energy, carbohydrate and TFA started to be synthesized.

According to Klok et al. (2013b) the carbohydrates accumulate during the day, moreover they reported that starch synthesis is linked to growth; in this experiment carbohydrate oscillation seems related the biomass light stress for similar growth rate.

6.2 Biomass growth modelling

The phenomena reported and described in the previous section are simulated in the present section according to two models. The first model was from the literature and it is based on the upper pathway of the microalgae. The second model was proposed in the present thesis and it is based on simple kinetics interpreting the reported observation.

6.1.1 The unsegregated and structured model

This model is based on the submodels available in the literature for the upper pathway of the microalgae (figure 6.9). The adopted submodels are typically applied for time-averaged simulations of culture growth (Janssen et al., 2002).

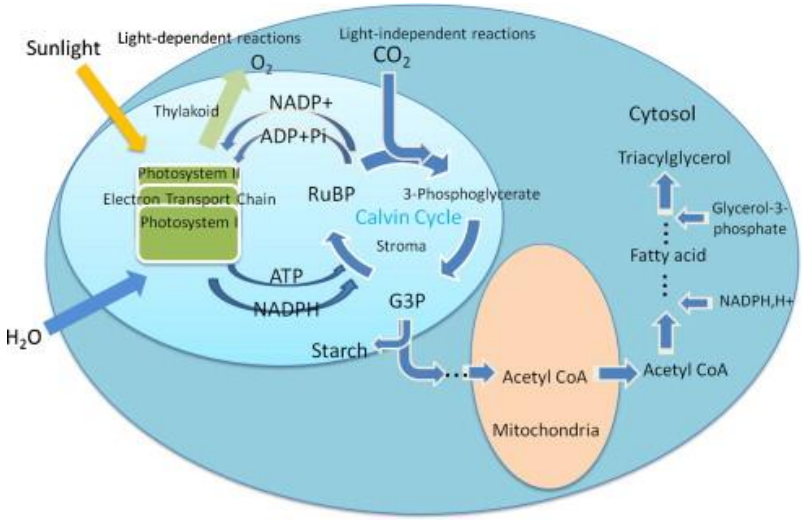

Figure 6.9: A sketch of a microalgal cell

In the chloroplast light energy is absorbed by the pigments of the photosystems. Only photons in the wavelength range of 400 to 700 nm are absorbed (the photosynthetic active radiation, PAR). The energy of the absorbed photons is used to produce NADPH, O_2 and ATP according to the Eq. [6.1]:

$$2\ H_2O + 2\ NADP^+ + \ 3\ ADP + 3\ Pi + photons\ \rightarrow\ O_2 + \ 2\ NADPH + 2\ H^+ + \ 3\ ATP \qquad [6.1]$$

The generated NADPH and ATP are used within the chloroplast to fix CO_2 and to convert it into the building block of sugars (CH_2O) according to eq. [6.2]:

$$CO_2 + \ 3\ ATP + 2\ NADPH + 2\ H^+ \ \rightarrow CH_2O + 3\ ADP + 3\ Pi + 2\ NADP^+ + \ H_2 \qquad [6.2]$$

The CH_2O flows out of the chloroplast and it is processed for the building of microalgal biomass according to the anabolic growth reactions (figure6.10). A fraction of CH_2O is processed in the mitochondria to generate energy as ATP. to drive the growth reactions and to support maintenance reactions.

The stechiometric request of photons needed to drive the reaction [6.1] is 8 photons per one molecule of CH_2O.

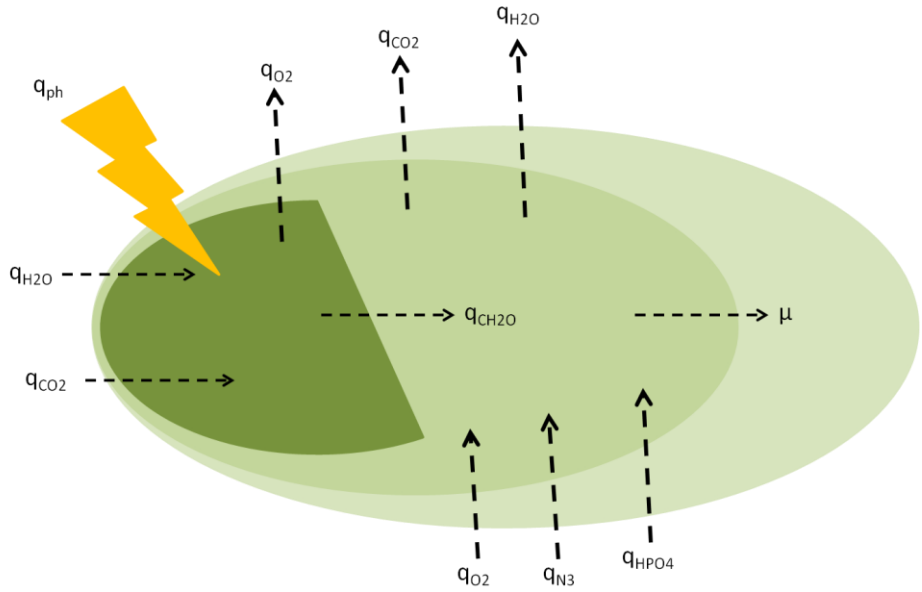

Figure 6.10: Sketch of the main mass flux (q_i, mol·s^{-1}) involved in the microalgal cells.

The stoichiometry of coupled reactions [6.1] and [6.2] suggests the flux relationships reported hereinafter:

$$-q^c_{CO2} = \ -q^c_{H2O} = \ q^c_{CH2O} = \ q^c_{O2} \qquad [6.3]$$

The Pirt's law describes the specific consumption rate of sugar outside of the chloroplast q_{CH2O} (mol_{CH2O} mol_x^{-1} s^{-1}). CH_2O produced by photosynthesis in the chloroplast is equal to the specific sugar consumption rate in the rest of the cell:

$$q^c_{CH2O} = -q_{CH2O} \quad [6.4]$$

Pirt et al. (1980) proposed a relationship between the specific consumption rate of sugar depend, the specific growth rate μ of the microalgae, and the maintenance demand for sugar m_{CH2O}:

$$q_{CH2O} = -\frac{\mu}{Y_{x/CH2O}} - m_{CH2O} \quad [6.5]$$

The maintenance m_{CH2O} depends on the microalgal species and growth conditions. Typical values for microalgae are in the range of 1.9 to 3.5·10-6 mol_{CH2O} mol_x^{-1} s^{-1}.

The specific sugar production rate in the chloroplast q^c_{CH2O} depends on the light intensity $I_{ph,PAR}$. This relationship can be described by the model of Jassby and Platt (1976) based on the hyperbolic tangent function (tanh):

$$q^c_{CH2O} = q^c_{CH2O,m} * \tanh\left(\frac{\alpha * I_{ph}}{q^c_{CH2O,m}}\right) \quad [6.6]$$

where α is a parameter of the Jassby and Platt model and may be calculated according to the Eq. [6.7]:

$$\alpha = Y^c_{CH2O/ph,m} * a_x \quad [6.7]$$

where $Y^c_{CH2O/ph,m}$ is the efficiency of the photosynthesis, a_x the spectrally averaged absorption coefficient.

Equation [6.6] yields:

$$q^c_{CH2O} = q^c_{CH2O,m} * \tanh\left(\frac{Y^c_{CH2O/ph,m} * a_x * I_{ph}}{q^c_{CH2O,m}}\right) \quad [6.8]$$

According to the Eq. [6.8] and the fig. 6.10 $Y^c_{CH2O/ph}$ is expressed as:

$$Y^c_{CH2O/ph} = \frac{q^c_{CH2O}}{-q_{ph}} \quad [6.9]$$

The yield is a measure of the actual conversion efficiency of the light energy by the photosynthesis. As the light intensity I_{ph} approaches 0 mol_{ph} m^{-2} s^{-1} the maximal yield is 0.10 mol_{CH2O} mol_{ph}^{-1}.

As the light intensity increases the yield drops. A fraction of the photons absorbed by the biomass are processed by the photosynthesis. The surplus of photons absorbed by the pigments in the photosystems is dissipated as heat by the photosystem itself. This decrease in the efficiency of photosynthesis at increasing light intensity is called photosaturation. The yield of biomass on photons absorbed can be calculated:

$$Y_{x/ph} = \frac{(q^{c}_{CH2O} - m_{CH2O}) * Y_{x/CH2O}}{-q_{ph}} \quad [6.10]$$

The application of the Eq. [6.8] require the knowledge of the light intensity field in the photobioreactor. Indeed, the light intensity decreases moving inside the photobioreactor (figure 6.11) and the decay depends on the specific absorption coefficient a_x of the microalgae. It is possible assume a plane-light. The law of Lambert-Beer reports the light intensity $I_{ph,\lambda(z)}$ at a given wavelength λ in a suspension as a function of the suspension depth (z) and of the specific absorption coefficient $a_{x,\lambda}$.

$$I_{ph,\lambda}(z) = I_{ph,\lambda}(0) * e^{-a_{x,\lambda} * C_x * z} \quad [6.11]$$

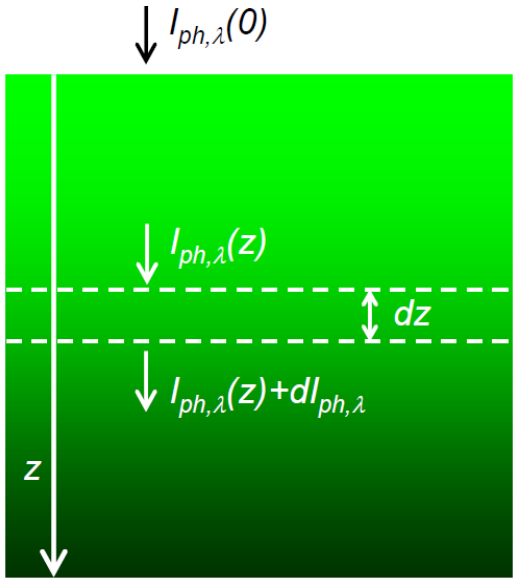

Figure 6.11: Light penetration inside photobioreactor: z=0 is the irradiated surface. A layer at constant irradiance is highlighted.

here the light intensity $I_{ph,\lambda}$ depends on the wavelength-photon flux density:

$$I_{ph,\lambda}(0) = I_{ph}(0) * E_{n,\lambda} \quad [6.12]$$

$I_{ph(0)}$ is the light intensity with reference at the PAR spectrum at the light-exposed surface of the photobioreactor. $E_{n,\lambda}$ is the PAR-normalized spectrum of the light used. The light intensity referred at

the PAR spectrum at a depth z ($I_{ph(z)}$) is the sum of the contributions of all individual wavelengths from 400 to 700 nm. The simplified relationship is:

$$I_{ph}(z) = I_{ph}(0) * e^{-a_x * C_x * z} \quad [6.13]$$

Where:

$$a_x = \sum_{\lambda=400}^{\lambda=700} a_{x,\lambda} * E_{n,\lambda} * \Delta\lambda \quad [6.14]$$

The biomass balance extended to the microalgal cultivation system assumed as a CSTR is:

$$V_R * \frac{dC_x}{dt} = F_{in} * C_{x,in} - F_{out} * C_x + r_x * V_R \quad [6.15]$$

where V_R [m^3] is the liquid volume in the photobioreactor, F_{in} and F_{out} the liquid flow rate [$m^3\ s^{-1}$] fed and withdraw to/from the photobioreactor, C_x [$mol_x\ m^{-3}$] the biomass concentration in the photobioreactor, $C_{x,in}$ [$mol_x\ m^{-3}$] the biomass concentration in the feeding, r_x [$mol_x\ m^{-3}\ s^{-1}$] the volumetric biomass production rate. The r_x is the product of the C_x and the specific growth rate of the microalgae, μ:

$$r_x = \mu * C_x \quad [6.16]$$

$$V_R \frac{dC_x}{dt} = F_{in}C_{x,in} - F_{out}C_x + \mu C_x V_R \quad [6.17]$$

Assuming sterile feeding and steady state conditions, Eq. [6.17] yields:

$$\frac{F_{out}}{V_R} = \mu = D \quad [6.18]$$

The specific growth rate may be expressed in terms of the production rate of sugar building block in the chloroplast:

$$\frac{F_{out}}{V_R} = [(\overline{q^c_{CH2O}} - m_{CH2O})Y_{x/CH2O}] = D \quad [6.19]$$

where $\overline{q^c_{CH2O}}$ is the q^c_{CH2O} averaged over the light path inside the photobioreactor. With reference to the light distribution inside a flat photobioreactor irradiated at the large surface (figure 6.11) the $\overline{q^c_{CH2O}}$ may be assessed according to the Eq. [6.20]:

$$\overline{q^c_{CH2O}} = \frac{\sum_{n=1}^{n=N}\left[q^c_{CH2O,m}\tanh\left(\frac{Y_{CH2O/ph,m}\left(\sum_{\lambda=400}^{\lambda=700}a_{x,\lambda}E_{n,\lambda}\Delta\lambda\right)\left(I_{ph(0)}e^{-a_x C_x z}\right)}{q^c_{CH2O,m}}\right)\right]\frac{d}{N}}{d} \qquad [6.20]$$

The equation [6.19] yields is a CSTR, it is possible write:

$$D = \left(\frac{\overline{\sum_{n=1}^{n=N}\left[q^c_{CH2O,m}\tanh\left(\frac{Y_{CH2O/ph,m}\left(\sum_{\lambda=400}^{\lambda=700}a_{x,\lambda}E_{n,\lambda}\Delta\lambda\right)\left(I_{ph(0)}e^{-a_x C_x z}\right)}{q^c_{CH2O,m}}\right)\right]\frac{d}{N}}}{d} - m_{CH2O}\right)Y_{x/CH2O} \qquad [6.21]$$

The dilution rate simulated according to equation [6.21] assuming the operating conditions set for the tests carried out with the turbidostat is reported in figures 6.12 and 6.13. The first figure refers to the test carried out assuming the "constant irradiation day/night cycle"; the second figure refers to the test carried out assuming the "circadian cycle".

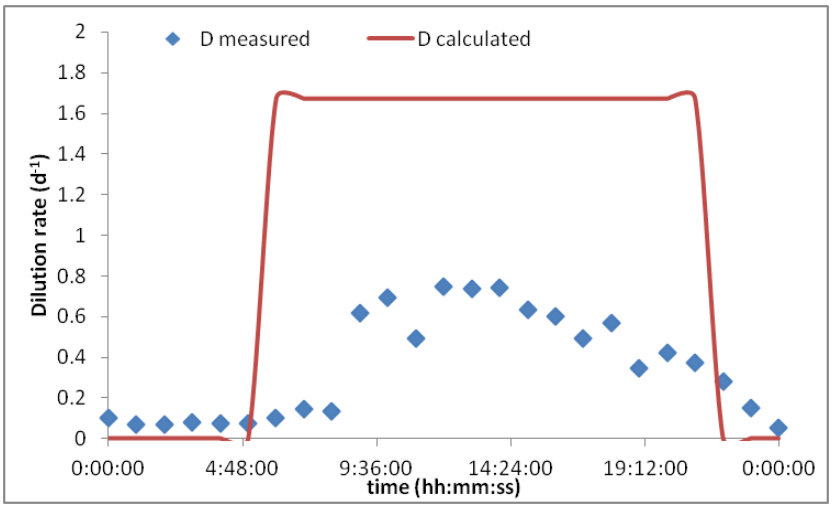

Figure 6.12: Calculated (red line) and measured (blue dot) growth rate for the test under "constant irradiation day/night cycle".

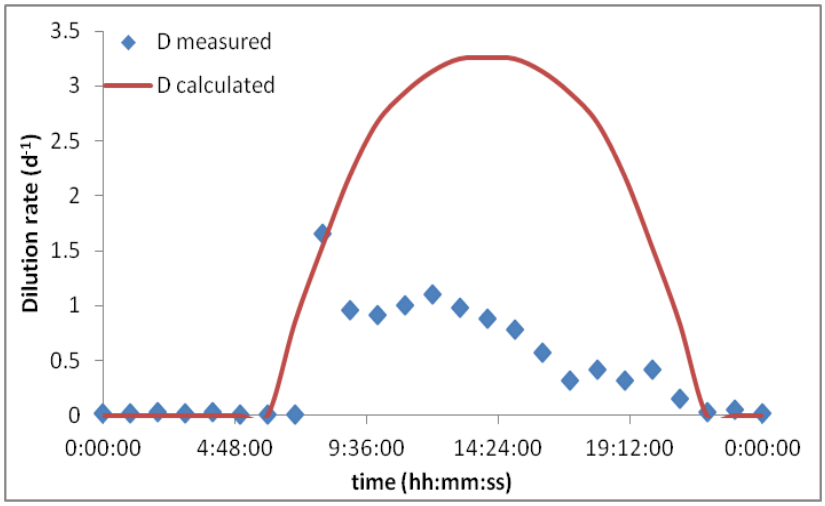

Figure 6.13: Calculated (red line) and measured (blue dot) growth rate for the test under "circadian cycle".

The comparison of the assessed dilution rate with the experimental values is not satisfactory. Indeed, the simulation was not able to return the experimental values. The most relevant result is that the simulation cannot reproduce the variation of the dilution rate during the day. Therefore, a model that take into account the change of the dilution rate – and the specific growth rate – with the time when the irradiance is constant must be introduced.

6.1.2 The empirical unsegregated and unstructured model

The specific growth rate measured during the tests carried out in the turbidostat (Eq.[6.1]) was not constant during the irradiation period even though the irradiance was constant ("constant irradiance day/night cycle"). Figure 6.14 shows a sketch of the dynamics observed during the "constant irradiance day/night cycle" test. The sketched dynamics was repeated each day for about two weeks during the test. The following features have been identified:

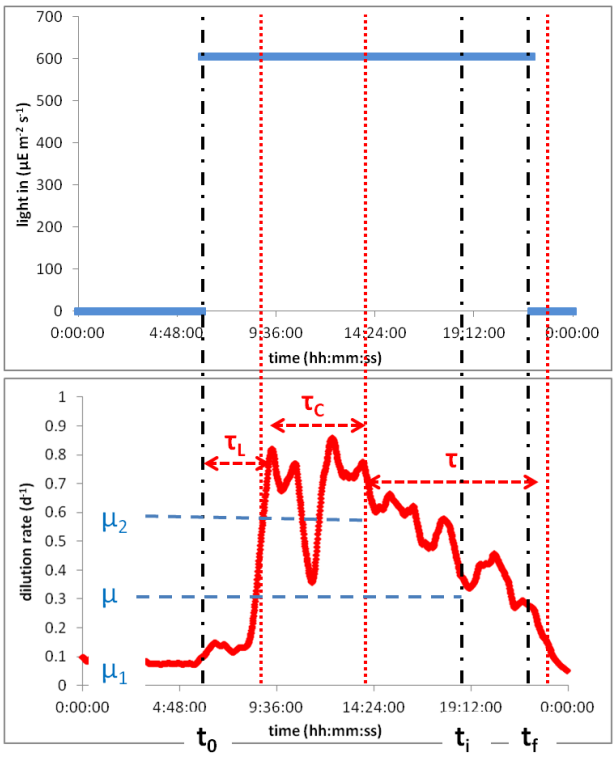

Figure 6.14: Sketch of the dilution rate (specific growth rate) as a function of time during a typical day of continuous culture. Irradiation strategy: "constant irradiation day/night cycle"

t_0 the instant at which the light is switched on;

t_f the instant at which the light is switched off;

τ_L interval time between t_0 and the beginning of the departure of the biomass growth rate from the dark-condition value τ_1 (almost equals to zero in the reported test);

τ_c interval of time during which the specific growth rate is constant and equal to μ_2;

τ interval of time during which the specific growth rate decreases from μ_2 down to μ_1;

t_i the instant at which the specific growth rate is the medium value between μ_2 and μ_1.

The time-resolved measurements of the specific growth rate between μ_2 and μ_1 was described according to the relationship reported in Eq. [6.22]. The relationship was able to report a smooth fit of the limiting case of low and high specific growth rate.

$$\ln\frac{\mu-\mu_1}{\mu_2-\mu} = -\frac{1}{\tau}(t-t_i) \qquad [6.22]$$

The specific growth rate may be expressed as a function of the time by processing the Eq. [6.22] and it was:

$$\mu = \frac{\mu_2 e^{-\frac{1}{\tau}(t-t_i)} + \mu_1}{1+e^{-\frac{1}{\tau}(t-t_i)}} \qquad [6.23]$$

The analysis of the time-resolved measurements of the dilution rate measured during the "constant irradiation day/night cycle" test allowed to assess the parameters of the Eq. [6.23]. The parameters are reported in table 6.1.

μ_1 (d^{-1})	μ_1 (d^{-1})	t_0 (h)	t_f (h)	t_i (h)	τ_L (h)	τ_C (h)	τ_L (h)
0.040	1.00	6:00	22:00	18:40	2.30	5.00	9.00

Table 6.1: Time characteristics of the time-resolved measurement of the D vs. time assessed during the continuous test in turbidostat adopting the "constant irradiation day/night cycle".

Figure 6.15 reports the time-resolved measurements of the dilution rate and the plot of the Eq. [6.23] using parameters reported in table 6.1; the time is expressed in day. The instant zero is $t_0+\tau_L$. The agreement between the experimental data and the result of the interpolating relationship is satisfactory.

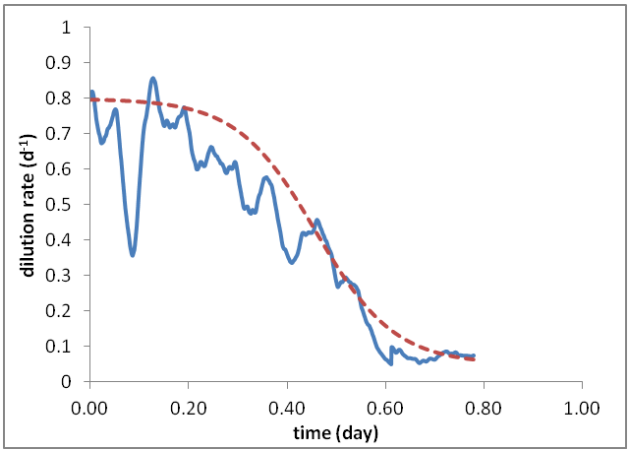

Figure 6.15: Specific growth rate measured (blue line) and from Eq. [6.23] (red dashed line) for the test at "constant irradiation day/night cycle".

The interpolating model Eq. [6.23] may be used to simulate the variation of the specific growth rate during a day provided the light cycle.

The parameters assessed during the tests "constant irradiation day/night cycle" (table 6.1) were assumed as features of the investigated microalgae except for μ_2. The maximum growth rate was assumed as a function of the light intensity according to the Monod kinetic (Molina Grima et al., 1994, 1999; Garcia-Malea et al., 2005; Concasa et al., 2010; Pegallapati et al., 2012):

$$\mu_2 = \frac{\mu_{max} I}{K_I + I} \qquad [6.24]$$

where μ_{max} is the maximum growth rate and K_I the light intensity at half the μ_{max}. The parameters of Eq. [6.24] assessed by Pegallapati et al. (2012) for *Nannochloropsis salina* were used for the simulations: μ_{max} =1.2 d^{-1}, K_I=181 µE m^{-2} s^{-1}.

The assessment of the specific growth rate as a function of the light cycle was carried out according to the following conditions:

$t \le t_0 \Rightarrow I = 0 \Rightarrow \mu = \mu_1$

$t > t_0 \Rightarrow I > 0 \Rightarrow \quad t < t_0 + \tau_L \Rightarrow \mu = \mu_1$

$t > t_0 + \tau_L \Rightarrow \mu = \mu\,(t, I(t))$ from Eq. [6.24] combined with Eq. [6.23]

The figure 6.16 reports the time-resolved measurements of the dilution rate and the plot of the Eq. [6.23] combined with Eq. [6.24] using parameters reported in table 6.1; the time is expressed in day. The instant zero is 0.00 AM. The agreement between the experimental data and the result of the interpolating relationship is satisfactory. It is note to worth that no fitting data was used for the plot of figure 6.16.

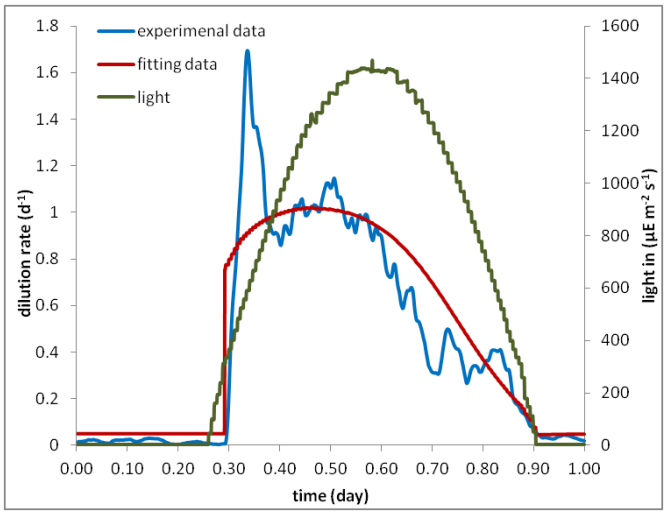

Figure 6.16: Specific growth rate measured (blue line) and from Eq.s [6.23] and [6.24] (red dashed line) for the "circadian cycle" test.

RESULTS: PHOTOSYNTHESIS CHARACTERIZATION

The kinetic model and the assessment procedure of the photochemical process are reported hereinafter. The equation set [7.1] through [7.4] derives from the model proposed by Eilers and Peeters (1988) (figure 2.4). It describes the behavior of reaction centres involved in the photochemical processes (see also figure 2.5):

$$\frac{dx_1}{dt} = -\alpha I x_1 + \gamma x_2 + \delta x_3 \quad [7.1]$$

$$\frac{dx_2}{dt} = \alpha I x_1 - \gamma x_2 - \beta I x_2 \quad [7.2]$$

$$\frac{dx_3}{dt} = \beta I x_2 - \delta x_3 \quad [7.3]$$

$$x_1 + x_2 + x_3 = 1 \quad [7.4]$$

where I is the irradiance, and α, β, γ and δ are the kinetic parameters to be assessed for microalgal photosynthesis.

7.1 Assessment of α and γ parameters

The parameters α and γ were assessed by processing fluorescence data measured during tests carried out with light pulse (LP) under ML conditions. The fluorescence under these conditions is due to the transition from x_1 to x_2 states. Provided a pulse sufficient to activate *closed-states* and to do not inhibite the reaction centres, the population of reaction centres is limited exclusively to x_1 and x_2 (x_3=0) and consequently only the transitions from x_1 to x_2 and from x_2 to x_1 are allowed. The equation set [7.1]-[7.4] is simplified as follow:

$$\frac{dx_1}{dt} = -\alpha I x_1 + \gamma x_2 \quad [7.5]$$

$$\frac{dx_2}{dt} = \alpha I x_1 - \gamma x_2 \quad [7.6]$$

$$x_1 + x_2 = 1 \quad [7.7]$$

The initial conditions are:

$$\begin{cases} x_1 = 1 \\ x_2 = 0 \end{cases} \quad [7.8]$$

Because under dark adapted conditions all reaction centres are in *open state*.

The integration of the eq. set [7.5] through [7.7] yields:

$$(\mathrm{t}) = \left(1 - \frac{\gamma}{\alpha I + \gamma}\right)\left(1 - e^{-(\alpha I+\gamma)t}\right) \quad [7.9]$$

At t=W_P the eq. [7.9] yields:

$$\chi_2 = \mathrm{x}_2(\mathrm{t} = W_P) = \left(1 - \frac{\gamma}{\alpha I + \gamma}\right)\left(1 - e^{-(\alpha I+\gamma)W_P}\right) \quad [7.10]$$

Where χ_2 is the fraction of operating centres in x_2 state at the end of the pulse. The integration of the set of eq.s [7.5] through [7.7] for t >W_P (I(t)=0) yields:

$$\mathrm{x}_2(\mathrm{t}) = \chi_2 e^{-\gamma(t-W_P)} \quad [7.11]$$

The x_2 time series depends on the LP intensity-time profile and α and γ parameters, and it may be simulated by the equation [7.9]. Given LP intensity-time profile, α and γ parameters, the calculated x_2 value was divided by the maximum calculated value ($\mathrm{x}_2^{\max} = \frac{\alpha I}{\alpha I+\gamma}$) to fulfil the condition $x_2 \in [0,1]$:

$$\mathrm{x}_2^* = \frac{\mathrm{x}_2}{\mathrm{x}_2^{\max}} \quad [7.12]$$

where x_2^* is the calculated *closed-state* fraction for the selected values of α and γ parameters. The cell irradiation by a light pulse under ML conditions is associated to the variation of fluorescence in the time due to the progressive displacement of the reaction centres from *open-state* to *closed-state*. To couple the measured fluorescence to the fraction of *close-state* reaction centres (x_2), the difference between the instantaneous fluorescence (F) and minimum measured fluorescence (F_0) has been made dimensionless with respect to F_V and equation [7.13] applies.

$$\mathrm{x}_2^{\mathrm{measured}} = \frac{\mathrm{F} - \mathrm{F}_0}{\mathrm{F}_\mathrm{M} - \mathrm{F}_0} \quad [7.13]$$

The parameters α and γ were estimated minimizing the sum of error (Eq. 7.14) between data of x_2^{measured} and x_2^* for tests carried out at light pulse intensity and width spanning over wide ranges.

$$\theta = \sum\left(\mathrm{x}_2^{\mathrm{measured}} - \mathrm{x}_2^*\right)^2 \quad [7.14]$$

7.2 Assessment of β parameter

The parameters β was assessed by processing fluorescence data measured during tests carried out with long light saturating pulse under ML conditions. Reaction centres exposed to light for long time are expected to have been excited to the closed state and to have chance to be inhibited. According to this scenario, the fluorescence vs. time profile is expected to be characterized by a rapid increase of the fluorescence in the first pulse period and a successive slow decrease even though the pulse is still active. The decay of the fluorescence when the pulse is still active may be associated to the

dynamics of the transition from x_2 to x_3 states because the latter state does not generate fluorescence. The transition from the *inhibited-state* to the *open-state* may be neglected because the time scale of the observed phenomena is definitively shorter than the repairing process. Therefore, the model of the reaction center dynamics – equation set [7.1]-[7.4] – is simplified as follow:

$$\frac{dx_1}{dt} = -\alpha I x_1 + \gamma \quad [7.15]$$

$$\frac{dx_2}{dt} = \alpha I x_1 - \gamma x_2 - \beta I x_2 \quad [7.16]$$

$$\frac{dx_3}{dt} = \beta I x_2 \quad [7.17]$$

$$x_1 + x_2 + x_3 = 1 \quad [7.18]$$

The initial conditions are:

$$\begin{cases} x_1 = 1 \\ x_2 = 0 \\ x_3 = 0 \end{cases} \quad [7.19]$$

because under dark adapted conditions all reaction centres are in *open state*.

The x_2 time series depends on the SP time profile, α, γ and β parameters, and it may be simulated by integrating the equation set [7.15]-[7.18]. The values of α and γ parameters assessed during the previous step are set during the calculation for the β assessment. Given the SP time profile, the calculated x_2 value was divided by the maximum calculated value (x_2^{max}) – Eq. [7.12] - to fulfil the condition $x_2 \in [0,1]$.

The cell irradiation by a saturating pulse under modulating light (ML) conditions is associated to the variation of fluorescence in the time due to the progressive displacement of the reaction centres from *open state* to *closed state* and the successive displacement of the reaction centres from *closed state* to *inhibited state*.

To couple the measured fluorescence to the fraction of *closed-state* reaction centres (x_2), the difference between the instantaneous fluorescence (F) and minimum measured fluorescence (F_0) has been made dimensionless with respect to F_V and Eq. [7.20] applies.

$$x_2^{measured} = \frac{F - F_0}{F_{M,max} - F_0} \quad [7.20]$$

The parameter β was estimated minimizing the sum of error (Eq. [7.14]) between data of $x_2^{measured}$ and x_2^* for tests carried out at saturating pulse characterized by width spanning over wide ranges.

7.3 Assessment of δ parameter

The parameter δ was assessed by processing fluorescence data measured during tests carried out with SP under AL conditions. The fluorescence dynamics under these conditions is due to the transition among the three states.

Under AL conditions, steady state of the three states is expected. The fraction of reaction centres of the three state under steady state conditions - $x_{1,ss}$, $x_{2,ss}$, $x_{2,ss}$ – may be assessed setting the Eq. set [7.1]-[7.4] equal to zero and they are:

$$x_{1,ss} = \frac{\gamma\left(\frac{\alpha\delta I}{\delta\gamma+\delta I(\alpha+\beta)+\alpha\beta I^2}\right)+\delta\left[\beta I\left(\frac{\alpha I}{\delta\gamma+\delta I(\alpha+\beta)+\alpha\beta I^2}\right)\right]}{\alpha I} \quad [7.21]$$

$$x_{2,ss} = \frac{\alpha\delta I}{\delta\gamma+\delta I(\alpha+\beta)+\alpha\beta I^2} \quad [7.22]$$

$$x_{3,ss} = \beta I \frac{\alpha I}{\delta\gamma+\delta I(\alpha+\beta)+\alpha\beta I^2} \quad [7.23]$$

The fluorescence of microalgae irradiated by a SP under AL conditions is characterized by F' and F'_M that allow to assess the ϕ_{PSII}. As AL increases the *inhibited-state* reaction centres (x_3) increases and the ϕ_{PSII} decreases because *inhibited-state* do not generate fluorescence. The processing of F' and F'_M values allows to assess Φ_{PSII} and x_3 by means of the Eq.s [7.24] and [7.25]:

$$\Phi_{PS\,II} = x_1 + x_2 = \frac{F'_M - F'}{F'_M} \quad [7.24]$$

$$x_3^{measured} = 1 - (x_1 + x_2) \approx 1 - \Phi_{PS\,II} = 1 - \frac{F'_M - F'}{F'_M} = \frac{F'}{F'_M} \quad [7.25]$$

where $x_3^{measured}$ is the inhibited center fraction measured when the fluorescence is maximum. Figure 3 shows a sketch of the fluorescence and x_3 vs. time. The x_3 fraction is constant under AL conditions ($x_{3,ss}$) and increases during SP. The instant of the fluorescence peak due to the SP is also marked by a dot-dashed vertical line.

The x_3 time series depends on the SP time profile, α, γ, β and δ and it may be simulated by integrating the equation set [7.1]-[7.4] by setting the initial conditions [7.21]-[7.23]. The values of α, γ and β parameters assessed during the previous steps are set during the calculation for the δ assessment. Given the SP time profile, the calculated x_3^* (figure 7.1) was compared with the measured value by Eq. [7.25].

The parameter δ was estimated minimizing the sum of error (Eq. [7.26]) between data of $x_3^{measured}$ and x_3^* for tests carried out at AL intensity spanning over a wide range.

$$\theta = \sum\left(x_3^{measured} - x_3^{*}\right)^2 \qquad [7.26]$$

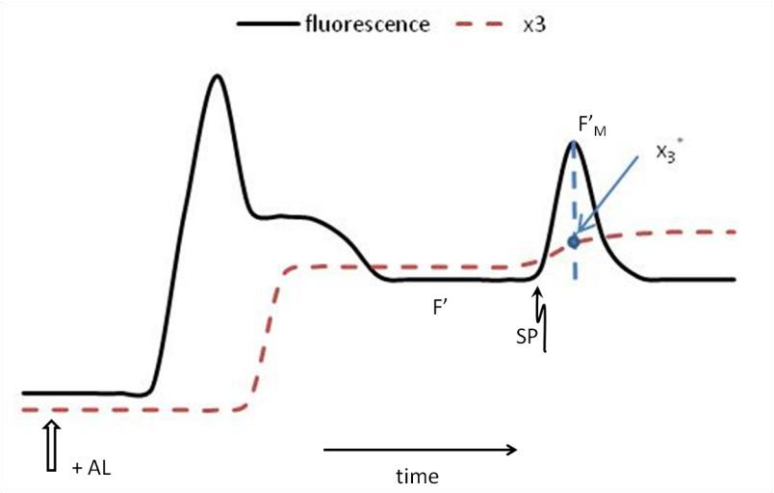

Figure 7.1: Sketch of the fluorescence vs. time for microalgae adapted at AL conditions and irradiated by SP. The dashed line is the expected x_3 fraction vs. time. The x_3^* marks the value of x_3 at the maximum fluorescence value F'_M.

7.4 The assessment of kinetic parameters of the photochemical processes

The procedure to assess the kinetic parameters of the photochemical processes is reported with reference to the irradiation of microalgae sampled from steady-state cultures of *Scenedesmus vacuolatus* in a cylindrical bubble column photobioreactor (CBC) irradiated with white light (140 µE m^{-2} s^{-1}).

Figure 7.2 reports the fraction of *closed-state* reaction centres measured ($x_2^{measured}$) according to Eq. [7.20] from fluorescence measurement (data points). Data refers to the irradiation of microalgal samples by light pulse (LP) under modulated measuring light (ML) conditions. Fluorescence tests refer to LP sufficient to activate *closed-states* and to do not inhibite the reaction centres: pulse intensity (I_P) ranged between 300 and 2000 µE m^{-2} s^{-1}; pulse width (W_P) ranged between 0.3 and 1 s. In particular, fluorescence measurements were carried out for LP characterized by the following W_P and I_P features: 1 s at 300 µE m^{-2} s^{-1} (figure 7.2a); 1 s at 600 µE m^{-2} s^{-1} (data not show); 1 s at 990 µE m^{-2} s^{-1} (figure 7.2b); 1 s at 1450 µE m^{-2} s^{-1} (data not show); 0.3 s at 2000 µE m^{-2} s^{-1} (figure 7.2c); 0.5 s at 2000 µE m^{-2} s^{-1} (figure 7.2d); 0.8 s at 2000 µE m^{-2} s^{-1} (data not show). The $x_2^{measured}$ time series were characterized by value almost constant during the pulse time for all LP investigated.

Figure 7.2 also shows the plot (continuous line) of the fraction of *closed-state* reaction centres calculated (x_2^*) according to Eq. [7.12] for the best set of α and γ parameters.

The best estimated values for α and γ parameters are $4.90 \cdot 10^{-3} \pm 1.25 \cdot 10^{-3}$ m^2 μE^{-1} and 5.55±0.50 s^{-1}, respectively.

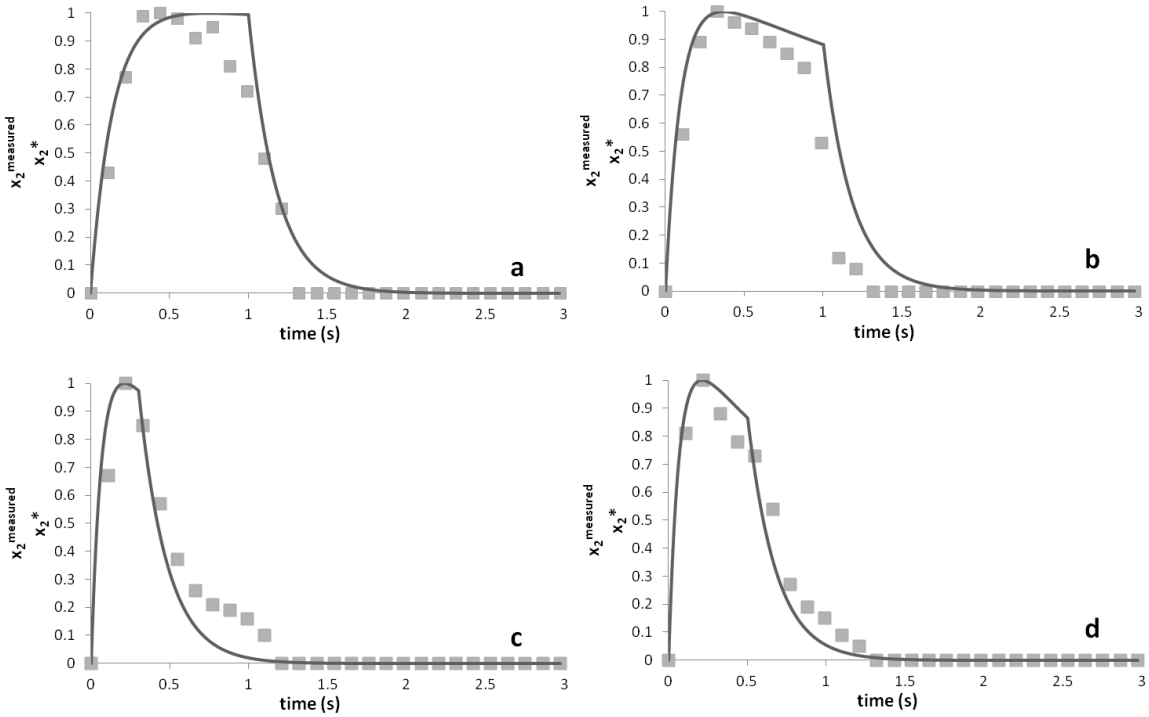

Figure 7.2: Fraction of reaction centres under *closed-state* measured (dots) and calculated (line). *S. vacuolatus* growth in CBC irradiated with white light (140 µE m^{-2} s^{-1}). Florescence tests carried out with LP under ML conditions. LP features: a) 1 s at 300 µE m^{-2} s^{-1}; b) 1 s at 990 µE m^{-2} s^{-1}; c) 0.3 s at 2000 µE m^{-2} s^{-1}; d) 0.5 s at 2000 µE m^{-2} s^{-1}.

Figure 7.3 reports the fraction of closed-state reaction centers measured ($x_2^{measured}$) according to Eq. [7.20] from fluorescence measurement (data points). Data refer to the irradiation of microalgal samples by saturating light pulse (SP) under ML conditions. Fluorescence tests refer to SP sufficient to activate inhibited state: I_P was set 2000 µE m^{-2} s^{-1}; W_P ranged between 1.5 and 3 s. The $x_2^{measured}$ time series were almost close to 1 for the first second of the pulse and then gradually decreased even though the pulse was still active.

Figure 7.3 also shows the plot (continuous line) of the fraction of closed-state reaction centres calculated (x_2^*) according to Eq. [7.12] for the best value of β parameter and $\alpha=4.90\cdot10^{-3}\pm1.25\cdot10^{-3}$ m^2 μE^{-1} and $\gamma=5.55\pm0.50$ s^{-1}.

The best values estimate for β is $5.14\cdot10^{-4}\pm3.60\cdot10^{-5}$ m^2 μE^{-1}.

Figure 7.4 reports the chlorophyll fluorescence parameters (Φ_{PSII} and NPQ) measured for SP (W_P=1 s; I_P=2000 µE m^{-2} s^{-1}) during fluorescence tests carried out at different actinic light (AL) levels. Data refer to microalgal cells adapted to AL for 3 minutes; AL irradiances ranged between 3 and 670 µE m^{-2} s^{-1}. As expected, Φ_{PSII} decreased with the intensity of the AL because the fraction of the inhibited reaction centres (x_3) increased.

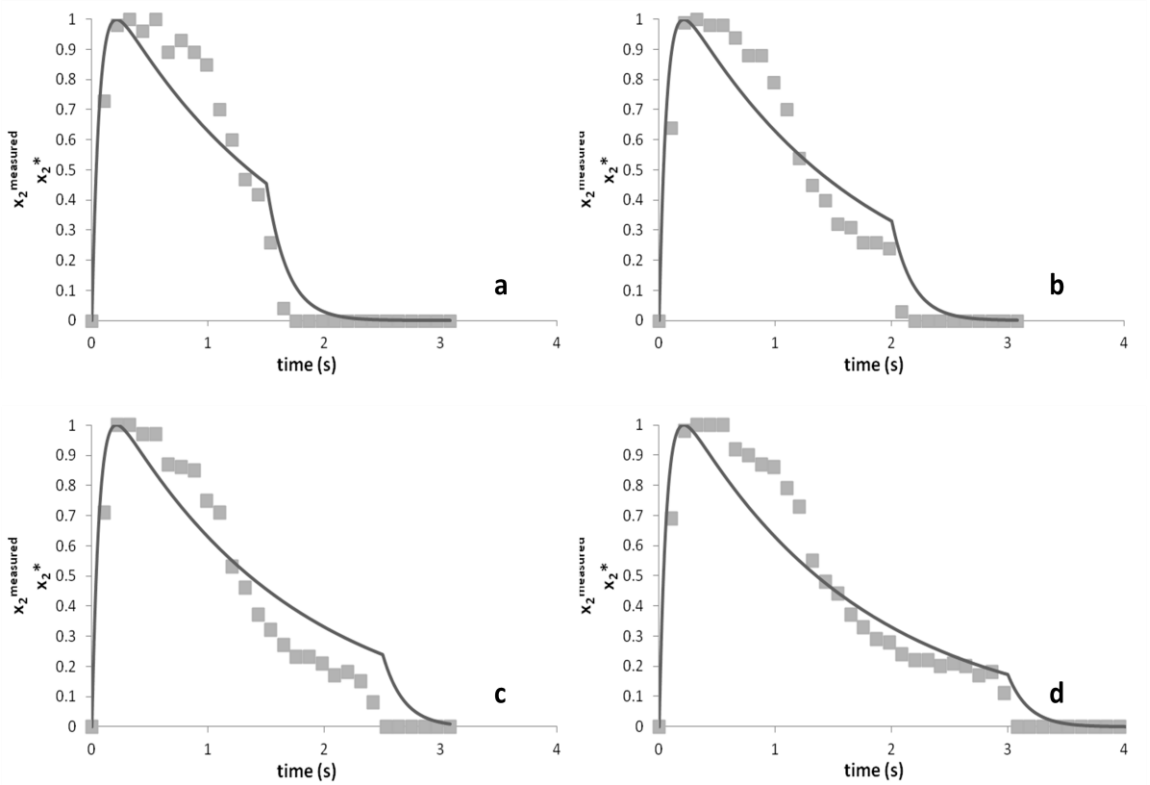

Figure 7.3: Fraction of reaction centres under *closed-state* measured (dots) and calculated (line). *S. vacuolatus* growth in CBC irradiated with white light (140 µE m^{-2} s^{-1}). Florescence tests carried out with SP under ML conditions. SP features are: I_P=2000 µE m^{-2} s^{-1}; W_P is 1.5 s (a), 2.0 s (b), 2.5 s (c) and 3.0 s (d).

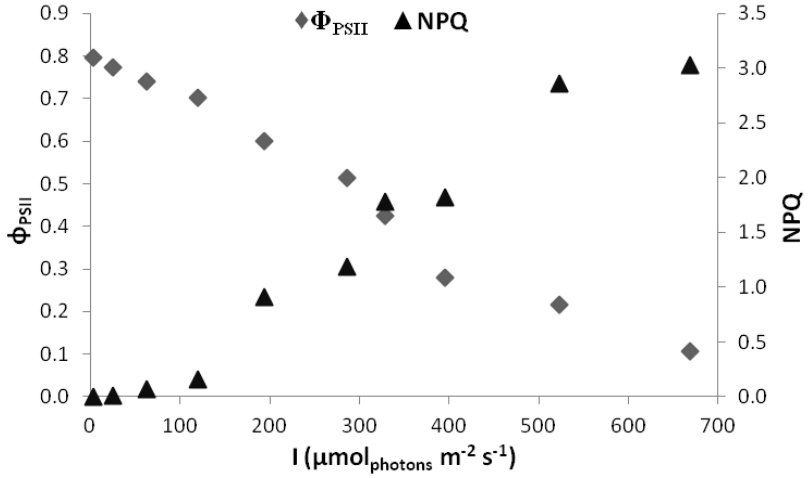

Figure 7.4: Chlorophyll fluorescence parameters (Φ_{PSII} and NPQ) measured under steady-state conditions at different AL levels.

Data of Φ_{PSII} vs. AL intensity were processed according to Eq. [7.25] to assess the fraction of the inhibited reaction centres ($x_3^{measured}$). $x_3^{measured}$ are reported as data point in figure 7.5. Figure 7.5 also shows the plot (continuous line) of the fraction of *inhibited-state* reaction centres calculated (x_3^*)

at the instant of the maximum fluorescence value (see figure 7.1) for the best value of δ parameter and $\alpha=4.90\cdot10^{-3}\pm1.25\cdot10^{-3}$ m^2 μE^{-1}, $\gamma=5.55\pm0.50$ s^{-1} and $\beta=5.14\cdot10^{-4}\pm3.60\cdot10^{-5}$ m^2 μE^{-1}.

The best values estimated for δ is $3.12\cdot10^{-2}\pm7.64\cdot10^{-3}$ s^{-1}.

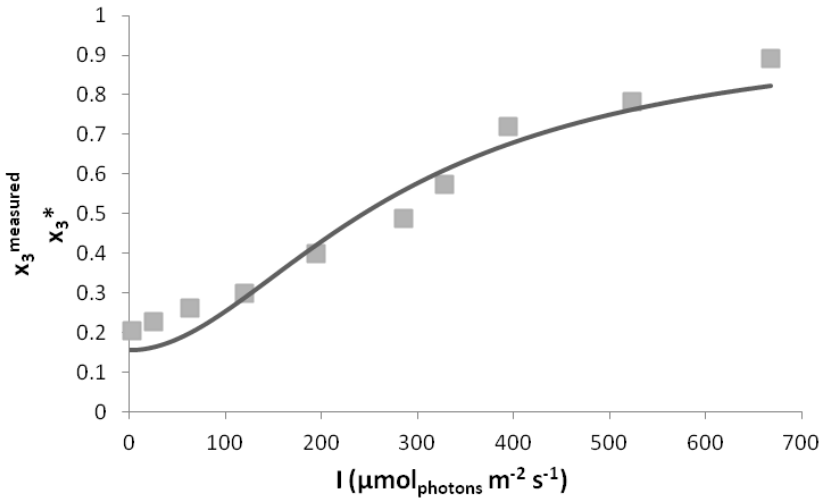

Figure 7.5: Fraction of reaction centres under inhibited state measured (dots) and calculated (line) vs. the light intensity (I) of AL. *S. vacuolatus* growth in CBC irradiated with white light (140 µE m^{-2} s^{-1}). Fluorescence tests carried out with SP under AL conditions. LP features: I_P=2000 µE m^{-2} s^{-1}; W_P=1 s.

7.5 Effect of microalgal culture conditions on kinetic parameters of the photochemical processes

The investigation of the effects of microalgal culture conditions on kinetic parameters of the photochemical processes is reported with reference to steady-state cultures of *S. vacuolatus*. Table 7.1 reports the kinetic parameters of the photochemical processes assessed for *S. vacuolatus* cultures carried out in vertical cylindrical bubble column photobioreactors (CBC) and parallelepiped-shape bubble column photobioreactor (RBC) irradiated with white light and red/blue light. The table also reports the data assessed for *Porphyridium sp*. by Wu and Merchuk (2001).

	CBC irradiated with white light	CBC irradiated with red and blue light	RBC irradiated with white light	Wu and Merchuk (2001)
α (m^2 μE^{-1})	$4.90\cdot10^{-3}\pm1.25\cdot10^{-3}$	$2.81\cdot10^{-3}\pm3.65\cdot10^{-4}$	$3.59\cdot10^{-3}\pm1.11\cdot10^{-3}$	$1.94\cdot10^{-3}$
β (m^2 μE^{-1})	$5.14\cdot10^{-4}\pm3.60\cdot10^{-5}$	$3.39\cdot10^{-4}\pm4.75\cdot10^{-5}$	$1.38\cdot10^{-4}\pm1.31\cdot10^{-5}$	$5.78\cdot10^{-7}$
γ (s^{-1})	5.55±0.50	6.27±0.60	2.45±0.242	0.146
δ (s^{-1})	$3.12\cdot10^{-2}\pm7.64\cdot10^{-3}$	$2.27\cdot10^{-3}\pm2.14\cdot10^{-3}$	$4.12\cdot10^{-4}\pm4.33\cdot10^{-4}$	$4.80*10^{-4}$

Table 7.11: α, β, γ and δ for *S. vacuolatus* growth under different operating conditions and photobioreactors. Data for *Porphyridium sp*. by Wu and Merchuk (2001) are also reported.

The analysis of the data reported in the table 7.1 points out that the operating conditions of microalgal cultures, the light spectrum, and the photobioreactor design affect the fluorescence kinetic parameters. Although affected by the culture conditions, the order of magnitude of the kinetic parameters α, β, and γ does not change for the investigated conditions. The parameters assessed in the present investigation are higher than those reported by Wu and Merchuk (2001) for *Porphyridium sp*. in a tubular photobioreactors but they are of the same order of magnitude. The difference may be due to the sensitivity of the photochemical processes to the stain.

Figure 7.6 highlights the potential effects of the variation of the kinetic parameters of the photochemical processes. Figure 7.6A reports the time scale of the reaction rates as a function of the irradiance at x_i=1 (i=1, 2 and 3) and assessed setting α=4.90·10^{-3} m^2 μE^{-1}, β=5.14·10^{-4} m^2 μE^{-1}, γ=5.55 s^{-1}, δ= 3.12·10^{-2} s^{-1}. As expected the time-scale of the rate of the reaction r_{PC} and r_{PI} decrease with I and they are smaller than the time-scale of the reaction r_{REP} for I larger than 30-40 μE m^{-2} s^{-1}. The comparison of the time scale of the four reactions supports the identification of the bottleneck for the photochemical process and it is discussed hereinafter.

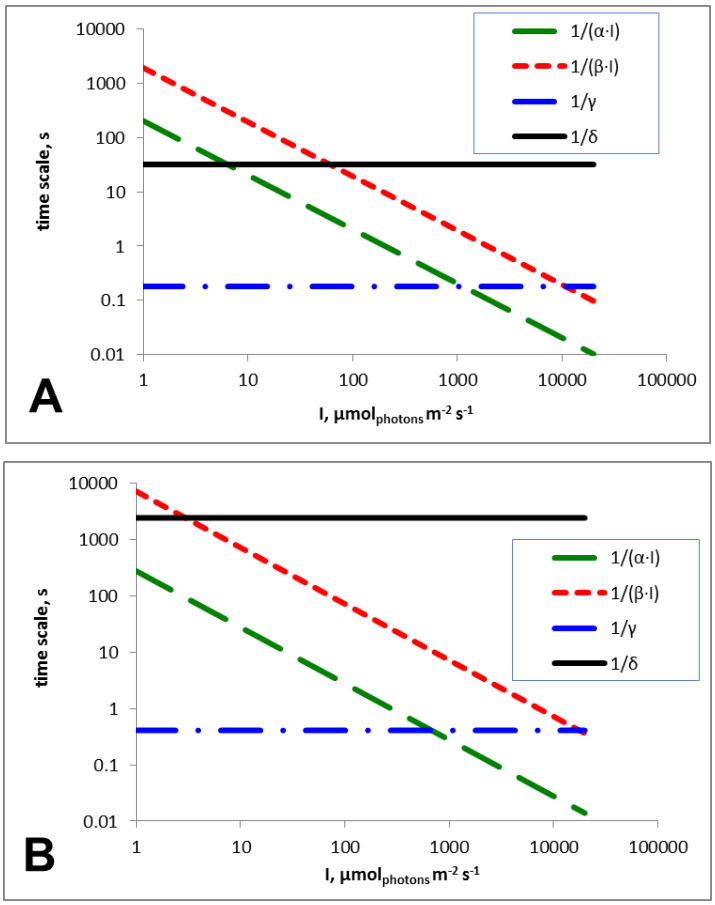

Figure 7.6: Time scale of the reactions in figure 2.4. A) α=4.90·10^{-3} m^2 μE^{-1}, β=5.14·10^{-4} m^2 μE^{-1}, γ=5.55 s^{-1}, δ= 3.12·10^{-2} s^{-1}. B) α=3.59·10^{-3} m^2 μE^{-1}, β=1.38·10^{-4} m^2 μE^{-1}, γ=2.45 s^{-1}, δ= 4.12·10^{-4} s^{-1}.

- $I < 1000$ µE m^{-2} s^{-1}: the photon capture process is the limiting step with respect to the photochemical quenching process, and the photoinhibition process is definitively slower than the photochemical quenching process. According to the time scales, the bottle neck of the process is the photon capture and the reaction centres are converted into open state as soon as they are formed. The x_1 fraction is expected to be the largest.

- $I > 10000$ µE m^{-2} s^{-1}: the photochemical quenching process is slower with respect to the photon capture and the photoinhibition processes. The time scale of the reaction r_{REP} is larger than the others. According to the time scales, the reaction centres are promptly converted into closed state and the photo-inhibition process is the dominating fate for the closed-state reaction centers. The x_3 fraction is expected to be the largest because inhibited states are slowly repaired.

- 1000 µE m^{-2} s^{-1}< I < 10000 µE m^{-2} s^{-1}: the photoinhibition process is slower with respect to the photochemical quenching process and both of them are slower than the photon capture process. According to the time scales, the reaction centres are promptly converted into closed state and the photoinhibition process becomes progressively competitive with respect to the photochemical quenching process. The x_2 fraction is expected to be the largest.

The time scale of the reaction r_{REP} is larger than the other for almost all the irradiance. Therefore, the repairing process is always the limiting step of the photochemical process when the operating conditions promote the formation of the inhibited-state of the reaction centres.

The figure 7.6B shows the time scale of the reaction rates as a function of the irradiance at x_i=1 (i=1, 2 and 3) and assessed setting α, β, γ and δ for *S. vacuolatus* growth in RBC irradiated with white light. Moving from the culture growth in CBC irradiated with white light (figure 7.6A) to that growth in RBC (figure 7.6B) it is possible no note that: i) the I range in which the photoinhibition process and the photochemical quenching process compete for the *closed-state* reaction centres moves at low I and it becomes larger; ii) at a fixed I the time scale of the photo-inhibition process increase and the *closed-state* reaction centres have high chance to be involved in the photochemical quenching process. This finding is in agreement with previous observation reported by Janssen et al. (2003) and Olivieri et al. (2013). Janssen et al. (2003) reported that rapid oscillations of light intensity greatly increase the photosynthetic efficiency and Olivieri et al. (2013) proved that biomass productivity was larger in inclined square bubble column photobioreactors than in vertical cylindrical bubble column photobioreactors. Indeed, Olivieri et al. (2013) suggested that the regular mixing active in the inclined photobioreactors provided a cyclic alternation of the microalgae between the light/surface region and the dark/inner region. It is expected that the cyclic exposure to the light promotes the

photochemical quenching process with respect to the photoinhibition process and a larger biomass production is expected.

The analysis of the results reported above suggests to take advantages of different time scales of the four routes of the reaction centres. The dominance of the photoinhibition with respect to the photochemical quenching disappears if irradiance is turned off. The irradiance of microalgae should be turned on for a time interval to excite the reaction center at the *closed-state* (time scale 1/αI) and turned off to allow the photochemical quenching (time scale 1/γ) without any competition with photoinhibition.

7.6 Effects of microalgal strain on the photochemical kinetic parameters

The photochemical kinetic parameters were assessed for several microalgal strains growth in parallelepiped-shape bubble column photobioreactor (RBC) under white light conditions. *Chlamydomonas reinharditii*, *Stichococcus bacillaris* and *Chlorella vulgaris* species were investigated. The estimated kinetic parameters are reported in table 7.2.

	Scenedesmus vacuolatus (*)	*Chlamydomonas reinhardtii*	*Stichococcus bacillaris*	*Chlorella vulgaris*
α ($m^2\,\mu E^{-1}$)	$3.59\cdot10^{-3}\pm1.11\cdot10^{-3}$	$1.68\cdot10^{-3}\pm4.86\cdot10^{-4}$	$1.41\cdot10^{-3}\pm6.05\cdot10^{-4}$	$2.74\cdot10^{-2}\pm9.32\cdot10^{-4}$
β ($m^2\,\mu E^{-1}$)	$1.38\cdot10^{-4}\pm1.31\cdot10^{-5}$	$2.39\cdot10^{-4}\pm1.67\cdot10^{-5}$	$2.37\cdot10^{-4}\pm2.25\cdot10^{-5}$	$9.50\cdot10^{-5}\pm3.28\cdot10^{-5}$
γ (s^{-1})	2.45±0.242	3.23±0.32	6.12±0.67	5.21±0.52
δ (s^{-1})	$4.12\cdot10^{-4}\pm4.33\cdot10^{-4}$	$1.41\cdot10^{-3}\pm2.19\cdot10^{-3}$	$8.55\cdot10^{-4}\pm1.11\cdot10^{-3}$	$3.06\cdot10^{-4}\pm8.11\cdot10^{-4}$

(*) from table 1

Table 7.2: α, β, γ and δ assessed for several strains growth in RBC photobioreactors under white light conditions.

For all investigated microalgal strains, the photochemical rate (α) results to be faster than photohinibitory process (β). The rate of repair, regulated by the constant δ, is slower compared to the nearly instantaneous change in photochemistry. The results demonstrated that the photochemical activity is equal in all algal strains, but the photochemical kinetic parameters, α, β, γ and δ, are specific for each algal strain.

RESULTS: LIPID EXTRACTION AND TRANSESTERIFICATION

For the characterization of the produced biodiesel, the determination of the fatty acid methyl esters (FAMEs) composition is an important step for. The conventional protocol consists of two phases: lipid extraction and transesterification. To reduce costs associated with lipids extraction, the attention was focused on the biodiesel production by a onepot process. This approach is known as in situ or direct transesterification. The attention was focused on the effects of operating conditions on FAMEs yield. The influence of type (acid or alkaline) and concentration of the catalyst, precontact time, methanol/biomass weight ratio, reaction time and temperature and water content of microalgal biomass was investigated too. The direct transesterification protocol was optimized per *Stichococcus bacillaris*. The optimized protocol of direct transesterification was tested on different *Stichococcus* microalgal strains, *Stichococcus cylindricus*, *Stichococcus fragilis*, *Stichococcus jenerensis*, *Stichococcus deasonii* and *Stichococcus chodatii* and on different microalgal species, *Scenedesmus vacuolatus*, *Maesotaenium caldariorum*, *Chlorella vulgaris, Chlamydomonas reinhrdtii* and *Nannochloropsis sp*., characterized by a different cell wall composition. The effects of these variables on triglyceride conversion were compared with data obtained with a conventional method of extraction-transesterification (Rashid and Anwar, 2008; Guckert et al., 1988). At the end of the extraction procedure, the total lipid content inside biomass was calculated as:

$$Lipids\ yield(\%) = \frac{Lipid\ weight}{Dry\ microalgal\ weight} \times 100 \quad [8.1]$$

After transesterification procedure and FAME analysis by Gas Cromatografy, the bio-oil yield was calculated and expressed as:

$$Bio - oil\ yield(\%) = \frac{Total\ FAME\ weight}{Microalgal\ weight} x\ 100 \quad [8.2]$$

8.1 Conventional alkaline-catalyzed transesterification

An amount of 0.4 g of dried biomass was used to determine the lipid yield within the biomass and the Bio-oil yield after conventional alkaline transesterification (1.5% NaOH w/w, 3 min of reaction, methanol/biomass weight ratio 79:1, 60°C) on *S. bacillaris, S. cylindricus, S. fragilis, S. jenerensis*, *S. deasonii* and *S. chodatii* (Figure 8.1).

To verify completeness of extraction, residual biomass was subjected to direct alkaline catalyzed transesterification. The same transesterification (1.5% NaOH w/w, 3 min of reaction, methanol/biomass weight ratio 79:1, 60°C) conditions were employed for the residual biomass. The

results in terms of bio-oil yield were close to zero, thus indicating that, after extraction, no further esterifiable lipids remain in the biomass residue.

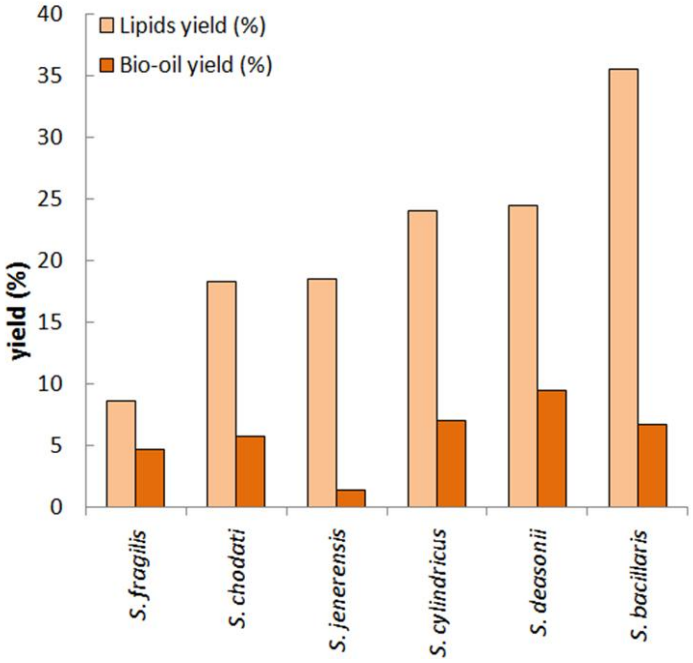

Figure 8.1: Lipid and Bio-oil yield under conventional method of extraction and transesterification

Lipids yield ranged from 8.6% (*S. fragilis*) to 35.5% (*S. bacillaris*) and was very similar for *S. cylindricus* and *S. deasonii* (~24%), and for *S. jenerensis* and *S. chodatii* (~18%) strains. Bio-oil yield ranged from 1.4% for *S. jenerensis* to 9.5% for *S. deasonii*. Based on these observations, it can be concluded that significant variations may be found in both extracted lipids and Bio-oil yield even within same genus. Because of its high lipid content among the investigated algal strains, *S. bacillaris* was selected to significantly improve the bio-oil yield by means of direct alkaline transesterification.

8.2 Effect of direct transesterification process on bio-oil production

✓ Effect of catalyst concentration

Figure 8.2 shows the results of direct alkaline catalyzed transesterification as a function of the catalyst concentration. Tests were carried out with freeze-dried algal biomass in alkaline-methanol solutions characterized by a wide interval of concentrations: NaOH catalyst in methanol was increased up to 2.0% by weight. Fixed operating conditions were: reaction temperature (T=60 °C), reaction time (t_r=3 min) and methanol/freeze-dried biomass weight ratio (r_{mb}=79:1).

The results indicated that bio-oil were produced only if NaOH was present. The yield was appreciably affected by catalyst concentration indicating that the maximum bio-oil yield was obtained with 1.5% NaOH. With a further increase of NaOH concentration, the saponification reaction led to a decreased

yield. These results were consistent with those reported by others (Dorado et al., 2004; Encinar et al., 1999). In particular, Dorado and Co-workers investigated the effect of KOH concentration in the range of 0 to 2.3% (w_{KOH} w_{oil}^{-1}) and Encinar and Coworkers studied the influence of NaOH concentration in the range of 0 to 1.0% (w_{NaOH} w_{oil}^{-1}). Literature results have shown that the ester conversion was zero without catalyst and that marked increases of alkaline catalyst concentration gave rise to a small decrease in the bio-oil production yield. Thus, a catalyst concentration of 1.5% NaOH was chosen for following investigations.

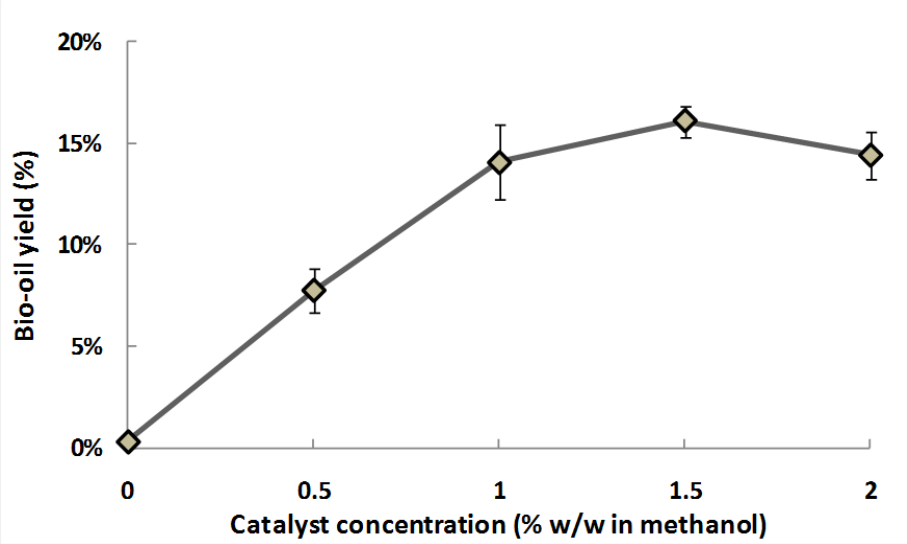

Figure 8.2: Direct alkaline catalyzed transesterification: effect of the catalyst concentration on the bio-oil yield. Operating condition: r_{mb} = 79:1, T = 60 °C, t_r = 3 min.

✓ **Effect of reaction temperature**

Bio-oil yield in tests at temperatures ranging between 20°C and 80°C are reported in Figure 8.3. Operating conditions of the tests were: freeze-dried biomass, methanol to biomass weight ratio 79:1, NaOH concentration in methanol 1.5% (by weight) and transesterification reaction time at 3 minutes.

The collected results indicated that bio-oil yield increased significantly with temperature and approached the highest values (16.25%) at 60°C. For the highest temperatures (80°C), there was a marked decrease of bio-oil yield, up to 7.7%. This can again be attributed to the increased relevance of the saponification process by the alkaline catalyst with respect to the methanolysis one (Ramadhas et al., 2005).

A reaction temperature of 60 °C was thus chosen for following investigations.

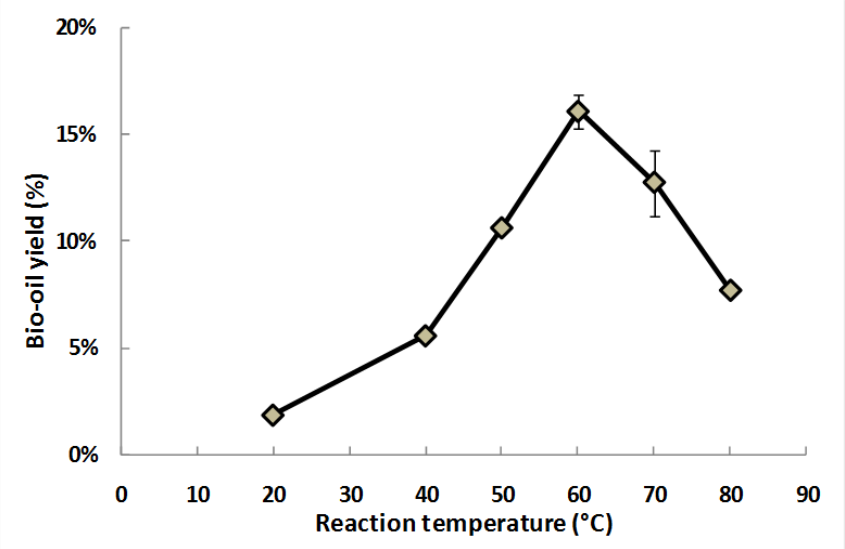

Figure 8.3: Direct alkaline catalyzed transesterification: effect of the reaction temperature on the bio-oil yield. Operating condition: C_{NaOH} 1.5% (w/w), r_{mb}=79:1, t_r=3 min.

✓ **Effect of reaction time**

The results concerning the performance of direct alkaline transesterification of freeze-dried algal biomass with a reaction time set in the range 1-20 minutes are reported in Figure 8.4. Operating conditions employed for the tests were: reaction temperature 60 °C, methanol to biomass weight ratio 79:1 and catalyst concentration of 1.5% NaOH (w/w).

Bio-oil yield increased with a reaction time between 1 and 3 minutes and was quite constant – about 17% - with a reaction time within the interval 3 -12 min and decreased for more prolonged reaction times. These results are partially in agreement with those reported elsewhere. Freedman et al., 1987, pointed out that the conversion of seed-oils (soybean, peanut, cotton seed, and sunflower) to FAMEs did not alter significantly (93-98%) for reaction times ranging between 1 and 60 minutes, whereas others (Rodrigues da Silva Baumgartner et al., 2013) observed high FAMEs yield from *Spirulina platensis* only after 10 min of reaction. Similar results were reported regarding the transesterification of beef tallow with methanol (Ma et al., 1998). They observed that the reaction was slow during the first minute due to the mixing of methanol and beef tallow, proceeding faster in the following 4 minutes. The amounts of mono and diglycerides increased at the beginning and decreased after 15 minutes of reaction time. It is reasonable that prolonged reaction times (12-20 min, under the adopted conditions) may lead to higher losses of FAMEs due to thermal degradation processes or different chemical reactions, such as alkaline hydrolysis to fatty acid (FA) (Mazo et al., 2010), "Claisen-like" condensation reactions (Ryckebosch et al., 2011], and alcoholysis with phytol and other alcohols derived from the lysis of algal material.

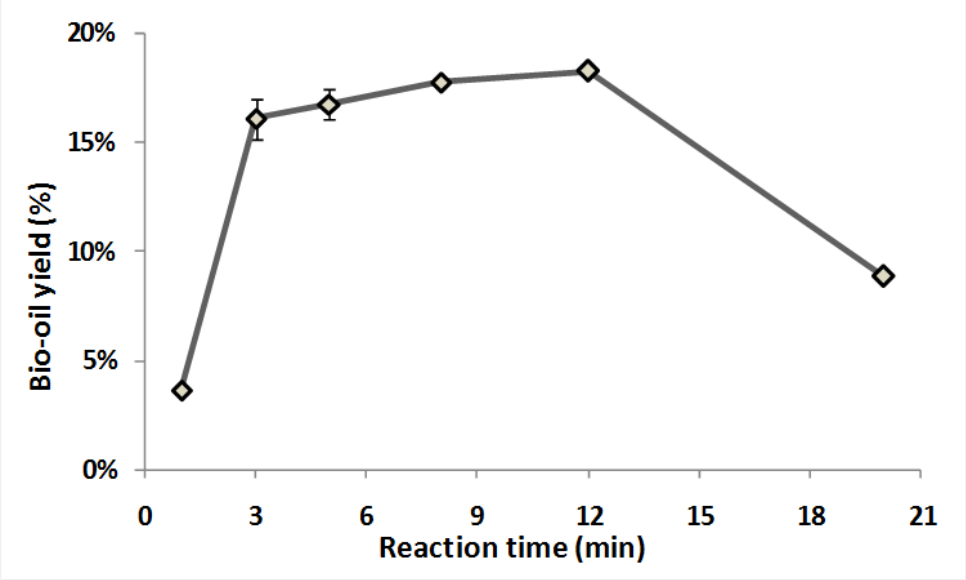

Figure 8.4: Direct alkaline catalyzed transesterification: effect of the reaction time on the bio-oil yield. Operating condition: C_{NaOH} 1.5% (w/w), r_{mb}=79:1, T=60 °C.

✓ **Effect of methanol/biomass weight ratio**

Direct transesterification experiments were carried out with methanol to freeze-dried biomass weight ratio (r_{mb}) set at 24:1, 39:1 and 79:1 (data not shown). The operating conditions were: alkaline catalyst concentration 1.5%% (w/w), reaction temperature 60°C and reaction time of 3 min. The bio-oil yield did not change with the methanol to biomass weight ratio within the range 39:1 - 79:1. The results are in accord with those previously reported (Wahlen et al., 2011). They also noticed that the FAMEs yield did not change with the methanol/freeze-dried biomass weight ratio even with a ratio as high as 118:1. These results seem to indicate the absence of methanol limitation under the investigated operating conditions and therefore to exclude any problem of methanol diffusion inside the biomass. If the methanol diffusion was a limiting step, a first order dependence by the methanol concentration would have been clearly observed.

Thus, the subsequent direct transesterification experiments were carried out with the same methanol/ biomass weight ratio used in the previous experiment (r_{mb} = 79:1).

✓ **Effect of pre-mixing**

The effect of pre-mixing time was also investigated in order to validate the previous consideration about a possible methanol diffusion-limiting process. Tests were carried out with freeze-dried algal biomass in 1.5% NaOH w/w alkaline-methanol solutions. Fixed operating conditions were: reaction temperature (T=60 °C), reaction time (t_r=3 min) and methanol/freeze-dried biomass weight ratio (r_{mb}=79:1).

On increasing the pre-mixing time from 0 to 6 hours, results of tests indicated that the bio-oil yield did not change significantly and it ranged from 16 to 18% (data not shown). As a consequence that the pre-mixing doesn't affect the reaction rate, the effect of diffusion-limited rate can be further excluded.

✓ **Effect of biomass water content**

The tests on biomass water content were carried out under the following operating conditions: methanol/biomass weight ratio =79:1, catalyst concentration =1.5% NaOH (w/w), reaction temperature =60 °C, reaction time =3 min and pre-mixing time =0 h. Figure 7.5 reports data referring to the bio-oil yield as a function of biomass water content. The results showed that the water content did not affect bio-oil yield (14-16%) if biomass/water content ratio was less than 10%, while water content higher than 10% reduced the bio-oil yield to 0.2%. This drastic reduction of bio-oil yield with increasing water content in the biomass is in agreement with results reported by others (Wahlen et al., 2011). They pointed out that the FAMEs yield decreases down to 50% of the expected FAMEs when the water content of biomass increases from 0 to 400 % (w/w % of biomass).

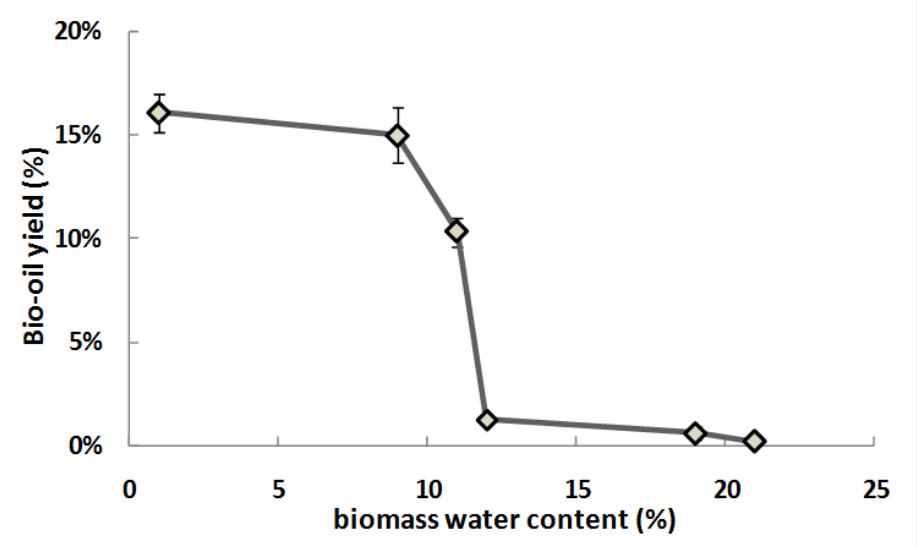

Figure 8.5: Direct alkaline catalyzed transesterification: effect of biomass water content. Operating conditions: t_p=0 h, t_r=3min, r_{mb}=79:1, T=60 °C, C_{NaOH}=1.5% (w/w) in methanol.

The explanation of this process is twofold. During direct transesterification, at temperatures higher than ambient, a competition between lipolysis, promoted by lipases present in the cells (Ryckebosch et al., 2011), and methoxy ions, present in the alkaline solution, takes place. It should be considered that although methoxy ions are more nucleophilic than water molecules and consequently capable of a faster attack on the lipids, these ions need first to enter the cells before reacting. Therefore, the transesterification yield is not only the result of a simple attack of methoxy ions on the lipid

molecules, but it is also influenced by their capability to diffuse from the external solution in the cell. A second explanation for the observed behaviour derives from some studies reporting that the lyophilisation process may break up the membrane protein matrix (Mat et al., 2010; Lee et al., 1998; Van Leeuwe et al., 2006; Molina Grima et al., 2004), or be sufficient to weaken the cell membrane (Pasquet et al., 2011), thus creating an easy access for the alkaline catalyst and promoting direct transesterification. Through this mechanism, the lower the residual water content, the higher will be the degree of cell membrane damage. From this point of view it could be assumed that, for a residual water content lower than 10%, a high degree of cell damage is obtained which enables methoxy ions to easily attack lipid molecules.

A possible solution is to counteract the detrimental effect of biomass water content on FAMEs yield by increasing the methanol volume. Figure 8.6 reported data obtained using biomass with a water content of 18% under the following operating conditions: catalyst concentration = 1.5% NaOH (w/w), reaction temperature = 60 °C, reaction time = 3 min and pre-mixing time = 0 h.

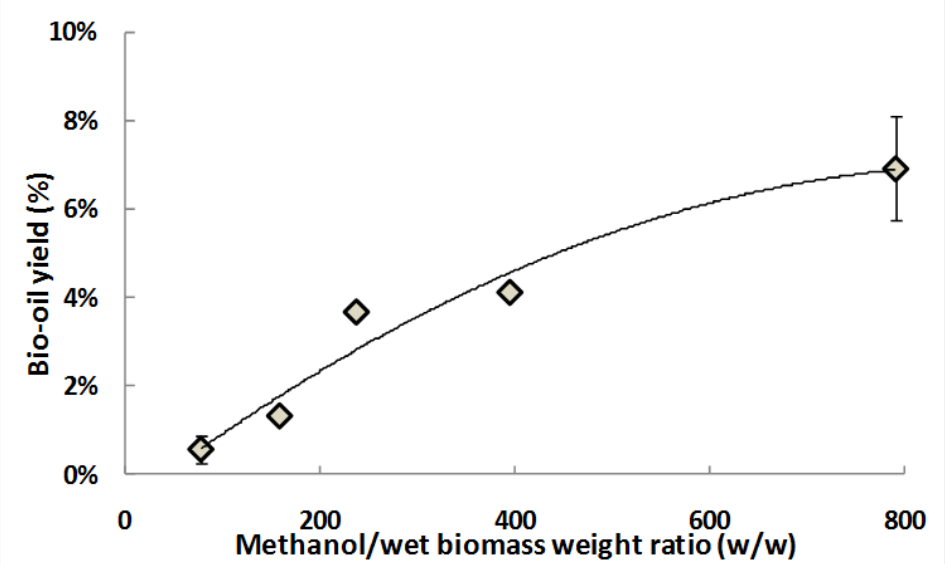

Figure 8.6: Direct alkaline catalyzed transesterification: effect of methanol/wet biomass weight ratio. Operating conditions: t_p=0 h, t_r=3min, r_{mb}=79:1, T=60 °C, C_{NaOH}=1.5% (w/w) in methanol, biomass water content = 18% (w/w). Curve fitting: 2nd order polynomial.

The analysis of the data showed that the bio-oil yield increased with the methanol/wet-biomass ratio in the range from 79:1 to 790:1. Notably, the yield increased from 0 to 7%, under the operating conditions investigated. In addition, the positive effect on the bio-oil yield of increasing the methanol volume could be ascribed to the fact that methanol, which is cell disruptive (Kusdiana et al., 2004), may additionally favour the cleavage of the algal wet agglomerates.

The results of alkaline direct transesterification experiments, carried out on *Stichococcus bacillaris,* indicated that triglycerides were not converted without an alkaline catalyst and approached a maximum value with a catalyst concentration of 1.5% NaOH (w/w). Under alkaline conditions this led to the following: (i) the pre-mixing time did not affect bio-oil yield (~17%); (ii) the bio-oil yield increased with temperature and approached a maximum at close to 65°C; (iii) the bio-oil yield did not change significantly with the methanol to biomass weight ratio within the range 39:1 - 79:1; iv) the bio-oil yield gradually increased within the first minutes of reaction, approached a constant value within the interval 3-12 minutes and decreased for times longer than 12 min. Biomass drying was observed to play an important role in direct transesterification: the bio-oil yield reduced with an increase in biomass water content. A higher bio-oil yield was obtained increasing the methanol/wet biomass ratio. Under alkaline catalyzed conditions the direct transesterification process was more efficient than the acidic ones producing higher bio-oil yield.

8.3 Conventional *vs* direct alkaline and acid transesterification on *Stichococcus* strains

For *Stichococcus* strains, the results for both direct and conventional alkaline transesterification are reported in Figure 8.7. Under the conditions adopted, methanol/biomass weight ratio = 79:1, catalyst concentration = 1.5% NaOH (w/w), reaction temperature = 60°C, reaction time = 3 min and pre-mixing time = 0 h, for all *Stichococcus* strains, with the sole exception of *S. fragilis*, a higher bio-oil yield was gained by applying direct transesterification compared to the conventional one.

The higher performance of direct *vs* conventional transesterification is in agreement with previous investigations (Wang et al., 2012). The direct transesterification of *Schizochytrium limacinum* was characterized by 10%–20% higher FAMEs yield compared to the conventional transesterification method. These results may be related to a partial thermal degradation of lipids resulting from elevated temperatures and prolonged times during the Soxhlet extraction step (McNichol et al., 2012) and/or to the release of fatty acids from the alkaline hydrolysis of cellular membranes and disruption of cell walls (Kim et al., 2013).

To compare, alkaline and acidic transesterification process, experiments were also performed under acidic conditions for all investigated *Stichococcus* strains (figure 8.7). Bio-oil yield, for direct transesterification, carried out under alkaline conditions, was higher than that measured for both direct and conventional processes under the adopted acidic conditions (90 °C, 40 min). Some acidic transesterification tests (data not reported), performed at the same temperature and reaction time for the alkaline process (60 °C, 3 min), showed lower bio-oil yield than that reached adopting the conditions reported by Johnson and Wen, 2009. In previous studies (Velasquez-Orta et al., 2012) it was reported that, in terms of time, the alkaline catalyst (sodium hydroxide) outperformed the acid

catalyst (sulphuric acid) obtaining higher conversions at lower reaction times. Moreover, there were no significant differences between results obtained for tests carried out according to the two acidic protocols. These results indicated that the presence of the solvent in acidic-catalyzed transesterification, under the adopted experimental conditions, is not essential. In contrast, Johnson and Wen reported that in a solvent free system, FAMEs yield obtained from *Schizochytrium limacinum* by direct transesterification, under acidic conditions, was very low, indicating that the solvent was essential for the reaction (Johnson and Wen, 2009).

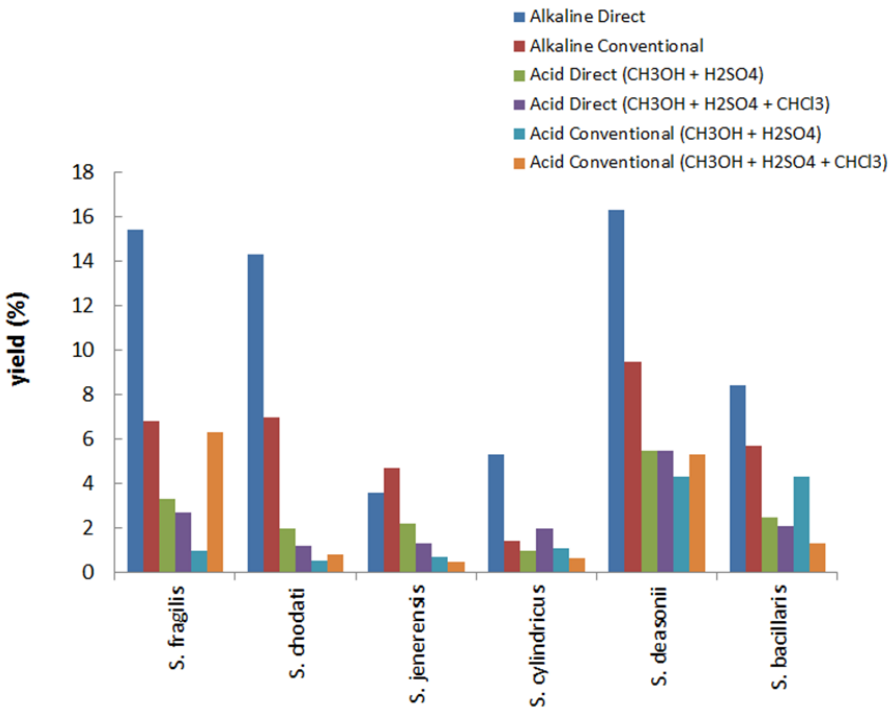

Figure 8.7: Bio-oil production under conventional method of extraction and transesterification and direct transesterification. Operating conditions adopted for direct alkaline transesterification were: t_p=0 h, t_r=3 min, T=60 °C, r_{mb}=79:1, C_{NaOH}=1.5% (w/w). For direct acidic transesterification, two protocols were adopted (Johnson and Wen, 2009).

8.4 Conventional *vs* direct alkaline and acid transesterification on different microalgal species

Direct and conventional transesterification under acid and alkaline condition were carried out for several microalgal species: *Chlorella vulgaris*, *Chlamydomonas reinhardtii, Scenedesmus vacuolaus*, *Nannochloropsis sp*., *and Maesotaenium caldariorum*. The strains were characterized by different cell wall composition. In particular the selected species are characterized by:

- ✓ *Chlorella vulgaris* (already known as *Chlorella fusca*): cell wall is very complex and resistant. Its composition was studied by Atkinson et al. (1972). Provided that cytokinesis has produced naked autospores within the mother cell wall, cell wall formation starts outside the autospore plasma membrane with the formation of small trilaminar plaques. The trilaminar plaques

expanded while the granular material mass inter-autospore decreases, and they eventually fuse to produce a complete trilaminar sheath around each autospore. A microfibrillar, cellulase digestible, layer is deposited between the trilaminar component and the plasma membrane. Meanwhile the corresponding microfibrillar component of the mother cell wall is digested leaving only its resistant trilaminar component. The trilaminar component includes a substance considered to be the polymerized carotenoid, sporopollenin, responsible of the resistance to extreme extraction procedures including acetolysis, and its infra red absorption spectrum.

- ✓ *Chlamydomonas reinhardtii*: cell wall of the biflagellate alga is a multilayered, extracellular matrix composed of carbohydrates and 20-25 polypeptides (Imam and Snell, 1985). This cellulose-deficient cell wall is composed of two separate domains: one made approximately 20 proteins held together by noncovalent interactions, and a second domain made of a few proteins, which are the framework of the wall.

- ✓ *Scenedesmus vacuolatus*: cell wall contains ketocarotenoids and sporopollenin (Burczyck et al., 1981). Canthaxanthin, astaxanthin and unidentified ketocarotenoid and lutein were found as integral cell wall components. They are bound to outer (trilaminar) layer of the complete cell wall which also contains sporopollenin.

- ✓ *Maesotaenium caldariorum*: the cell wall is very fragile. To the author knoweledge, there is no study reported in the literature regarding the cell wall composition.

Operating conditions used for direct transesterification were: dried biomass, t_p=0 h, t_r=3 min, T=60 °C, r_{mb}=79:1, C_{NaOH}=1.5% (w/w). Two protocols were adopted for direct acidic transesterification (Johnson and Wen, 2009). Table 8.1 reports the results of the transesterification process for the investigated strains.

Bio-oil yield(%)				
	Scenedesmus vacuolatus	*Maesotaenium caldariorum*	*Chlorella vulgaris*	*Chlamydomonas reinhrdtii*
Alkaline transesterification				
Direct	2.9	5.6	6.5	7.6
Conventional	6.3	5.8	1.7	1.7
Acidic transesterification				
Direct (CH_3OH+H_2SO_4+$CHCl_3$)	2.3	2.6	5.8	2.0
Conventional (CH_3OH+H_2SO_4+$CHCl_3$)	1.0	0.4	2.4	2.4

Table 8.1: Direct (alkaline or acidic) and conventional (alkaline or acidic) transesterification. Bio-oil yield assessed for tests carried out under acidic and alkaline conditions.

Bio-oil yield assessed for conventional and direct transesterification under alkaline conditions was higher than that measured for direct and conventional processes under acidic conditions reported by Johnson and Wen (2009) (90 °C, 40 min). For all strains, bio-oil yield obtained by direct transesterification was higher or similar than/to the yield of the conventional process. Moreover, the process under alkaline conditions was more efficient than the acidic ones because it produced higher bio-oil yield.

CONSIDERATIONS ON INTENSIVE MICROALGAL CULTURES AS ENERGY/MATTER SOURCE

The investigation on the microalgal cultures in the turbidostat mentioned in chapter 6 pointed out some critical issues. These issues play a key role in: addressing the tests for the specific growth rate assessment; defining guide lines for the continuous production of microalgal biomass and its components.

The specific growth rate was not constant during the day even though the operating conditions were constant, irradiance included. As a result, attention should be paid when considering the data of the specific growth rate reported in the literature. Indeed, the reported data were assessed by processing biomass concentration dynamics under batch conditions and the biomass concentration measurement was typically carried out once a day. In other words, the specific growth rate reported in the literature is a value averaged over a day: the assessed growth rate underestimates the maximum specific growth rate (say μ_2 in section 6.2) under the selected operating conditions. It could become critical to assess the maximum specific growth rate for a fixed set of operating conditions. The maximum specific growth rate for a fixed set of operating conditions (μ_2) may be assessed during the day fraction during which the circadian clock of the microalgal cells is set on "growth".

The design and the operation of continuous photobioreactor systems may take advantages from the results reported in the chapter 6 and 7.

The dilution rate set for a continuous photobioreactor dedicated to the intensive production of the biomass and/or its contents must take into account the fluctuating nature of the specific growth rate. Typically, plants operate under chemostat conditions rather than under turbidostat conditions because chemostat requires cheaper apparatus and it is easier to use. Plants operated at dilution rate (constant) (chemostat control) equals to the day-averaged specific growth rate are subject to: i) the increase of biomass concentration during the fraction of the day during which the circadian clock of the microalgal cells is set on "growth"; and ii) the decrease of biomass concentration during the other fraction of the day.

The circadian clock affects the intensive production rate of biomass constituents too. Indeed, the harvesting during the day of the biomass should be carried out when the concentration of the selected constituent is high. However, attention should be paid because the maximum concentration of some contents is high when the instantaneous growth rate is minimum (even zero). The

compromise between production rate of the selected constituent and its concentration in the stream is matter of economic optimization.

The kinetics of the photochemical process may be used as a tool to enhance the productivity of the photobioreactor. The design of the photobioreactor should be selected to exploit the maximum photon capture rate having care to keeping the photoinhibition rate negligible. The analysis of the results reported in the chapter 7 suggests to take advantages from different time scales of the four routes of the reaction centres. Irradiance along the photobioreactor should be tuned: i) the irradiance should be turned on for a time interval enough to excite the reaction centres at the *closed-state* (time scale $1/\alpha I$); the irradiance should be turned off to allow the photochemical quenching (time scale $1/\gamma$) without any competition with photoinhibition.

The effects of the suggested sequence of irradiance levels may interpret the results reported in the section 5.1.1 and those proved by Liao et al. (2014) for a novel tubular photobioreactor (TPBR).

The operation of the inclined bubble column photobioreactors produced high biomass production rate than vertical bubble column photobioreactors. The exposure of microalgae at the irradiated surface was alternated to longer period under lower irradiance (inner/shaded culture): a condition that enhances the photochemical conversion of the light. Liao et al (2014) investigated a novel tubular photobioreactor (TPBR) as that sketched in figure 9.1. They alternated dark and transparent regions of equal length along the TPBR and operated the plant under several flow velocities. They pointed out that the presence of dark/light alternate regions improved the TPBR productivity and that the enhancement increased with the irradiance. The reported results are in agreement with the results of chapter 7, explain the productivity enhancement and suggest guidelines to further improve the photobioreactor performances. Indeed, the length of the light and dark regions should be proportional to the identified time scale: $1/\alpha I$ and $1/\gamma$, respectively. Moreover, the length of the light region should depend on the irradiance.

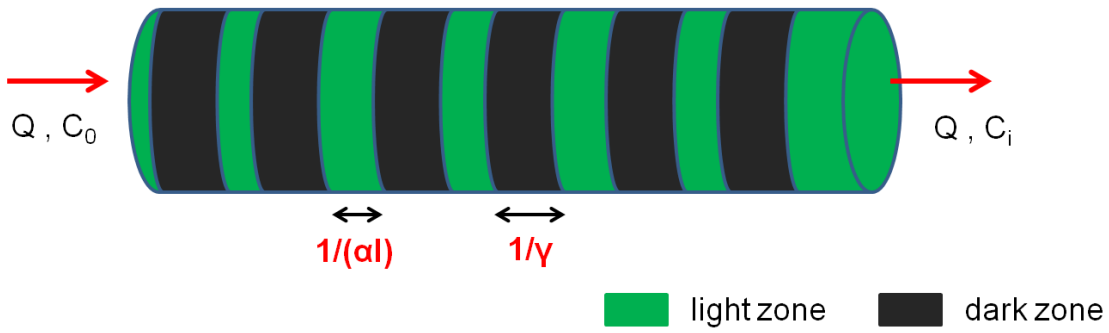

Figure 9.1: Sketch of the photobioreactor proposed by Liao et al. (2014). The extension of the light/dark zone are proposed as results of the present study.

CONCLUSIONS

The study carried out during the PhD thesis has been dedicated to the characterization of the process to produce energy vectors from intensive culture of autotrophic microalgae. The activities have regarded issues supporting the design of photobioreactors and the innovative process to produce biofuels. Eleven microalgal strains have been investigated: *Nannochloropsis sp.*, *Scenedesmus vacuolatus*, *Stichococcus bacillaris*, *Stichococcus fragilis*, *Stichococcus cylindricus*, *Stichococcus deasonii*, *Stichococcus jenerensis*, *Stichococcus chodatii, Chlorella vulgaris*, *Chlamydomonas reinhardtii*, *and Maesotaenium caldariorum.* These strains have been selected because they are characterized by high lipid content and different cell wall structure.
Main conclusions are:

1. A procedure to assess the kinetic parameters that characterize the model of photosynthetic reaction-centres reported by Eilers and Peeters (1988) has been proposed. The characterization has been assessed by processing microalgal fluorescence measurements on four microalgal strains growth under different operating conditions.

   - The assessed parameters indicate that: at irradiance lower than 1000 µE m^{-2} s^{-1} the photochemical process is controlled by the photons capture while at higher irradiance the photoinhibition competes with the photochemical quenching.

   - Irradiance effects on microalgal growth has been interpreted taking into account the time-scale of the photochemical quenching process vs. the time-scale of the photoinhibition process.

2. Bio-oil has been produced according to the innovative direct transesterification process.

   ✓ The optimization of the alkaline direct transesterification was carried out on *Stichococcus bacillaris.* Triglycerides were not converted without an alkaline catalyst and approached a maximum value at a catalyst concentration of 1.5% NaOH (w/w). Under alkaline conditions this led to the following: (i) the pre-mixing time did not affect bio-oil yield (~17%); (ii) the bio-oil yield increased with temperature and approached a maximum at around 65°C; (iii) the bio-oil yield did not change significantly with the methanol to biomass weight ratio within the range 39:1 - 79:1; iv) the bio-oil yield gradually increased within the first minutes of reaction, approached a constant value within the interval 3-12 minutes and decreased for times longer than 12 min.

- ✓ Biomass drying was observed to play an important role in direct transesterification: the bio-oil yield reduced with an increase in biomass water content. A higher bio-oil yield was obtained increasing the methanol/wet biomass ratio.

- ✓ Under alkaline catalyzed conditions the direct transesterification process was more efficient than the acidic ones producing higher bio-oil yield.

- ✓ Direct transesterification process was characterized by bio-oil yield – assessed for the investigated microalgal strains – higher than that assessed for conventional transesterification process.

3. The studies on microalgal culture were focused on effects of hydrodynamics, light, CO_2 in the gas phase, medium composition and medium pH on microalgal cultures in lab-scale photobioreactors. The effects of each operating condition on the biomass and lipid productivities were analysed. Two configurations of photobioreactors were investigated: cylindrical bubble column photobioreactors (CBC), and parallelepiped bubble column photobioreactors (RBC).

- ✓ Microalgal growth was successfully carried out in several photobioreactor design.

- ✓ The CO_2 concentration typical of power plant exhaust gas (up to 15-18%) enhances lipid productivity, notwithstanding the inhibition effects on pigment synthesis.

- ✓ The optimal pH has been found to be 7.0.

- ✓ Satisfactory microalgae and lipid productivities have been obtained at low pH, thus suggesting the real possibility to adopt acid conditions to preserve cultures from contamination.

- ✓ A proper photobioreactor design can significantly improve the process performance up to doubling the specific volumetric biomass productivity (see figure 4.4).

4. A turbidosotat photobioreactor has been operated to characterize the specific growth rate and the distribution of biomass content during the day. Two irradiation strategy have been investigated :“constant irradiance day/night cycle” 16 h of light at 600 µE m^{-2} s^{-1} and 8 h of dark; “circadian cycle” 16 h of irradiation at intensity characterized by time-sinusoidal path and maximum of 1500 µE m^{-2} s^{-1} and 8 h of dark.

- ✓ The circadian clock and cell division of *Nannochoropsis sp.* have been highlighted during tests.

- ✓ The fraction of carbohydrate, protein and TFA of the biomass changes over the day: the lower value has been measured after the cell division, while the maximal values were obtained before cell division. the harvesting during the day of the biomass should be carried out when the concentration of the selected constituent is high.

- ✓ A model to describe the change of the specific growth rate of microalgae during the day has been proposed and validated.

The reported results suggest that future activities should be focused on:

- ✓ the systematic extension of the photosynthesis kinetic characterization to microalgae cultivated under a wide spectrum of operating conditions, reactor design included. This data book should provide the basis to model how the photosynthetic systems adapt themselves to the operating conditions and in particular to the light/dark regimes;

- ✓ the study of the proteins responsible of the photoinhibition process. The aim is to increase the threshold irradiance and to propose an engineered strain able to operate at high irradiance at high energy efficiency. The actions may include both systems: the inhibition and the repair systems of the photosynthesis;

- ✓ the development of photobioreactor systems able to take advantage from the different time scale of the photochemical process. In particular, the system proposed by Liao et al (2014) and the inclined bubble columns should be improved designed to exploit the different time scale of the photochemical process;

- ✓ the characterization of the instantaneous growth kinetics taking into account the circadian clock of the strains;

- ✓ the development of systems to maximize the production of microalgal fractions (carbohydrates, lipids, proteins) according to the application of the process. The maximization of the exploitation of a fraction may not be in agreement with the maximum economic profit of the process and the contribute of all fractions should be carefully taken into account.

REFERENCES

Alabi AO, Tampier M, Bibeau E. Microalgae technologies and process for biofuels/bioenergy production in British Columbia: current technology, suitability and barriers to implementation: final report. British Columbia Innovation Council, Victoria, British Columbia 2009.

Arnold AA, Genard B, Zito F, Tremblay R, Warschawski DE, Marcotte I. Identification of lipid and saccharide constituents of whole microalgal cells by 13C solid-state NMR. BBA-Biomembranes 2015; 1848 (1B): 369-377.

Atkinson Jr AW, Gunning BES, John PCL. Sporopollenin in the cell wall of *Chlorella* and other algae: ultrastructure, chemistry, and incorporation of 14C-acetate, studied in synchronous cultures. Planta 1972; 107 (1): 1-32.

Becker EW. Nutritional properties of microalgae: potentials and constraints. Handbook of Microalgal Mass Culture. CRC Press, Boca Raton, Florida. 1986; 339-420.

Benemann JR, Oswald WJ. Systems and economic analysis of microalgae pond for conversion of CO_2 to biomass. Final report, Pittsburgh Energy Technology Center 1996.

Benemann JR, Weissman JC, Koopman JL, Oswald WJ. Energy production by microbial photosynthesis. Nature 1977; 268: 19-23.

Benvenuti G, Bosma R, Cuaresma M, Janssen M, Barbosa MJ, Wijffels RH. Selecting microalgae with high lipid productivity and photosynthetic activity under nitrogen starvation. J Appl Phycol 2014; DOI 10.1007/s10811-014-0470-8.

Berchmans HJ, Morishita K, Takarada T. Kinetic study of hydroxide-catalyzed methanolysis of *Jatropha curcas*–waste food oil mixture for biodiesel production. Fuel 2013: 104: 46-52.

Bernardi A, Perin G, Sforza E, Galvanin F, Morosinotto T, Bezzo F. An identifiable state model to describe light intensity influence on microalgae growth. Ind Eng Chem Res 2014; 53: 6738-6749.

Bertucco A, Beraldi M, Sforza E. Continuous microalgal cultivation in a laboratory-scale photobioreactor under seasonal day–night irradiation: experiments and simulation. Bioprocess Biosyst Eng 2014; 37(8): 1535-1542.

Bischoff, H.W. and Bold, H.C. 1963. Phycological Studies IV. Some soil algae from Enchanted Rock and related algal species. Univ Texas Publ 1963; 6318: 1-95.

Bold HC. The morphology of *Chlamydomonas chlamydogama* sp. nov. Bull Torrey Bot Club 1949; 76: 101-108.

Borodyanski G, Konstantinov I. Microalgae separator apparatus and method. United States patent US 2002/0079270A1; Jun 1, 2002.

Boyle NR, Morgan JA. Flux balance analysis of primary metabolism in *Chlamydomonas reinhardtii*. BMC Syst Biol 2009; 3:4.

Brányiková I, Maršálková B, Doucha J, Brányik T, Bišová K, ZachlederV. Microalgae—novel highly efficient starch producers. Biotechnol. Bioeng. 2011; 108: 766–776.

Breuer G, Lamers PP, Martens DE, Draaisma RB, Wijffels RH. Effect of light intensity, pH, and temperature on triacylglycerol (TAG) accumulation induced by nitrogen starvation in *Scenedesmus obliquus.* Bioresour Technol 2013; 143: 1–9.

Breuer G, Lamers PP, Martens DE, Draaisma RB, Wijffels RH. The impact of nitrogen starvation on the dynamics of triacylglycerol accumulation in nine microalgae strains. Bioresour Technol 2012; 124: 217-226.

Broady PA. Survey of algae and other terrestrial biota at Edward VII Peninsula Maria, Byrd Land, Antarctica. Antarct Sci 1989; 3:215-224.

Burczyk J, Szkawran H, Zontek I, Czygan FC. Carotenoids in the outed cell-wall layer of Scenedesmus (Chlorophyceae). Planta 1981; 151: 247-250.

Camacho Rubio F., Acién Fernández FG, García Camacho F, Sánchez Pérez JA, Molina Grima E. Prediction of dissolved oxygen and carbon dioxide concentration profiles in tubular photobioreactors for microalgal culture. Biotechnology and Bioengineering 1999; 62: 71-86.

Carlsson AS, Van Beilen JB, Moeller R, Clayton D. Micro and Macro algae: utility for industrial application. CPL Press, Newbury, 2007.

Cheng Y, Zhou W, Gao CF, Lan K, Gao Y, Wu Q. Biodiesel production from Jerusalem artichoke (Helianthus tuberosus L.) tuber by heterotrophic microalgae Chlorella protothecoides. J Chem Technol Biotechnol 2009; 85(5): 777-781.

Chisti Y. Research review paper: biodiesel from microalgae. Biotechnol Adv 2007; 25: 294-306.

Chiu SY, Kao CY, Tsai MT, Ong SC, Chen CH, Lin CS. Lipid accumulation and CO2 utilization of *Nannochloropsis oculata* in response to CO2 aeration. Bioresour Technol 2009; 100: 833-8.

Crill PA. The photosynthesis – light curve: a simple analog model. J Theor Biol 1977; 6: 503-516.

Cuhel RL, Ortner PB, Lean DRS. Night synthesis of protein by algae. Limnol. Oceanogr. 1984; 731–744.

Dorado MP, Ballesteros E, Lopez FJ, Mittelbach M. Optimization of alkali-catalyzed transesterification of *Brassica Carinata* oil for biodiesel production. Energ Fuel 2004; 18: 77-83.

Eichenberger W, Gribi C. Lipids of *Pavlova lutheri*: cellular site and metabolic role of DGCC. Phytochemistry 1997; 45: 1561-1567.

Eilers PHC, Peeters JCH. A model for the relationship between light intensity and the rate of photosynthesis in phytoplankton. Ecological Modelling 1998; 42: 199-215.

Etheridge DM, Steele LP, Langenfelds RL, Francey RJ, Barnola JM, Morgan VI. Historical CO_2 record from the Law Dome DE08, DE08-2, and DSS ice cores (atmospheric CO_2 concentrations, Antarctic ice cores). A Compendium of Data on Global Change, on line at the Carbon Dioxide Information Analysis Center, http://cdiac.esd.ornl.gov/, June 1998.

Fábregas J, Maseda A, Domínguez A, Ferreira M, Otero A. Changes in the cell composition of the marine microalga, *Nannochloropsis gaditana* during a light:dark cycle. Biotechnol. Lett. 2002, 24: 1699–1703.

Falkowski PG, Raven JA. Aquatic Photosynthesis, Princeton University Press, 2007.

Fawley KP, Fawley MW. Observations on the diversity and ecology of freshwater *Nannochloropsis* (*Eustigmatophyceae*), with descriptions of new taxa. Protist 2007; 158: 325-336.

Flickinger M, Drew SW. Encyclopedia of bioprocess technology: fermentation, biocatalysis, and bioseparation 1999; volumes 1-5.

Folch J, Lees M, Stanley GHS. A simple method for the isolation and purification of total lipids from animal tissues. J Biol Chem 1957; 226: 497-509.

Francisco EC, Neves DB, Jacob-Lopes E, Franco TT. Microalgae as feedstock for biodiesel production: carbon dioxide sequestration, lipid production and biofuel quality. J Chem Technol Biotechnol 2010; 85: 309-403.

Gao C, Zhai Y, Ding Y, Wu Q. Application of sweet sorghum for biodiesel production by heterotrophic microalga *Chlorella protothecoides*. Appl Energy 2010; 87: 756-761.

Ghasemi Y, Rasoul-Amini S, Naseri AT. Microalgae biofuel potentials (Review). Appl Biochem Microbiol 2012; 48:126–144.

Gonzàlez-Lòpez CV, Acièn Fernàndez FG, Fernàndez-Sevilla JM. Development of a process for efficient use of CO_2 from flue gases in the production of photosynthetic microorganisms. Biotechnol Bioeng 2012; 109:1637–1650.

Griffiths MJ, van Hill RP, Harrison STL. Selection of direct transesterification as the preferred method for assay of fatty acid content of microalgae. Lipids 2010; 45: 1053-1060.

Gross W. Ecophysiology of algae living in highly acidic environments. Hydrobiologia 2000; 433: 31-37.

Gutierrez-Wing MT, Benson BC, Rusch KA. Impact of light quality and quantity on growth rate kinetics of *Selenastrum capricornutum*. Eng Life Sci 2012; 12:79–88.

Halim R, Rupasinghe TWT, Tull DL, Webley PA. Modelling the kinetics of lipid extraction from wet microalgal

Hindersin S, Leupold M, Kerner M, Hanelt D. Irradiance optimization of outdoor microalgal cultures using solar tracked photobioreactors. Bioprocess Biosyst Eng 2013; 36:345–355.

Hu Q, Sommerfeld M, Jarvis E, Ghirardi M, Posewitz M, Seibert M, Darzins A. Microalgal triacylglycerols as feedstocks for biofuel production: perspectives and advances. Plant J 2008; 54: 621-639

Imam SH, Snell WJ. The *Chlamydomonas* cell wall: characterization of the wall framework. J Cell Biol 1985; 101(4): 1599–1607.

Janssen M, Tramper J, Mur LR, Wijffels RH. Enclosed outdoor photobioreactors: light regime, photosynthetic efficiency, scale-up, and future prospects. Biotechnol Bioeng 2003; 81:193–210.

Johnson MB, Wen Z. Production of biodiesel fuel from the microalga Schizochytrium limacium by direct transesterification of algal biomass. Energ Fuel 2009; 23: 5179-5183.

Kim CW, Sung MG, Nam K, Moon M, Kwon JH, Yang JW. Effect of monochromatic illumination on lipid accumulation of Nannochloropsis gaditana under continuous cultivation. Bioresource Technology 2014; 159: 30-35.

Kirk JTO. Light and Photosynthesis in Aquatic Ecosystems. Cambridge University Press 1994.

Klok AJ, Martens DE, Wijffels RH, Lamers PP. Simultaneous growth and neutral lipid accumulation in microalgae. Bioresour Technol 2013; 134: 233-243.

Kok B. On the inhibition of photosynthesis by intense light. Biochem Biophys Acta 1956; 21: 234-244.

Kolber Z, Falkowski PG. Use of active fluorescence to estimate phytoplankton photosynthesis in situ. Limnol Oceanogr 1993; 38: 1646-1665.

Krienitza L, Wirth M. The high content of polyunsaturated fatty acids in *Nannochloropsis limnetica* (*Eustigmatophyceae*) and its implication for food web interactions, freshwater aquaculture and biotechnology. Limnologica 2006; 36: 204-210.

Lam MK, Lee KT, Mohamed AR. Homogeneous, heterogeneous and enzymatic catalyst for transesterification of high free fatty acid oil (waste cooking oil) to biodiesel: A review. Biotechnology advances 2010; 28: 500-518.

Lardon L, Hèlias A, Sialve B, Steyer J, Bernard O. life-cycle assessment of biodiesel production from microalgae. Environ Sci Technol 2009; 43: 6475-6481.

Lepage G, Roy CC. Direct transesterification of all classes of lipids in a onestep reaction. J Lipid Res 1986; 27: 114-120.

Lepage G, Roy CC. Improved recovery of fatty acid through direct transesterification without prior extraction or purification. J Lipid Res 1984; 25: 1391-1396.

Liang Y, Sarkany N, Cui Y, Yesuf J, Trushenski J, Blackburn JW. Use of sweet sorghum juice for lipid production by *Schizochytrium limacinum* SR21. Bioresour Technol 2010; 101: 3623-3627.

Lubiàn LM, Montero O, Moreno-Garrido I, I. Huertas E, Sobrino C, Gonzalez-del Valle M, Parès G. *Nannochloropsis* (*Eustigmatophyceae*) as source of commercially valuable pigments. J Appl Phycol 2000; 12: 249-255.

Lürling M, Van Donk E. Grazer-induced colony formation in *Scenedesmus acutus* (*Chlorophyceae*): ecomorph expression at different temperatures. J Phycol 1999; 35: 1120-1126.

Ma F, Hanna MA. Biodiesel production: a review. Bioresour Technol 1999; 70: 1-15.

Masojìdek J, Koblìzèk M, Torzillo, G. Photosynthesis in microalgae, in: Amos Richmond (Eds.), Handbook of Microalgal Culture: Biotechnology and Applied Phycology, Blackwell Publishing Ltd, 2004; pp. 20-39.

Mata TM, Martins A, Caetano NS. Microalgae for biodiesel production and other applications: A review. Renew Sustain Energy Rev 2010; 14 (1): 217-232.

Mathews CK, Van Holde KE. Biochemistry. Benjamin/Cummings Publishing Company, Redwood City 1990.

Maxwell K, Johnson GN. Chorophyll fruorescence – a pratical guide. J Exp Bot 2000; 51: 659-668.

McNichol J, MacDougall KM, Melanson JE, McGinn PJ. Suitability of Soxhlet extraction to quantify microalgal fatty acids as determined by comparison with in situ transesterification. Lipids 2012; 47: 195-207.

Mittag M, Kiaulehn S, Johnson CH. The circadian clock in *Chlamydomonas reinhardtii*. What is it for? What is it similar to? Plant Physiol. 2005; 137: 399–409.

Molina Grima E, Acien Fernandez FG, Rogbies Medina A. Handbook of microalgal culture, ed. A. Richmond, Blackwells 2004: 215-251.

Molina Grima E, Fernández J, Acién Fernández FG, Chisti Y. Tubular photobioreactor design for algal cultures. Journal of Biotechnology 2001; 92: 113-131.

Noureddini H, Zhu D. Kinetics of transesterification of soybean oil. JAOCS 1997; 74: 1457-1463.

Olivieri G, Gargano I, Andreozzi R, Marotta R, Marzocchella A, Pinto G, Pollio A. Effects of CO_2 and pH on *Stichococcus bacillaris* in Laboratory Scale Photobioreactors. Chemical Engineering transactions 2012; 27: 127-132.

Olivieri G, Gargano I, Andreozzi R, Marotta R, Marzocchella A, Pinto G, Pollio A. Effects of photobioreactors design and operating conditions on *Stichococcus bacillaris* biomass and biodiesel production. Biochem Eng J 2013; 74: 8-14.

Olivieri G, Marzocchella A, Andreozzi R, Pinto G., Pollio A, Biodiesel production from *Stichococcus* strains at laboratory scale. J Chem Technol Biotechnol 2011; 86: 776-783.

Olivieri G, Salatino P, Marzocchella A. Advances in photobioreactors for intensive microalgal production: configurations, operating strategies and applications. J Chem Technol Biotechnol 2014; 89: 178–195.

Oswald I, Taylor AM, Treisman M. Discriminative responses to stimulation during human sleep. Brain 1960; 83: 440-453.

Pienkos PT, Darzins A. Biofuels. Bioprod Biorefin. 2009; 3: 431-440.

Pirt SJ, Lee YK, Richmond A, Watts Pirt M. The photosynthetic efficiency of Chlorella biomass growth with reference to solar energy utilization. J Chem Tech Biotechnol 1980; 30: 25-34.

Pirt SJ. The thermodynamic efficiency (quantum demand) and dynamics of photosynthetic growth. New Phytol 1986; 102: 3-37.

Pollio A, Aliotta G, Pinto G, Patern `M, Bevilacqua A. Ecophysiological characters and biochemical composition of *Stichococcus bacillaris* Naegeli strains from low pH environments. Algologic Stud/Arch Hydrobiol 1997; 84: 129-143.

Pollio A, Pinto G, Ligrone R, Aliotta G. Effects of the potential allelochemical α-asarone on growth, physiology and ultrastructure of two unicellular green algae. J Appl Phycol 1993; 5: 395–403.

Post AF, loogman JG, MurLR. Regulation of growth and photosynthesis by *Oscillatoria agardhii* grown with a light/dark cycle. FEMS Microbiol. Lett. 1985; 31: 97–102.

Posten C, Schaub G. Microalgal and terrestrial biomass as source of fuels – a process view. J Biotechnol 2009; 142: 64-69.

Pratoomyot J, Srivilas P, Noiraksar T. Fatty acids composition of 10 microalgal species. Songklanakarin J Sci Technol 2005; 27: 1179-87.

Randawa MS. A note on species of Stichococcus and Phormidium from Dehli. J Indian Bot Soc 1959; 38: 398-399.

Rashid U, Anwar F. Production of biodiesel through optimized alkaline-catalyzed transesterification of rapeseed oil. Fuel 2008; 87: 265-273.

Rawat I, Ranjith Kumar R, Mutanda T, Bux F. Biodiesel from microalgae: a critical evaluation from laboratory to large scale production. Appl Energy 2013; 103:444–467.

Rodolfi L, Chini Zittelli G, Bassi N, Giulia Padovani G, Biondi N, Bonini G, Tredici MR. Microalgae for oil: strain selection, induction of lipid synthesis and outdoor mass cultivation in a low-cost photobioreactor. Biotechnol Bioeng 2009; 102: 100-112.

Rodolfi L, Chini-Zitelli G, Bassi N, Padovani G, Biondi N, Bonini G, Tredici MR. Microalgae for oil: Strain selection, induction of lipid synthesis and outdoor mass cultivation in a low-cost photobioreactor. Biotechnol Bioeng 2009; 102 (1): 100-112.

Ruiz NJ, Garcia MDCC, Miron AS, Haftalaui EHB, Camacho FG, Grima EM. Lipids accumulation in *Chlorella protothecoides* through mixotrophic and heterotrophic cultures for biodiesel production. New Biotechnol 2009; 25(S1):S266.

Ryan TW, Dodge LG, Callahan TJ. The effect of vegetable oil properties on injection and combustion in two different diesel engines. J Am Oil Chem Soc 1984; 61: 1610-1619.

Schenk PM, Thomas-hall AR, Stephen E, Marx UC, Mussgnung JH and Posten C. Second generation biofuels: high efficiency microalgae for biodiesel production. Bioenergy Res 2008; 1: 20-43.

Scragg AH, Iliman AM, Carden A, Shales SW. Growth of microalgae with increased calorific values in a tubular reactor. Biomass Bioenergy 2002; 23: 67-73.

Sforza E, Grisa B, de Farias Silva CE, Morosinotto T, Bertucco A. Effects of light on cultivation of *Scenedesmus obliquus* in batch and continuous flat plate photobioreactor. Chem eng tran 2014; 38: 211-216.

Sharma YC, Singh B. Development of biodiesel: current scenario. Renewable Sustainable Energy Rev 2009; 13: 1646-1651.

Sheehan J, Dunahay T, Benemann J, Roessler P. A Look Back at the U.S. Department of Energy's Aquatic Species Program. Biodiesel from Algae 1998.

Shenbaga Devi A, Santhanam P, Rekha V, Ananth S, Balaji Prasath B, Nandakumar R, Jeyanthi S, Dinesh Kumar S. Culture and biofuel producing efficacy of marine microalgae *Dunaliella salina* and *Nannochloropsis sp*.. J Algal Biomass Utln 2012; 3 (4): 38-44.

Singh J, Gu S. Commercialization potential of microalgae for biofuels production. Renew Sustain Energy Rev 2010; 14:2596–2610.

Slegers PM, Wijffels RH, Van Straten G, Van Boxtel AJB. Design scenarios for flat panel photobioreactors. Appl Energy 2011; 88:3342–3353.

Solovchenko E, Khozin-Goldberg I, Didi-Cohen S, Cohen Z, Merzlyak MN. Effect of light intensity and nitrogen starvation on growth, total fatty acids and arachinidic acid in the green microalga Parietocholir incise. J. Appl. Phycol 2008; 20: 245-251.

Spolaore P, Joannis-Cassan C, Duran E, Isambert A. Commercial application of microalgae. J Biosci Bioeng 2006; 101(2): 87-96.

Suali E, Sarbatly R. Conversion of microalgae to biofuel. Renew Sustain Energy Rev 2012; 16:4316–4342.

Sukenik A, Carmeli Y. Lipid synthesis and fatty acid composition in *Nannochloropsis sp.* (Eustigmatophyceae) grown in a light–dark cycle. J. Phycol. 1990; 26: 463–469.

Tang D, Han W, Li P, Miao X, Yhong J. CO_2 biofixation and fatty acid composition *of Scenedesmus obliquus* and *Chlorella pyrenoidosa* in response to different CO_2 levels. Bioresour Technol 2011; 102: 3071-3076.

Torzillo G. Tubular Bioreactors. In: *Spirulina platensis* (*Arthrospira*): Physiology, Cell-biology and Biotechnology (ed. A. Vonshak), pp. 101–15. Taylor & Francis, London

U.S. Department of Energy 2010 - National Algal Biofuels Technology Roadmap.

Vasudevan PT, Briggs M. Biodiesel production – current state of the art and challenges. J Ind Microbiol Biotechnol 2008; 35: 421-430.

Vicente G, Bautista LF, Rodríguez R, Gutiérrez FJ, Sádaba I, Ruiz-Vázquez RM, Torres-Martínez S, Garre V. Biodiesel production from biomass of an oleaginous fungus. Biochem Eng J 2009; 48: 22-27.

Waltz E. Biotech's green gold?. Nature Biotechnology 2009; 27(1): 15-18.

Weissman J, Benemann JR. Photobioreactor Design: Comparison of Open Ponds. Bioeng Biotech 1988; 31: 336-344.

Widjaja A, Chien CC, Ju YH. Study of increasing lipid production from fresh water microalgae *Chlorella vulgaris*. J Taiwan Inst Chem Eng 2009; 40: 13-20.

Wijffels RH, Barbosa MJ. An outlook on microalgal biofuels. Science 2010; 329: 796–799.

Williams PJB, Laurens LML. Microalgae as biodiesel & biomass feedstocks: Review & analysis of the biochemistry, energetic & economics. Energy & Enviromental Science 2010; 3: 554-590.

Winter de L, Klok AJ, Cuaresma Franco M, Barbosa MJ, Wijffels RH. The synchronized cell cycle of *Neochloris oleoabundans* and its influence on biomass composition under constant light conditions. Algal Research 2013: 313-320.

Winter de L, Schepers LW, Cuaresma M, Barbosa MJ, Martens DE, Wijffels RH. 2014. Circadian rhythms in the cell cycle and biomass composition of *Neochloris oleoabundans* under nitrogen limitation. J Biotechnol 2014; 187: 25–33.

Wu X, Merchuk JC. Simulation of algae growth in a bench-scale bubble column reactor. Biotechnol Bioeng 2002; 80(2): 156-168.

Xu H, Miao X, Wu Q. High quality biodiesel production from a microalga *Chlorella protothecoides* by heterotrophic growth in fermenters. J Biotechnol 2006; 126: 499-507.

Zheng M, Tian J, Yang G, Zheng L, Chen G, Chen J, Wang B. Transcriptome sequencing, annotation and expression analysis of *Nannochloropsis sp*. at different growth phases. Gene 2013; 523 (2): 117-121.

Zheng MG, Huang YJ, Zheng L, Sun ZT, Wang L. Cloning, expression and stress-respondent transcription of long-chain acyl-coenzyme A synthetase cDNA gene of *Nannochloropsis gaditana* and its involvement in the biosynthesis of eicosapentaenoic and decosahexaenoic acids. Biotechnol Lett 2014; 36: 141-145.

Zhu L. Biorefinery as a promising approach to promote microalgae industry: An innovative framework. Renew Sustain Energy Rev 2015; 41: 1376-1384.

Zijffers JWF, Schippers KJ, Zheng K. Maximum photosynthetic yield of green microalgae in photobioreactors. Mar Biotechnol 2010; 12: 708-718.